ISSN 1000-9620

Marine Science Bulletin

海洋通报

Volume 11 • Number 1 2009

ISSN 1000-9620

9 771000 962001 01>

NATIONAL MARINE DATA AND
INFORMATION SERVICE OF CHINA

MARINE SCIENCE BULLETIN

Vol. 11 No. 1 May 2009

CONTENTS

Influence on Northern Pacific Storm Track of the Okhotsk Sea Ice during Winter ····· HE Dong-yan et al. (01)

An Optimal Algorithm for the Retrieval of Chlorophyll, Suspended Sediments and Gelbstoff of Case II Waters in the Pearl River Estuary ····· YANG Jin-kun et al. (13)

Dissolved Inorganic Arsenic in the Yellow Sea and the East China Sea—Distributions and Seasonal Variations ····· REN Jing-ling et al. (24)

Regulatory Analysis of IPP Isomerase Gene in *Haematococcus pluvialis* ····· GAO Zheng-quan et al. (37)

Distribution of Biogenic Silica Content in Surface Sediments from the Southern South China Sea and Its Environmental Significance ····· ZHANG Lan-lan et al. (43)

Growth Strategy of Seagrass *Thalassia hemprichii* in Xincun Bay near Hainan Island of China ····· XU Zhan-zhou et al. (53)

Influence of Microstructure Change of Seafloor Sediments on the Sound Velocity in them in the Course of Stress-strain ····· LI Gan-xian et al. (62)

Fractal Analysis of Spatial Fault Distribution in the Southern South China Sea····· YAO Yan-tao et al. (70)

Research on the Model of Coastline Demarcation and Management ····· LIN Ning et al. (82)

Development and Management Status of Voluntary Observing Ships in China ····· LIU Jia-yi (90)

Influence on Northern Pacific Storm Track of the Okhotsk Sea Ice during Winter

LIBRARY
Pacific Islands Fisheries Science Cente
NOAA Fisheries
Honolulu, Hawai'i

HE Dong-yan[1], DENG Xue-liang[2], ZHU Wei-jun[3]

1. *Anhui Climate Centre, Hefei* 230031, *Anhui province, China;*

2. *Anhui Institute of Meteorology, Key Laboratory of Atmospheric Science and Satellite Remote Sensing, Hefei* 230031, *Anhui province, China;*

3. *Jiangsu Key Laboratory of Meteorological Disaster, Nanjing University of Information and Science Technology, Nanjing* 210044, *Jiangsu province, China*

Abstract: Based on Arctic sea ice concentration data and NCEP\NCAR reanalysis data, relationship between sea ice anomaly over the sea of Okhotsk and its vicinage and northern Pacific storm track during winter is discussed by statistic analysis methods. It is found that with northern Pacific SSTA, sea ice area anomaly over southwest of the sea of Okhotsk can except crucial influence on the variation in vigor and extension (contraction) from northwest to southeast of northern Pacific storm track. But with the influence of SSTA, sea ice area anomaly over northeast of the sea of Okhotsk and the gulf of Shelikhow works mainly on the strength and the south-north movement of the storm track.

Keywords: storm track, sea ice, SVD analysis

Many meteorologists have studied on the impact of sea ice on the atmospheric circulation and the climate before. High reflectivity of the sea ice surface reduces its absorptivity to the solar radiation and weakens the transportation of sensible and latent heat from ocean to atmosphere, which makes the atmosphere colder, the meridional temperature gradient in local bigger, and finally the zonal circulation strengthen. Hao et al. [1] point out that in northern Pacific, drift ice flows from Arctic Ocean to the sea of Okhotsk, even more south, which can evidently influence the coastal climate in northeast Asia. Zhao et al. [2-3] find out that the sea of Okhotsk is one of the sea where sea ice expands southerly remarkably during winter and spring, whose primary periods are 5 - 6 a and 2 - 4 a, and in the season when there is more sea ice, there is more remarkable influence of the sea ice on the atmospheric circulation, especially in the sea where the interannual change is acute in every season. Honda et al. [4] find sea ice anomaly in the sea of Okhotsk during winter can not only influence its upper circulation but also excite a peculiar wave train in its lower from the Bering sea vas Alaska to the north America.

Storm track is defined as an area where the 2.5 - 6 d synoptic transient eddy is the most violent, which has prominent seasonal variation, and some interannual even some interdecadal variation each season [5]. And it plays an important role in the short-term anomaly of the atmospheric circulation for its close association with the time-mean flow. Gudrun et al. [9] point out that when sea ice on the border of the

Received on May 23, 2008

Arctic and the northern Atlantic increases, the Atlantic storm track turns weaker, more southward, and more longitudinal.

In this paper, we mainly introduce our studies on the influence of the sea ice over the sea of Okhotsk and its vicinage on the simultaneously interannual variation of northern Pacific storm track during winter. And our attempts to find some physical explanations are mentioned.

1 Dataset and methods

1.1 Dataset

The primary data we use are monthly 1° × 1° sea ice concentration data from Hadley center, daily 2.5° × 2.5° wind and geopotential height reanalysis data, and monthly 2° × 2° SST reanalysis data from NCEP/NCAR. Time series are all selected from Jan. 1953 to Feb. 1999.

1.2 Analysis methods

Referring to the literature[10], 500hPa mean geopotential height is band-pass filtered to retain variance with period between 2.5 and 6 days to describe the position and intensity of storm track in winter (from December to February next year), and the 31 points digital filter [11] is used in band-pass filtering. When calculating the total ice area over one sea, an index named as *Q* index is used to express the monthly summation of all the grid value, which is named as *DQ* index for standardization. By the way, sea ice concentration correlates to the unit area, which increases when the latitude decreases, so we use the latitudinal revisal coefficient α (α = COS ($\alpha \times \pi$/180)) to eliminate this departure (α stands for the latitude of the grid). Then we use SVD analysis between the band-pass filtered variance of the 500hPa mean geopotential height field and the mean sea ice concentration field to find out the coupling mutative correlative distributions between northern Pacific storm track and Arctic sea ice in winter.

1.3 Selecting the key sea ice region

Fig. 1 shows the average of the northern Pacific storm track of 46 years from 1953/1954 to 1998/1999. Then we choose the strongest region of the storm track over 140°E - 160°W, 35° - 50°N as the central region, average all the band-pass filtered variance of 500 hPa geopotential height in it, and finally execute correlation analysis between the mean values and the sea ice concentration field by north of 45°N. The result shows that there is better correlation of the mean with the sea of Okhotsk and its vicinage, which also passes the t-test of the reliability α =0.05. So we choose the region 130° - 170° E, 45°- 62°N as the key region of sea ice (concluding the sea of Okhotsk, the gulf of Shelikhow, and the channel of Tatar).

In SVD analysis, the spacial scope we choose includes: the storm track : 110°E - 110°W, 30° - 60°N, the key region of sea ice (called sea ice field hereinafter for short): 130° - 170°E, 45° - 62°N, and of which the time series are all 46 years.

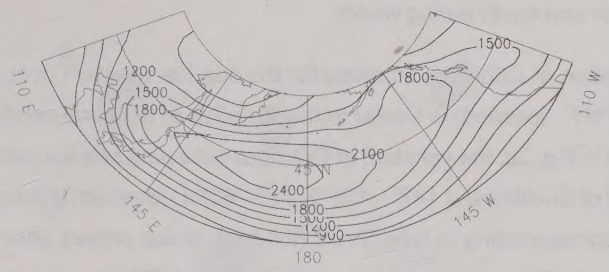

Fig. 1 Climatological position of northern Pacific storm track during winter with contour interval of 300 gpm^2

2 Analysis of results

2.1 The result of the SVD analysis

Because of the SVD result (Tab. 1) that the first two spacial canonical patterns explain 80.52% of the square covariance in all, we just analyze these two patterns in this paper mostly (called as type SVD 1 and SVD 2 respectively hereinafter for short).

Tab. 1 Parameters of the first two coupled mode of SVD analysis

		VF_1/%	CVF_1/%	VF_2%	CVF_2/%	r	SCF/%	$CSCF$/%
SVD 1	Left	17	17	7	7	0.694	61.68	61.68
	Right	13	13	6	6			
SVD 2	Left	13	30	3	10	0.613	18.84	80.52
	Right	6	19	3	9			

Type SVD 1 (Fig. 2a and 2b) mainly describes the relation of the opposite phase, while sea ice increases (decreases) in southwest of the Okhotsk sea but decreases (increase) in its north coast and the gulf of Shelikhow, the northwest, central and south parts of the northern Pacific storm track strengthen (weaken) but its north part weakens (strengthens). 61.68% of the square covariance is explained in the type, and the correlation coefficient between the two corresponding temporal coefficients reaches 0.694, which means both the interannual variations of the intensity and flex in the direction between northeast and southwest of the northern Pacific storm track relate well to the sea ice distribution , which is of opposite variation in the southwest Okhotsk sea to that in the north coast of Okhotsk sea and in the gulf of Shelikhow during winter.

But type SVD2 mainly puts up the different change, when the northern part of northern Pacific storm track strengthens (weakens), the southern part weakens (strengthens) (Fig. 3a), which relates closely to sea ice's variation occurring over the northeast Okhotsk sea and the gulf of Shelikhow (Fig. 3b). The square covariance these typical distributions explain is 18.84%, and the correlation coefficient between the two temporal coefficients reaches 0.613, which proves again that sea ice acreage change over the northeast Okhotsk sea and the gulf of Shelikhow counts much for the displacement of the northern Pacific

storm track between north and south during winter.

In Fig. 2c, the variation of *DQ* index standing for the sea ice variation over southwest Okhotsk sea (138° - 155°E, 45° - 57°N) (dashed) is similar to the variation of temporal coefficients corresponding to type SVD1 (full line), and in Fig. 3c, the variation of *DQ* index reflecting sea ice variation over the northeast Okhotsk sea and the gulf of Shelikhow (147° - 159°E, 48° - 62°N)(dashed) is consistent with the variation of temporal coefficients corresponding to type SVD2 (full line), which proves once again that both sea ice anomaly over the southwest Okhotsk sea and over the northeast Okhotsk sea and the gulf of Shelikhow relate well with the northern Pacific storm track in winter. And in the following text, we use statistical composite analytical method to further discuss the impact of sea ice anomaly in acreage over the sea of Okhotsk and its vicinage on the northern Pacific storm track in winter, and try to find some possible intrinsic physical mechanism. And the examples selected for composite analyzing are presented in Tab. 2. (For facility, the southwest Okhotsk sea is named as region Ⅰ and the northeast Okhotsk sea and the gulf of Shelikhow is named as region Ⅱ.)

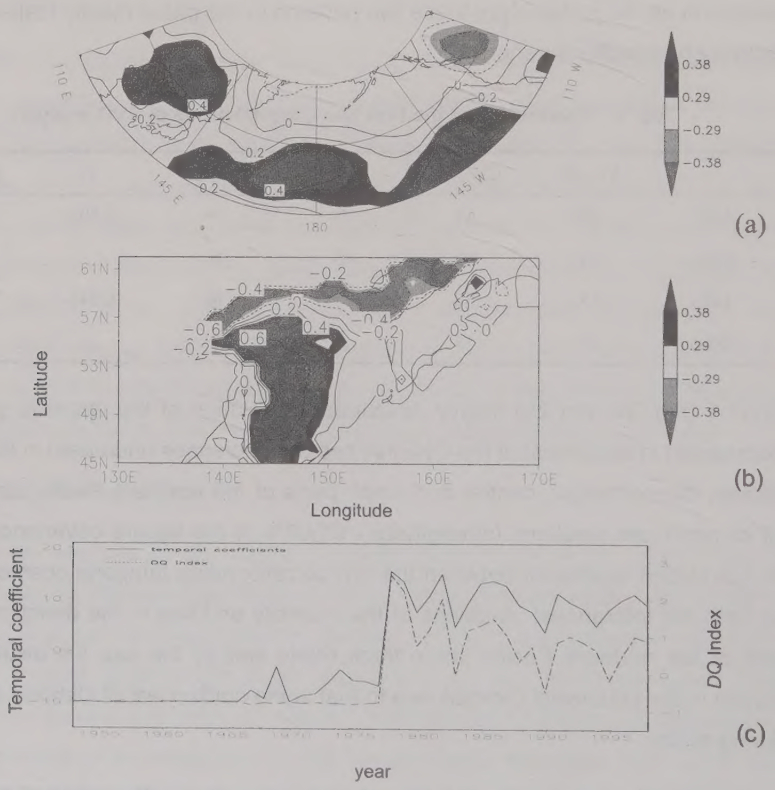

Fig. 2 Heterogeneous correlation patterns for the first SVD mode in winter 500 hPa synoptic height variance (a) and the sea ice (b) and (c) is the temporal coefficients related to the sea ice (full line) and the *DQ* index for the southwest part of thesea of Okhotsk (dashed). Regions with correlation values above 0.29 and below -0.29 is shaded.

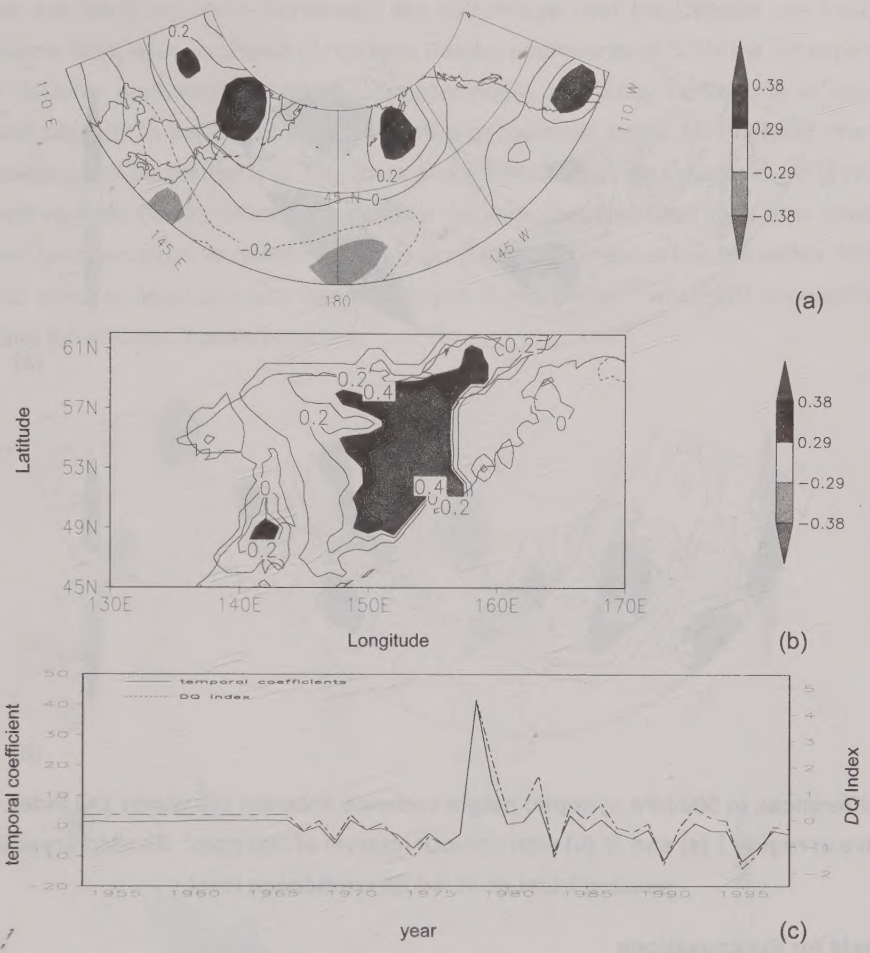

Fig. 3 Heterogeneous correlation patterns for the second SVD mode in winter 500 hPa synoptic height variance (a) and the sea ice (b) And (c) is the temporal coefficients related to the sea ice field (full line) and the *DQ* index for the northeast part of the sea of Okhotsk and the gulf of Shelikhow (dashed). Regions with correlation values above 0.29 and below -0.29 is shaded.

2.2 The result of the composite analysis

Fig. 4 shows the differences in 500 hPa geopotential height band-pass filtered field between the sea ice anomaly is positive and negative. When sea ice in region Ⅰ increases, the center of the northern Pacific storm track strengthens evidently, disturbance-enhancing area tends towards northwest to southeast, but over its northern and coastland of western North America, the disturbance weaken obviously (Fig. 4a). For region Ⅱ (Fig. 4b), when sea ice increases, disturbance-enhancing area of the storm track moves northwards, there are two strengthening centers in northwest and northeast respectively, but disturbance in southwest and south central weakens. After comparing, we also find that those characters (Fig. 4a, 4b) are consistent with the typical distributions of the storm track in SVD (Fig. 2a, 3a).

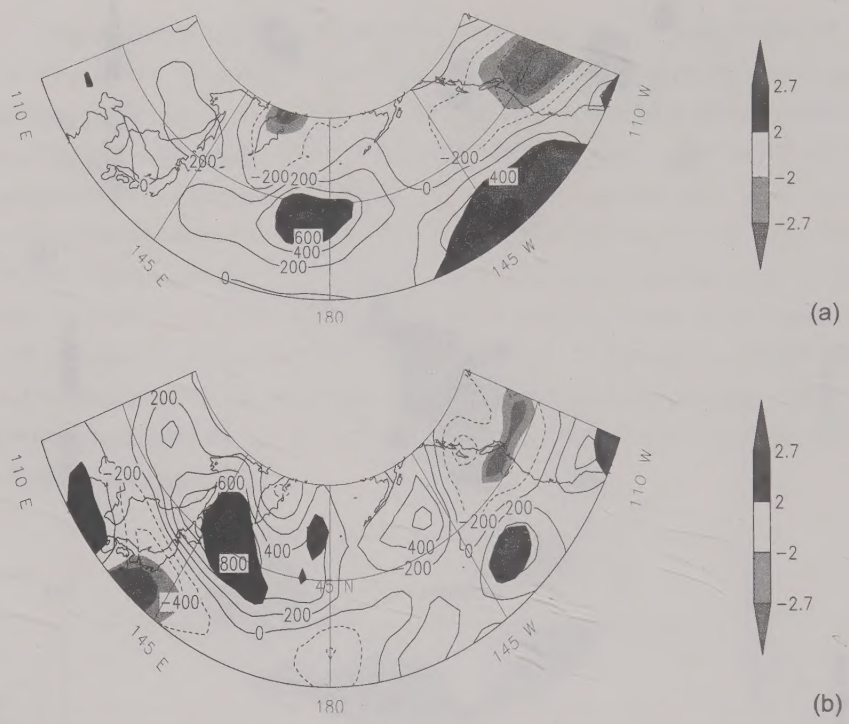

Fig. 4 Differences in 500 hPa synoptic height variance between the winter *DQ* index is positive and negative in region Ⅰ (a) and Ⅱ (b) with contour interval of 200 gpm^2. Shaded areas indicate that passing t-test at $\alpha = 0.05$ confidence level.

2.3 Analysis for the causations

As the baroclinity of the basic flow influences the intensity of storm track crucially[5, 12, 13], we draw baroclinic index [14] into our work to find out possible factors leading the storm track to transforming. Fig. 5a shows us when the acreage of sea ice in region Ⅰ is larger, baroclinity in south and northwest of the northern Pacific storm track increases, which also passes the t-text at the confidence level $\alpha = 0.05$. And it is well consistent with Fig. 4a, which indicates when sea ice in region Ⅰ increases during winter, synoptic eddy motion enhances northwards of the baroclinity-increasing area, reflecting that the baroclinity enhancing in northwest and south parts of the storm track leads its northwest and south central to strengthening. Like wise, when sea ice in region Ⅱ increases, baroclinity in western of the storm track enhances evidently (Fig. 5b), which causes the storm track enhancing northward its 4 latitudes (Fig. 4b).

Further more, storm track relates well with the jet on middle and upper troposphere[16, 18]. From the differences of 500 hPa geopotential height field between sea ice in region Ⅰ increased and decreased (Fig. 6a), there is a dipole over middle and high latitude of eastern Eurasia, of which positive and negative center are over Leptev Sea and Mongolia respectively, both expands eastward, and southwards of 50°N over the Okhotsk sea, the allohyps is positive, while northwards of 50°N the allohyps is negative, which

indicates when sea ice in region Ⅰ increases, the 500 hPa jet over the Okhotsk sea enhances near 50°N .At the same time, over southeast of northern Pacific, southwards of 30°N the allohyps is positive, while that is negative northwards of 30°N. Correspondingly, baroclinity northwards of these regions enhances obviously. And in the differences of 500 hPa geopotential height field between the sea ice in region Ⅱ increased and decreased (Fig. 6b), there is positive allohyps southwards of 45°N and negative northwards over western Pacific, which indicates that the jet accelerates near 45°N over western Pacific and makes baroclinity enhance its northwards. This circulation is somewhat like the pattern WP, though a little northward, which is accordant with that pointed out in reference [20] when WP is negative, both the Aleutian low and the jet over Japan strengthen.

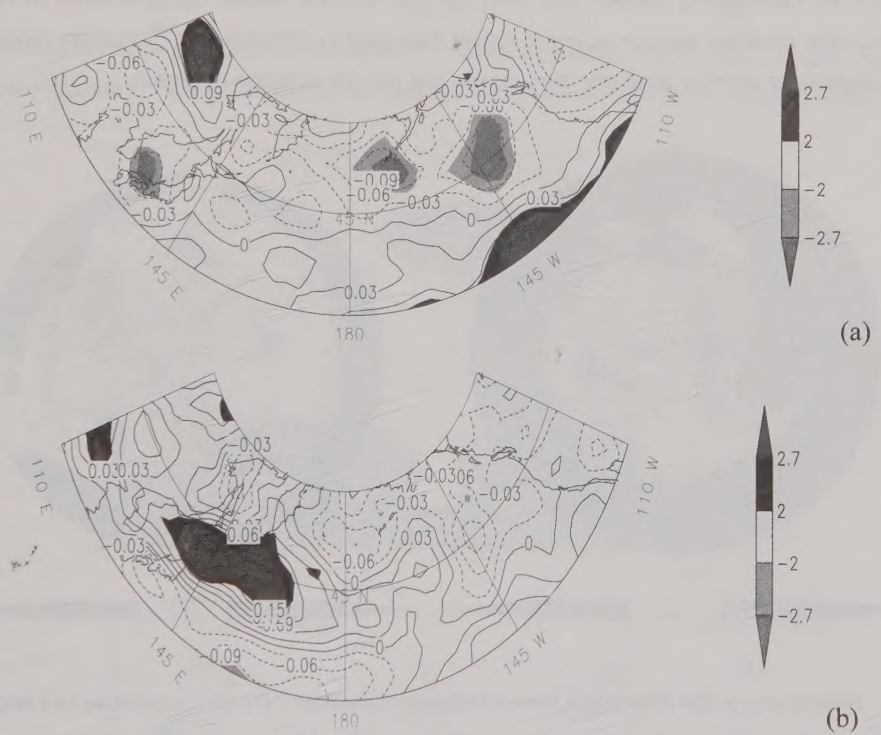

Fig. 5 Differences in 775 hPa mean barocliticay between the winter *DQ* index is positive and negative in region Ⅰ (a) and Ⅱ (b) with contour interval of 0.03 d^{-1}. Shaded areas indicate that passing t-test at $\alpha = 0.05$ confidence level.

It is figured out in references[15-18], SSTA (sea surface temperature anomaly) over Pacific affects storm track greatly, so we discuss variation of storm track with SSTA together (we select sea area: 110°E - 80°W, 30°S - 55°N here). When sea ice in region Ⅰ increase, SST over equatorial central and eastern Pacific turns hotter, but colder over the middle of northern Pacific (Fig. 7a), and because of this diabatic heating, the tropical Walker circulation weakens, the Hadley circulation strengthens, mean meridional temperature gradient over central and south parts of the northern Pacific storm track augments (Fig. 8a), the average available potential energy increases, and finally the baroclinity enhances. In west of the storm track, SSTA over Kuroshio is positive, while negative northwards, and more northward is region Ⅰ, which

causes local mean meridional temperature gradient increasing over northward of Kuroshio (Fig. 8a) through local diabatic heating and cooling, then heat energy transmitting more acutely from middle and high latitude to higher latitude, and finally baroclinity in northwest of the storm track enhancing. But in northeast of the storm track, SST increases over north Pacific, and decreases over its central (Fig. 7a), which makes mean meridional temperature gradient here decreases (Fig. 8a), and is disadvantageous for heat exchanging between south and north, so baroclinity weakens. Here we should explain that in analysis foregoing it seems discrepant that SST increases over western Pacific and the sea of Okhotsk (Fig. 7a) but sea ice in region Ⅰ still increases. But former soviet experts pointed out when it turns colder during autumn and winter, the SST is higher, the vertical temperature gradient is bigger, which prevents heat energy from transmitting deeper, and lead the thin surface heated up in autumn to refrigerating rapidly, and on the contrary, sea ice appears earlier that year in Okhotsk sea[19]. Further more, rupturing floating ice causing by warmer seawater also makes the sea ice acreage augment.

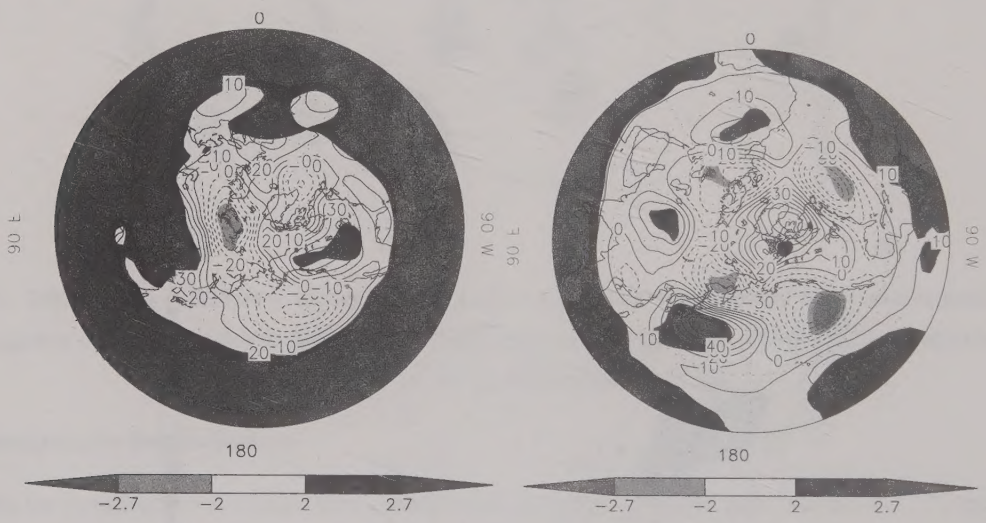

Fig. 6 Differences in 500 hPa height values between the winter *DQ* index is positive and negative in region Ⅰ (a) and Ⅱ (b) with contour interval of 10 gpm. Shaded areas indicate that passing t-test at $\alpha = 0.05$ confidence level.

When sea ice in region Ⅱ increase, there is positive SSTA in equatorial central and eastern Pacific, but negative SSTA in northern Pacific (Fig. 7b), so the mean meridional temperature gradient over southeast of northern Pacific turns larger (Fig. 8b), and from Kuroshio to the Okhotsk sea, diabatic heating arousing by the positive SSTA over northern Kuroshio causes air temperature higher, but local cooling effect in region Ⅱ makes the temperature lower, local mean meridional temperature gradient increases, and baroclinity enhance.

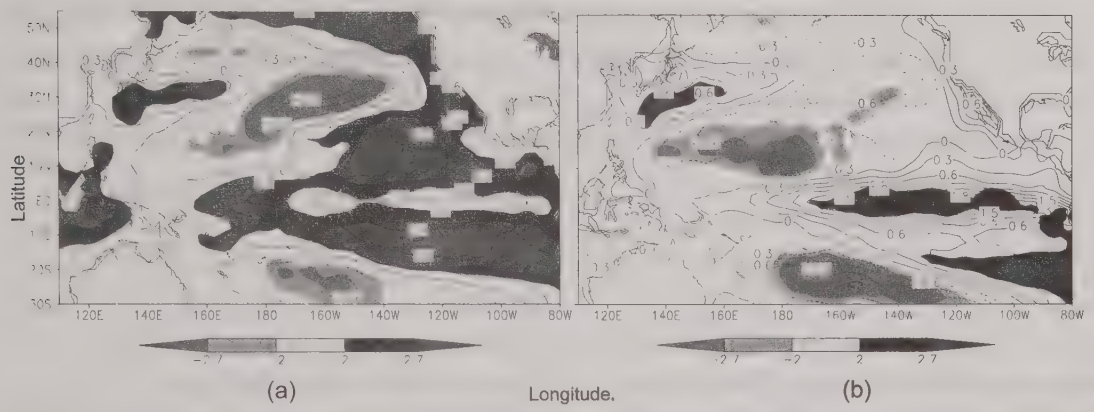

Fig. 7 Differences in Pacific SST between the winter *DQ* index is positive and negative in region Ⅰ (a) and Ⅱ (b) with contour interval of 0.3 °C. Shaded areas indicate that passing t-test at $\alpha = 0.05$ confidence level.

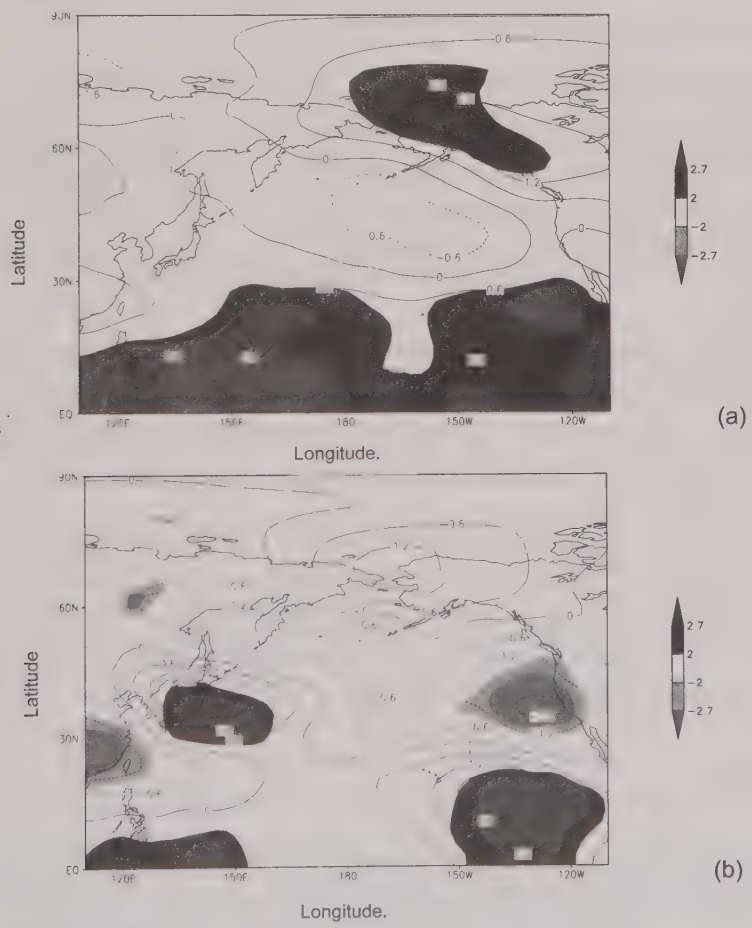

Fig. 8 Differences in 500 hPa temperature between the winter *DQ* index is positive and negative in region Ⅰ (a) and Ⅱ (b) with contour interval of 0.6 °C. Shaded areas indicate that passing t-test at $\alpha = 0.05$ confidence level.

In preceding analysis, we find that through affecting air circulation, influencing intensity and position of the jet, and making local mean meridional temperature gradient in middle and high latitude change by its local cooling function, sea ice over the Okhotsk sea and its vicinage can work on baroclinity and lead the position and the intensity of the northern Pacific storm track to changing. With the action of SSTA, this variation turns more complicated.

3 Conclusion

(a) Through SVD analysis, we find that type SVD1 mainly describes the correlative distributions between anomalous variation of sea ice over the southwest Okhotsk sea and the opposite variations in different parts of the northern Pacific storm track, while its northwest, central and south parts enhance (weaken), its north part weakens (enhances). While type SVD2 primarily reflects the impact of sea ice anomaly over the northeast Okhotsk sea and the gulf of Shelikhow on the intensity and the position in south and north direction of the storm track

(b) The composite analysis shows that anomalous variation of sea ice over the southwest Okhotsk sea can make baroclinity in northwest and southeast of the storm track change, and then influence flex and intensity in the northwest and southeast direction of the storm track. When sea ice over the northeast Okhotsk sea and the gulf of Shelikhow increase, local cooling function makes the jet over speedup, local meridional temperature gradient larger, baroclinity enhance, the storm track partials to northward, and strengthen.

(c) When we discuss the impact of the sea ice anomaly on the storm track, we consider SSTA together, and find that there is some correlativity in SSTA over northern Pacific with sea ice anomaly no matter over the southwest Okhotsk sea or over the northeast Okhotsk sea and the gulf of Shelikhow, and they work together to influence the intensity and the position of the storm track.

Finally, it should be noticed that sea ice is of perplexing state, different kinds, distribution, thickness of sea ice can all influence heat exchange between ocean and atmosphere, we just study the simultaneous impact of the sea ice over a small sea area of Okhotsk and its vicinage in acreage on the northern Pacific storm track during winter, and consider the effect of SSTA together, so individual impact of sea ice on the storm track still need more and further study.

Acknowledgements

This article is supported by the key project of Science and Technology Development Foundation of Regional Meteorological Center of Wuhan (No. QY-Z-200902), subsidized project of Key Laboratory of Meteorological Disaster of Jiangsu Province (KLME050202) and subsidized project of “Qing-lan” for the Young and Middle-aged Academic Pathfinders in Colleges and Universities of Jiangsu province.

References

[1] Hao C J, Xie S M, Li T J. The variation features of the Arctic sea ice [J]. Transactions of oceanology and limnology, 1994, (2): 84 - 91.

[2] Zhao Y C, Shun Z B, Ni D H. The variations of the Arctic and Antarctic sea ice [J]. Journal of Nanjing institude of meteorology, 2000, 23(3): 330 - 337.

[3] Zhao Y C, Shun Z B, Wang H Y. Linear trend and abrupt change of sea ice in Arctic and Antarctic with its relation to atmospheric circulation [J]. Journal of Nanjing institude of meteorology, 2001, 24(1): 119 - 126.

[4] Honda M, Yamazaki K, Nakamura H, et al. Dynamic and thermodynamic characteristics of atmospheric response to anomalous sea-ice extent in the sea of Okhotsk [J]. J Climate, 1999, 12(12): 3 347 - 3 358.

[5] Chang E K, Lee M S, Swanson K L. Storm track dynamic [J]. J Climate,2002,15(6): 2 163 - 2 183.

[6] Zhu W J, Shun Z B. A review on storm track research [J]. Journal of Nanjing institude of meteorology, 1999, 22(1):121 - 127.

[7] Lorenz D J, Hartmann D L. Eddy-zonal flow feedback in the northern hemisphere winter [J]. J Climate, 2003, 16(8): 1 212 - 1 227.

[8] Kimoto M ,J F-F ,Watanabe M, et al. Zonal-eddy coupling and a neutral mode theory for the Arctic Oscillation [J]. Geophys Res Lett, 2001, 28(4): 731 - 740.

[9] Gudrun M, Deser C, Saravanan R. The effects of northen Atlantic SST and sea ice anomalies on the winter circulation in CCM3.Part I: Main features and storm track characteristics of the response [J]. J Climate, 2004, 17(5): 857 - 876.

[10] Zhu W J, Shun Z B. Interannual variability of northern winter Pacific storm track i and its association with 500hPa height and tropical and northern Pacific sea surface temperature [J]. ACTA meteorological sinica, 2000, 58(3): 309 - 320.

[11] Zhang J J. Thesis volume of the long-term weather forecast [M]. Beijing: Ocean Press, 1992. 29 - 35.

[12] Deng X X, Shun Z B. Energy conversionin the vicinity of northern storm track [J]. Journal of Nanjing institude of meteorology, 1995, 18(2): 172 - 178.

[13] Shun Z B, Zhu W J. A case study of energy temporal variation for synoptic disturbance over the northern winter storm track [J]. Journal of Nanjing institude of meteorology, 2000, 23(2): 147 - 155.

[14] Hoskins B J, Valdes P J. On the existence of storm-tracks [J]. Atmos Sci, 1990, 47(15): 1 854 - 1 864.

[15] Shun Z B, Zhu W J. A possible mechanism for the maintenance of the Northern hemisphere wintertime storm track [J]. Journal of Nanjing institude of meteorology, 1998, 21(3): 299 - 306.

[16] Zhu W J, Shun Z B, Peng J Y. Effects of winter Pacific SSTA on the storm track and jet stream [J]. Journal of Nanjing institude of meteorology, 1999, 22(4): 575 - 581.

[17] Zhu W J, Shun Z B, Min J Z, et al. Influence on northern Pacific storm track of equatorial central and eastern Pacific SSTA during winter [J]. Journal of tropical meteorology, 2000, 16(1): 91 - 96.

[18] Zhu W J, Shun Z B. Impacts of Kuroshio SSTA on storm track over northern Pacific in winter [J]. Quaterl journal of applied meteorology, 2000,11(2): 145 - 153.

[19] Qu W Z, Li R D. A view of marine ice researches in U.S.S.R. [J]. Marine forecasts, 1993, 10 (3): 31 - 42.

[20] Pu Y K. Basic of the atmospheric circulation [M]. Beijing: China meteorological press, 1994. 136 - 142.

冬季鄂霍次克海海冰对北太平洋风暴轴年际变化的影响

何冬燕[1]，邓学良[2]，朱伟军[3]

（1. 安徽省气候中心，安徽 合肥 230031；2. 安徽省气象科学研究所 安徽省大气科学与卫星遥感重点实验室，安徽 合肥 230031；3. 南京信息工程大学 江苏省气象灾害重点实验室，江苏 南京 210044）

摘 要：利用北极海冰密集度资料和 NCEP\NCAR 再分析资料，运用统计方法讨论了冬季鄂霍次克海及其邻近海区海冰异常与同期北太平洋风暴轴的联系。结果发现,冬季鄂霍次克海西南部海区海冰面积异常与北太平洋海温异常共同作用对北太平洋风暴轴在西北-东南方向的伸缩及强度的年际变化有重要影响，而在海温异常的共同作用下，鄂霍次克海东北部及舍列霍夫海海区海冰面积异常则主要影响风暴轴的南北位移和强弱。

关键词：风暴轴；海冰；SVD 分析

An Optimal Algorithm for the Retrieval of Chlorophyll, Suspended Sediments and Gelbstoff of Case II Waters in the Pearl River Estuary

YANG Jin-kun[1], CHEN Chu-qun[2]

1. *Oceanographic Data Center, National Marine Data & Information Service, Tianjin* 300171, *China;*

2. *LED,South China Sea Institute of Oceanology, Chinese Academy of Sciences, Guangzhou* 510301, *Guangdong province, China*

Abstract: An optimal algorithm for the retrieval of chlorophyll, suspended sediments and gelbstoff of case II waters in the Pearl River estuary was established with the optical parameters derived from the in-situ data obtained in Jan. 2003 in the same area. And then, the chlorophyll, suspended sediments and gelbstoff of the SeaWiFS pixels on Jan. 29, 2003 corresponding to the in-situ sites of Jan. 25 and 26, 2003 were synchronously retrieved, with average relative errors of 14.9%, 12.1% and 13.6% for chlorophyll, suspended sediments and gelbstoff, respectively. The research results indicated that the optimal retrieval algorithm established here was relatively fit for the retrieval of the chlorophyll, suspended sediments and gelbstoff of case II waters in the Pearl River estuary, and had quite good retrieval accuracy.

Keywords: Case II Waters; Optimal Retrieval; Ocean Color Constituent; Forward Model; Atmospheric Correction; Pearl River Estuary

Introduction

Chlorophyll, suspended sediments and gelbstoff are customarily taken for the Ocean Color Three Constituents, which are the most important factors that infect the optical properties of case II waters in coastal and inland areas [1]. The retrieval of chlorophyll, suspended sediments and gelbstoff of case II waters in coastal and inland waters has been the difficult and import aspect of ocean color remote sensing until now. The key points for the retrieval are algorithm development and atmospheric correction. Because of the various components and complex optical properties of case II waters, it is difficult to develop a universal algorithm for all waters, which results in the algorithms bound to be regional and, or seasonal [2]. On the other hand, the atmospheric correction is also more difficult to carry out in case II waters than in case I waters. The detections of ocean color properties in case I waters are most taken into consideration in developed countries, however, which in case II waters where have crucial relationships with the development of economy and society are paid much attention to in China. Establishing

Received on January 4, 2008

appropriate retrieval algorithm and accomplishing accurate atmospheric correction to ocean color remote sensing data, are crucial to retrieval chlorophyll, suspended sediments and gelbstoff for a given case II waters, which plays a significant role in the aspects of oceanic biology, oceanic ecology, oceanic dynamics, environmental pollution, fishery, and so on.

In this study, a forward model for simulation of remote sensing reflectance was firstly set up with the optical parameters derived from the in-situ data of Jan. 2003 in Pearl River estuary. And then, the atmospheric correction was done to the SeaWiFS (Sea viewing Wide Field-of-view Sensor) data on Jan. 29, 2003 in Pearl River estuary with an improved atmospheric correction method fit for this area, after which the remote sensing reflectance of the SeaWiFS bands 1 - 6 were derived. The last but the most important, an optimal retrieval algorithm that fit for the research area was established, and the chlorophyll, suspended sediments and gelbstoff were synchronously retrieved with the developed algorithm. The analysis of the retrieval precision and error sources and the comparison with the other existing retrieval results were described in the end of this paper.

1 Materials and methods

1.1 Study area and experiment data

In this paper, the Pearl River estuary locating at 21°08' - 22°45'N and 112°50' - 114°20'E where present case II waters [3] was chosen as study area. Filed observations were carried out in 37 sites by China-British cooperation project in Jan. 2003 and Jan. 2004(see Fig. 1 for the Sampling sites). The remote sensing reflectance with bandwidth of 0.38 nm were detected by the SD2000 Spectrometer made in OOI Co. of USA. The absorption coefficients of gelbstoff at 400 nm were derived by the Gelbstoff Optics Analysis Laboratory System. The concentrations of chlorophyll were measured by the acetone extraction and fluorescence analysis [4]. The concentrations of suspended sediments expect for the 2003 S1 site were estimated by gravimetric method [5], and 2003 S1 site had no estimated result. Filed observation and data quality control were both kept to the NASA protocols [6]. The ranges of the in-situ concentrations of chlorophyll, suspended sediments and absorption coefficients of gelbstoff at 400 nm were 0.830 μg/L - 220.142 μg/L, 3.3 mg/L - 126.6 mg/L, and 0.312 05 / m - 1.134 12 / m, respectively. However, the in-situ concentration of chlorophyll at the 2003S7b site where was found red tide showing as 220.142 μg/L which was markedly greater than other sites was abandoned in this study.

1.2 Establishing forward model for the simulation of *Rrs*

Based on the relationships between ocean color three constituents and inherent optical properties, and the relationships between the inherent optical properties and *Rrs* (remote sensing reflectance), a forward model for the simulation of *Rrs* was established with the optical parameters derived from the in-situ data of Jan. 2003 in Pearl River estuary. The relationships between optical properties and *Rrs* would be distinct from variously regional and temporal factors. And different researchers have set up congruent *Rrs* simulation models depending on their corresponding study areas and experiment data. In

this paper, the model for the simulation of hyperspectral *Rrs* founded by Lee et al. [7] was employed, which could be described as follows:

$$R_{rs} = 0.518 r_{rs} / (1 - 1.562 r_{rs}) \tag{1}$$

Where r_{rs} is the subsurface remote sensing reflectance described as $r_{rs} = (0.0949u + 0.0794u)u$. Defining that $u \equiv b_b / (a + b_b)$, where *a* and b_b are the total absorption coefficient and total backscattering coefficient, respectively, which could be described as [8-10]:

$$a = a_w + a_g + a_s + a_c \tag{2}$$

$$b_b = r_w b_w + r_c b_c + r_s b_s \tag{3}$$

Where a_w and b_w are the absorption and backscattering coefficient by pure seawater, respectively, whose values could be inquired in relative literatures [11, 12]. a_c, a_s, a_g and b_c, b_s are the absorption coefficient of chlorophyll, suspended sediments, gelbstoff and the backscattering coefficient of chlorophyll and suspended sediments, respectively. r_w, r_c and r_s are the backscattering ratio of pure seawater, chlorophyll and suspended sediments with value of 0.5, 0.005 and 0.015 [2], respectively. Generally, the scattering coefficient of gelbstoff could be ignored [13].

(a) Absorption Coefficients of Gelbstoff a_g [14]

$$a_g(\lambda) = a_g(400) \exp(-S_g(\lambda - 400)) \tag{4}$$

Where S_g is the gelbstoff absorption slope ranging from 0.011 to 0.021 nm^{-1} [15], which fixes on 0.015 and 0.014 nm^{-1} for case II waters by Lee et al. [16] and Tassan [2], respectively. In this paper, the S_g was determined as 0.014 4 nm^{-1} evaluated from the in-situ data of 8 cruises measured in the Pearl River estuary from July 2002 to Jan. 2004 [17], which was almost equal to the theoretical value of 0.014 nm^{-1} that was recognized internationally. The absorption coefficient at 400 nm of gelbstoff $a_g(400)$ is expressed as *Y* for convenience in the following of this paper.

(b) Absorption Coefficients of Suspended Sedments a_s

$$a_s(\lambda) = a_s^*(440) \cdot a_s^{*'}(\lambda) \cdot S \tag{5}$$

Where *S* is the concentration of suspended sediments. $a_s^*(440)$,whose value was confirmed as 0.004 55, is the specific absorption coefficient at 440 nm of suspended sediments fitting for Pearl River estuary, which was retrieved by the in-situ absorption coefficients and concentrations of suspended sediments measured in Pearl River estuary in Jan. 2003. $a_s^{*'}(\lambda)$ are the normalized specific absorption coefficients at λ band of suspended sediments, whose values could be seen in reference [18].

(c) Absorption Coefficients of Chlorophyll a_c

The values of absorption coefficient of chlorophyll a_c could be affected by various factors, such as alga species, optical conditions, vegetal periods, cell sizes, pigments package effects, and so on [19, 20]. In this paper, the single-parameter expression founded by Lee et al. [21] was employed, which could be

expressed as follows:

$$a_c(\lambda) = [a_0(\lambda) + a_1(\lambda) \ln P] P \quad (6)$$

Where $a_0(\lambda)$ and $a_1(\lambda)$ are constants. *P* is the absorption coefficient at 440 nm of chlorophyll that is described as $P = 0.06C^{0.65}$ by Lee et al. [21], where *C* is the concentrations of chlorophyll. And in this paper, a new expression of *P* fitting for Pearl River estuary was derived by the in-situ absorption coefficients collected in this area by Cao et al. [22], which could be expressed as $P = 0.0681 \cdot C^{0.6058}$.

(d) Scattering Coefficients of Chlorophyll b_c [23]

$$b_c(\lambda) = 0.12 C^x a_c^*(550) / a_c^*(\lambda) \quad (7)$$

Where $a_c^*(\lambda)$ is the specific absorption coefficient of chlorophyll. In this paper, the normalized specific absorption coefficients of chlorophyll $a_c^{*'}(\lambda)$ [18] were employed to take place of $a_c^*(\lambda)$. And the scattering coefficients of chlorophyll b_c could be described as follows:

$$b_c(\lambda) = 0.12 C^x a_c^{*'}(550) / a_c^{*'}(\lambda) \quad (8)$$

Where *x* is the exponent constant determined as 0.63 by Sathyendranath [23] and Tassan [2] and 1 by YANG et al. [24], respectively. In this paper, x would be adjusted to fit for Pearl River estuary.

(e) Scattering Coefficients of Suspended Sediments b_s

There are few research results about b_s till now. In this paper, the expression founded by Tassan[2] was chosen to describe scattering coefficients of suspended sediments b_s :

$$b_s(\lambda) = b_s(550)(\lambda / 550)^{n_s} \cdot S \quad (9)$$

Where $b_s(550)$ and n_s is the scattering coefficients at 550 nm of suspended sediments and scattering spectral ratio fixed as [2] 1 m^2/g and -1, respectively. In this paper, $b_s(550)$ and n_s would also be adjusted to fit for Pearl River estuary.

(f) Determining of *x*, $b_s(550)$ and n_s

x, $b_s(550)$ and n_s were determined by optimal methods in this paper. Firstly, the absorption coefficients of gelbstoff, suspended sediments and chlorophyll at each site were evaluated through (4), (5) and (6) expressions with the in-situ *Y*, *C* and *S*. Secondly, *x*, $b_s(550)$ and n_s were set as unknown constants iteratively circulating in a reasonable initial value, range and iterative step, and then, scattering coefficients of suspended sediments and chlorophyll at each site corresponding to each group of *x*, $b_s(550)$ and n_s were estimated out. Thirdly, with the above evaluated absorption coefficients of gelbstoff, suspended sediments and chlorophyll and estimated scattering coefficients of suspended sediments and chlorophyll at each site, the modeled *Rrs* corresponding to each group of *x*, $b_s(550)$ and n_s were carried out. When the average relative error *RMS* between modeled Rrs noted as R_{rs}^{model} and in-situ Rrs noted as $R_{rs}^{in\text{-}situ}$ came to the minimum value with the range less than 0.1, the *x*, $b_s(550)$ and

n_s here were the required values that fit for the study area. *RMS* could be described as follows:

$$RMS = \sqrt{\frac{\sum_{n=1}^{N} (\ln(R_{rs}^{model}) - \ln(R_{rs}^{in-situ}))^2}{N}} \tag{10}$$

Where *N* ranges from 1 to 301. In this paper, the initial value of *x*, $b_s(550)$ and n_s were set as 0.01, 0.01 and -2.0 and with ranges of (0.01, 1.5), (0.01, 1.5) and (-2.0, 2.0), respectively. As a result, the *x*, $b_s(550)$ and n_s were finally determined as 0.8, 1.4 and -0.5, respectively.

Then, the scattering coefficient of chlorophyll b_c and suspended sediments b_s fitting for Pearl River estuary could be expressed as follows:

$$b_c(\lambda) = 0.12C^{0.8} a_c^{*'}(550) / a_c^{*'}(\lambda) \tag{11}$$

$$b_s(\lambda) = 1.4 \cdot (\lambda / 550)^{-0.5} \cdot S \tag{12}$$

As described above, the forward model for simulation of *Rrs* was established with the expression of (1)-(6) and (12) and (13). The modeled *Rrs* at spectrum of 400 to 700 nm with 1 nm bandwidth were simulated with the in-situ *Y*, *C* and *S* collected at Pearl River estuary in Jan. 2004. Comparing the modeled *Rrs* to the synchronous in-situ *Rrs*, the following results were summarized to two points: (a) There showed a high correlation relationship between the modeled and in-situ *Rrs* at the same site, with the maximum, minimum and average of the correlation square r^2 of 0.988, 0.976 and 0.953, respectively. (b) The maximum, minimum and average of the relative errors of the modeled and in-situ *Rrs* at the same site and same band presented as 37.5%, 0 and 6.5%, respectively. The percent of the modeled Rrs with the relative error less than 10% to the total modeled Rrs came to 86.2%.

Morel et al. [25] firstly established the model for simulation *Rrs*, but with relative low precision. The three-component *Rrs* model founded by Thomas et al. [26] had not take the suspended sediments absorption and chlorophyll scattering into account. Bukata et al. [27,28] had set up a *Rrs* model considered about algous organisms, nor-algous organisms, gelbstoff and minerals, however, the model aimed only at the optical properties at the *Lake Ontario* and referred to the bands set of CZCS. Fischer et al. [29] employed the Radiative Transfer Equation to simulate *Rrs* with the specific absorption and scattering coefficients, but the calculation was extraordinarily complex and the retrieval precision was infected. Comparison with above research results, the forward model for simulation *Rrs* established in this paper had much higher retrieval precision and quite fit for the water properties of Pearl River estuary.

a b

Fig. 1 Sampling sites of Pear River in Jan. 2003(a) and Jan. 2004(b)

1.3 Evaluating *Rrs* of SeaWiFS

The in-situ data were collected on 25th and 26th, Jan. 2003 on which two days the remote sensing data had low quality because of the effect of cloud. Thus, the SeaWiFS data on 29th, Jan. 2003 with good quality were chosen to carry on atmospheric correction. On account of the reasons that the leaving water radiance $L_w(\lambda)$ of the SeaWiFS bands for atmospheric correction of case II waters is nonzero and the signals between atmosphere and aerosol could not be distinguished from each other lightly, and the SeaDAS standard atmospheric correction algorithm regularity has failing results for the case II waters, which shows that the values of the atmospheric corrected $L_w(\lambda)$ are obviously lower and even negative values come. In this paper, the practical algorithm for atmospheric correction of SeaWiFS data of case II waters established by WEI J. [30] and CHEN et al. [31] was employed to complete the atmospheric correction for the chosen SeaWiFS data. Then, the relative accurate $L_w(\lambda)$ were derived, and the normalized leaving water radiance $L_{WN}(\lambda)$ of the atmospheric corrected SeaWiFS pixels corresponding to the in-situ sites on 25th and 26th, Jan. 2003 were evaluated out with the following expression[32]:

$$L_{WN}(\lambda)=\frac{L_W(\lambda)}{t(\lambda)[1-\rho(\theta_s)]\cos\theta_s}(r/\overline{R})^2 \tag{13}$$

Where $L_W(\lambda)$ were the atmospheric corrected leaving water radiance of SeaWiFS pixels corresponding to the in-situ sites. $t(\lambda)$ was the Atmospheric transmittance with value of 0.98. $\rho(\theta_s)$ was the water-air Fresnel reflectivity with value of 0.022. $\overline{R}$ was the mean sun-earth distance. *r* was the sun-earth distance on 29th, Jan. 2003. θ_s was the sun angle of the time of day when the SeaWiFS data was produced. The precise methods of calculating θ_s and $(r/\overline{R})^2$ could be seen in reference [33].

Considering that the R_{rs} could be defined as follows [34]:

$$R_{rs}(\lambda)=L_w(\lambda)/E_d(\lambda,0^+) \tag{14}$$

and the field $L_{WN}(\lambda)$ could be expressed as follows[35]:

$$L_{\mathrm{WN}}(\lambda) = L_{\mathrm{w}}(\lambda) \cdot F_0(\lambda) / E_{\mathrm{d}}(\lambda, 0^+) \tag{15}$$

Where $E_{\mathrm{d}}(\lambda, 0^+)$ was the above water downward irradiance. $F_0(\lambda)$ was the effective exoatmospheric solar irradiance, corrected by astronomical day, whose values were known.

Then, the R_{rs} could be derived with the $L_{WN}(\lambda)$, which could be described as:

$$R_{\mathrm{rs}}(\lambda) = L_{\mathrm{WN}}(\lambda) / F_0(\lambda) \tag{16}$$

1.4 Optimal retrieval of *Y*, *C*, *S*

In this paper, an optimal algorithm for the retrieval of chlorophyll *C*, suspended sediments *S* and gelbstoff *Y* of case Ⅱ waters in the Pearl River estuary was established. The bands 1 - 6 remote sensing reflectance of SeaWiFS pixels corresponding to the in-situ sites were defined as known quantities (the inputted quantities) and the *Y*, *C*, *S* as unknown quantities with initial values, value-ranges and interval values. With each group of *Y*, *C*, *S*, a set of remote sensing reflectance could be simulated with the forward model for simulating R_{rs} established before in this paper, and the simulated remote sensing reflectance would be compared with the inputted remote sensing reflectance of the research SeaWiFS pixels. When the RMS (estimated by expression (10)) between the simulated and inputted remote sensing reflectance reached minimum value in the range of less than 0.1, the *Y*, *C*, *S* here would be the retrieval results.

A five steps program developed under IDL environment was employed to reduce the retrieval time, and the retrieval for each site took 1 min. The initial values, value-ranges and interval values of *Y*, *C*, *S* were set in the first step, and then, in the next four steps, the value-ranges and interval values of *Y*, *C*, *S* were reduced on the base of retrieval results of forward step. The retrieval precisions gradually increased. When the fifth retrieval step was completed, the third value after radix point were essentially invariant and the retrieval precisions arrived at the requirement, and now the retrieval was successfully accomplished.

2 Results and analysis

The chlorophyll *C*, suspended sediments *S* and gelbstoff *Y* of SeaWiFS pixels corresponding to the in-situ sites in the Pearl River estuary were retrieved with the optimal algorithm established in this paper. The retrieval showed that the average relative error were 14.9%, 12.1%, 13.6% and the maximum relative error 22.1%, 17.7%, 21.1% for *C*, *S* and *Y*, respectively. The comparison and relative errors of in-situ and retrieved results could be seen in the Fig. 2. Where in the Fig. 2, a, b, c were the comparison of in-situ and retrieved results for *Y*, *C*, *S*, respectively, and d was the relative error of in-situ and retrieved results at each site for *Y*, *C*, *S*, respectively.

There are not similar reports about the synchronous retrieval for chlorophyll *C*, suspended sediments *S* and gelbstoff *Y* in the Pearl River estuary until now. However, TANG et al. [36, 37] have got the

retrieval result for the chlorophyll, total suspended matter, and gelbstoff concentrations in the Case II waters of Yellow Sea and East China Sea with Statistical Inversion Models and Neural Network Models, which showed that the statistical inversion average relative errors were 36% - 45%, 20% - 30%, 20% and the Neural Network retrieval average relative errors 44.4%, 40.5%, 48.8%, respectively. ZHONG et al. [38] have taken out the average relative errors 32.5%, 24.2%, 8.9% of chlorophyll, total suspended matter, and gelbstoff concentration of Case II waters in Yellow Sea and East China Sea based on artificial Neural Network Models.

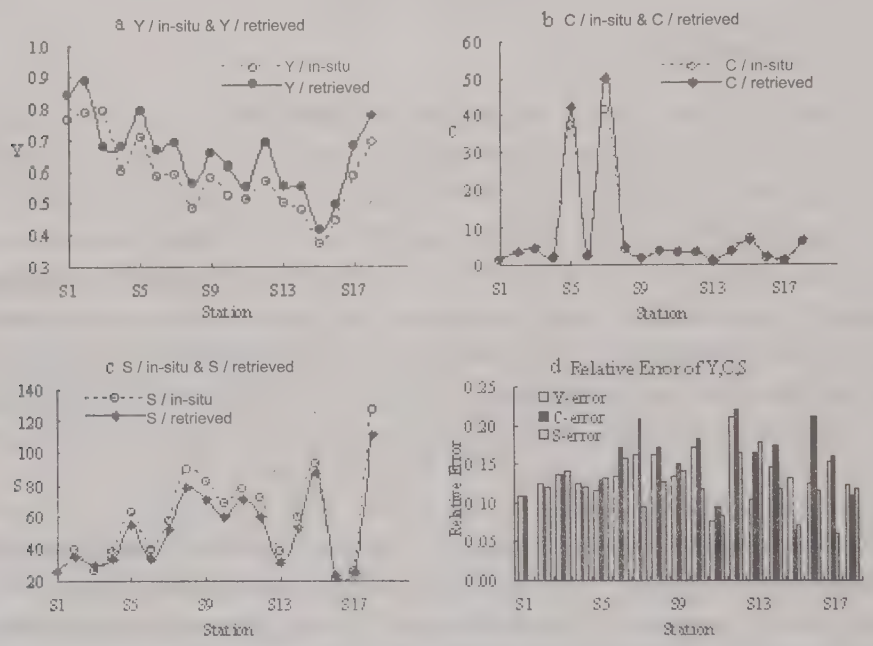

Fig. 2 Comparison and relative errors of in-situ and retrieved three constiuendts

It has better estimated the retrieval precision with the synchronous in-situ data. However, due to the actual reasons mentioned in the 2.3 section of this paper, the retrieval results here had to compare with the in-situ data collected on 25th and 26th, Jan. 2003. At the same time, the suspended sediments and gelbstoff in the Pearl River estuary most come from potamic portage, and the dimensional distributions of the three constituents are most infected by the effect of tide in Jan. when is drouthy and the influent magnitude is relative steady in 3 - 4 days time. Much more, if the in-situ data collected time is not the same as the satellite passed time especially the tide level appearing big difference in the temporal interval, the retrieval precision estimation could be only taken as a reference even employing the synchronous in-situ data to estimate the retrieval precision. Thus, the retrieval errors here may be from the nor-synchronousness, atmospheric correction and some experiential parameters, and so on.

3 Discussion

The model parameters fit for the Case II waters of Pearl River estuary were first fixed on in this

paper, and then an optimal algorithm for the retrieval of chlorophyll, suspended sediments and gelbstoff of case II waters in the same area was established, with which the chlorophyll, suspended sediments and gelbstoff of the SeaWiFS pixels corresponding to the in-situ sites were synchronously retrieved for the first time in China. The optimal algorithm here could avoid the spectrum frequency interference between different constituents and took on better retrieval precision compared with the exiting research results. The retrieval results here indicated that the optimal algorithm established in this paper was relatively fit for the retrieval of the chlorophyll, suspended sediments and gelbstoff of Case II waters in the Pearl River estuary, which could be also used as reference if the algorithms are not valid for other coastal and inland waters. As the test for validation of the optimal algorithm here was limited in this study, there is still a long way to go for the application of the optimal algorithm for operational system. One of the disadvantages of the optimal algorithm is that the calculation is time-consuming. More works on validation of the optimal algorithm with abundant in-situ data should be conducted in order to improve the algorithm.

References

[1] Kirk J T O. Light and photosynthesis in aquatic ecosystems [M]. Cambridge: Cambridge University Press, 1983.

[2] Tassan S. Local algorithms using SeaWiFs data for the retrieval of phytoplankton pigments, suspended sediment, and yellow substance in coastal waters [J]. Applied Optics, 1994, 33(12): 2 369 - 2 378.

[3] CHEN Chu-qun, SHI Ping, Magnus L, et al. Estimation of chlorophyll-a concentration in the Zhujiang River Estuary from SeaWiFS data [J]. Acta Oceanologica Sinica, 2002, 21(1): 27 - 36.

[4] Strickland J D H, Parsons T R. A practical handbook of seawater analysis. Bulletin Fisheries Research Board of Canada, 1972, 167: 207 - 211.

[5] Doxaran D, Cherukuru R C N, Lavender S J. Use of reflectance band ratios to estimate suspended and dissolved matter concentrations in estuarine waters [J]. International Journal of Remote Sensing, 2005, 26(8): 1 763 - 1 769.

[6] Mueller J L, Austin R W. Ocean Optics Protocols for SeaWiFS Validation, Revision 1, SeaWiFS Technical Report Series [M]. 1995. 25: HOOKER S B, FIRESTONE E R and ACKER J G (eds.), NASA Technical Memorandum 104566, Greenbelt, Maryland.

[7] Lee Z P, Carder K L, Mobley C D, et al. Hyperspectral remote sensing for shallow waters. I. A semianalytical model [J]. Applied Optics, 1998, 37(27): 6 329 - 6 338.

[8] Roesler C S, Perry M J, Carder K L. Modeling in suit phytoplankton absorption from total absorption spectra in productive inland marine waters [J]. Limnol Oceanogr, 1989, 34: 1 510 - 1 523.

[9] Carder K L, Hawes S K, Baker K A, et al. Reflectance model for quantifying chlorophyll a in the presence of productivity degradation products [J]. J Geophys Res, 1991, 96: 20 599 - 20 611.

[10] Gordon H R, Smith R C, Zaneveld J R V. Introduction to ocean optics [J]. SPIE: Ocean Optics, 1980, 208: 1 - 43.

[11] Smith R C, Baker K S. Optical properties of the clearest natural waters (200 - 800 nm) [J]. Applied Optics, 1981, 20: 177 - 184.

[12] Pope R M, Fry E S. Absorption spectrum (380 - 700 nm) of pure water. II. Integrating cavity measurements [J]. Applied Optics, 1997, 36(33): 8 710 - 8 723.

[13] CHEN Chu-qun, SHI Ping, PAN Zhi-lin. Simulation of sea water reflectance and its application in retrieval of yellow substance by remote sensing data [J]. Journal of Tropical Oceanography, 2003, 22(5): 34 - 39.

[14] Bricaud A, Morel A, Prieur L. Absorption by dissolved organic matter of the sea (yellow substance) in the UV and visible domains [J]. Limnol Oceanogr, 1981, 26: 43 - 53.

[15] Carder K L, Steward R G, Harvey G R, et al. Marine humic and fulvic acids: Their effects on remote sen sing of ocean chlorophyll [J]. Limnol Oceanogr, 1989, 34: 68 - 81.

[16] Lee Z P, Carder K L, Mobley C, et al. Hyperspectral remote sensing for shallow waters 2, Deriving bottom depths and water properties by optimization [J]. Applied Optics, 1999, 38: 3 831 - 3 843.

[17] CHEN Chu-qun. Research for the gelbstoff and its remote sensing detection in Pearl River estuary [M]. Ph.D.Dissertation (Graduate University of Chinese Academy of Sciences), Guangzhou, China, 2005.

[18] Prieur L, Sathyendranath S. An optical classification of coastal and oceanic waters based on the specific spectral absorption curves of phytoplankton pigments, dissolved organic matter, and other articulate materials [J]. Limnol Oceanogr, 1981, 26: 671 - 689.

[19] Stramski D, Sciandra A, Claustre H. Effect of temperature, nitrogen, and light limitation on the optical properties of the marine diatom Thalassiosira pseudoana [J]. Limnol Oceanogr, 2002, 47: 392 - 403.

[20] Ciotti A M, Lewis M R, Cullen J J. Assessment of the relationships between dominant dell size in natural phytoplankton communities and the spectral shape of the absorption coefficient [J]. Limnol Oceanogr, 2002, 47: 404 - 417.

[21] Lee Z P. Visible-infrared Remote-sensing Model and Application for Ocean Water [M]. Ph.D. Dissertation (University of South Florida, Department of Marine Science, St. Petersburg, Fl.,). 1994. 145pp.

[22] CAO Wen-xi, YANG Yue-zhong, XU Xiao-qiang, et al. Spectral absorption coefficient of suspended sediments and its regional model in Pearl River [J]. Chinese Science Bulletin, 2003, 48(17): 1 876 - 1 882.

[23] Sathyendranath S, Prieur L, Morel A. A three-component model of ocean color and its application to remote sensing of phytoplankton pigments in coastal waters [J]. International Journal of Remote Sensing, 1989, 10: 1 373 - 1 394.

[24] YANG Ding-tian, CAO Wen-xi, YANG Yue-zhong, et al. Optical characteristics of water in the Pearl River mouth [J]. Ecologic Science, 2004, 23(1): 1 - 4.

[25] Morel A, Prieur L. Analysis of variations in ocean color [J]. Limnol Oceanogr, 1977, 22: 709 - 722.

[26] Thomas Y F. Utilisation des données Landsat pour la mise en évidence de la turbidité en zones littorales; limites des méthodes. Publications Scientifiques et Techniques du CNEXO: Actes des Colloques, 1978, 5: 109 - 121.

[27] Bukata R P, Jerome J H, Burton J E, et al. Optical water quality model of Lake Ontario. 1: Determination of the optical cross section of organic and inorganic particulates in Lake Ontario [J]. Applied Optics, 1981, 20: 1 696 - 1 703.

[28] Bukata R P, Burton J E, Jerome J H, et al. Optical water quality model of Lake Ontario. 2: Determination of chlorophyll a and suspended mineral concentrations of natural waters from submersible and low altitude optical sensors [J]. Applied Optics, 1981, 20: 1 704 - 1 714.

[29] Fischer J, Doerffer R, Grass L H. Factoranalysis of multispectral rediances over coaltal and open ocean waters based on radiative transfer calculations [J]. Applied Optics, 1986, 25: 448 - 456.

[30] WEI Jun, CHEN Chun-qun, SHI Ping. A practical algorithm for atmospheric correction of SeaWiFS data [J]. Acta

Oceanologica Sinica, 2002, 24(4): 118 - 125.

[31] CHEN C Q, WEI J, SHI P. Atmospheric correction of SeaWiFs imagery for turbid waters in Southern China coastal areas [J]. SPIE: Ocean Remote Sensing and Applications, 2003, 4892: 80 - 86.

[32] Gordon H R, Brown O B, Evans R H, et al. A Semianalytic Radiance Model of Ocean Color [J]. J Geophys Res, 1988, 93(.D9): 10 909 - 10 924.

[33] WANG Bing-zhong. Calculation of astronomical parameters in energiae solaris [J]. Acta Energiae Solaris Sinica, 1999, 2: 8 - 10.

[34] Carder K L, Steward R G. A remote-sensing reflectance model for red-tide dinoflagellate off West Florida [J]. Limnol Oceanogr, 1985, 30: 286 - 298.

[35] Gordon H R, Clark D K. Clear water radiance for atmospheric correction of coastal zone color scanner imagery [J]. Applied Optics, 1981, 20: 4 175 - 4 180.

[36] TANG Jun-wu, WANG Xiao-mei, SONG Qing-jun, et al. Statistical inversion models for Case Ⅱ waters color elements in the Yellow Sea and East China Sea [J]. Advances in Marine Science, 2004, 22: 1 - 7.

[37] TANG Jun-wu, DING Jing, TIAN Ji-wei, et al. Neural Network models for the retrieval of chlorophyll, total suspended matter, and gelbstoff concentrations of Case Ⅱ waters in Yellow Sea and East China Sea [J]. High Technology Letters, 2005, 03: 83 - 88.

[38] ZHONG Jing-chen, WANG Xiao-yong, CHEN Qing-lian. A retrieval method on the chlorophyll, total suspended matter, and gelbstoff concentration of Case Ⅱ waters in Yellow Sea and East China Sea based on the artificial Neural Network [J]. Ocean Technology, 2005, 04: 118 - 121.

珠江口二类水体水色三要素的优化反演

杨锦坤[1]，陈楚群[2]

（1. 国家海洋信息中心数据中心，天津 300171；

2. 中国科学院南海海洋研究所 LED 实验室，广东 广州 510301）

摘 要：根据 2003 年 1 月份珠江口实测资料获得了适合该海域的相关参数，建立了适用于该海域的二类水体水色三要素优化反演模型，同步优化反演得到了与 2003 年 1 月 25 ~ 26 日实测站点相对应的 2003 年 1 月 29 日的 SeaWiFs 图像像元点的水色三要素，反演与实测水色三要素的平均相对误差分别为：叶绿素 14.9%，悬浮泥沙 12.1%，黄色物质 13.6%。研究结果说明本研究建立的优化反演模型比较适用于珠江口二类水体水色三要素的反演，且具有较高的反演精度。

关键词：二类水体；优化反演；水色三要素；正演模型；大气校正；珠江口

Dissolved Inorganic Arsenic in the Yellow Sea and the East China Sea—Distributions and Seasonal Variations

REN Jing-ling[1], LIU Su-mei [1], ZHANG Jing[2]

1. *Key Laboratory of Marine Chemistry Theory and Technology, Ministry of Education, Ocean University of China*, 238 *Songling Road, Qingdao* 266100, *Shandong province, China;*

2. *State Key Laboratory of Estuarine and Coastal Research, East China Normal University, Shanghai* 200062, *China*

Abstract: The distributions and seasonal variations of total dissolved inorganic arsenic (TDIAs, [TDIAs] = [As^{5+}]+[As^{3+}]) and arsenite (As^{3+}) in the Yellow Sea and East China Sea are presented here based on the observations of 9 cruises carried out in 2000 - 2003. The study area covers a broad range of hydrographic and chemical properties. The emphasis is put on a southeast transect from Changjiang Estuary to the Ryukyu Islands (i.e. PN section) in the East China Sea to discuss the impact of terrestrial input on the marginal seas of China. Arsenic species (TDIAs and arsenite) are determined by selective hydride generation - atomic fluorescence spectrometry (HG-AFS). TDIAs concentrations were high in the coastal area of Changjiang Estuary and decreased slightly towards the shelf region. High concentrations of TDIAs were also existed in the near bottom layer of shelf edge of the East China Sea which indicated another source of arsenic from the incursion of Kuroshio Waters. The seasonal variations of TDIAs in the study area depend on the hydrographic stages of Changjiang and the incursion intensity of Kuroshio Waters. Arsenite showed opposite distributions with TDIAs, with higher concentrations appeared at the surface layer of shelf region, which was positive correlated with the chlorophyll *a*. Biological conversion of arsenate into arsenite was hypothesized for the observed distribution pattern and its seasonal variations. The stoichoimetric ratios of As to P were estimated to be about 2×10^{-3} at PN Section in summer. The concentrations of dissolved arsenic in the Yellow Sea and East China Sea were comparable with other areas in the world.

Keywords: dissolved arsenic, species, Yellow Sea and East China Sea, distributions and seasonal variations

Introduction

Arsenic is of great concern in the terrestrial as well as aquatic environments because of its high toxicity. The behavior of Arsenic is complicated by the existence of different oxidation states (+5, +3, 0, -3) and multiple organic compounds, each of them having its own biogeochemical and geochemical reactivity. Arsenate shows nutrient-like profiles in the ocean, with minor surface depletion and deep water enrichment, which indicates uptake by phytoplankton in the surface and regeneration from degradation of

Received on June 5, 2008

organic detritus in deep water [1-7]. The similarity between arsenate and phosphate in chemical properties is largely responsible for the toxicity of arsenate to phytoplankton.

The distributions of dissolved arsenic have been investigated intensively in the open ocean [1, 6-9] and estuaries [10-18]. There were some arsenic results for the polluted river/estuary/inner bay systems of China [14, 19-23]. However, the study of biogeochemical cycle of dissolved arsenic for the marginal seas of China only remains in the initial stage. This manuscript mainly aims to understand the distributions and seasonal variations of arsenic and its speciation in the Yellow Sea (YS) and East China Sea (ECS). The impact of Changjiang discharge and Kuroshio incursion on the distributions of arsenic in the ECS Shelf was also discussed.

1 Research area and methods

1.1 Sample locations and sampling

The data were obtained on 9 cruises during 2000 and 2003 in the YS and ECS, ranging from lower reaches of the Changjiang to the Ryukyu Islands in the ECS Shelf (Tab. 1 and Fig. 1). Two areas were emphasized during these cruises, one was Changjiang Estuary and its adjacent area and the other one was PN section located from the Changjiang Estuary to the Ryukyu Islands in the ECS Shelf, where the impacts of Changjiang discharge and Kuroshio incursion on the biogeochemical behavior of arsenic in the marginal seas of China were studied.

The water samples were collected with the help of associated research programs with different logistical requirements, which resulted in several observational techniques. Discrete water samples were taken by Niskin bottles from various depths chosen from CTD reading. Profiles of temperature and salinity were made by Sea-Bird 911^{plus} CTD Rosette during the cruises of R/V "Dong Fang Hong 2" in the YS and ECS and by CTD and YSI in other cruises near the Changjiang Estuary. After collection, samples were filtered through pre-cleaned 0.45 μm pore-size cellulose filters in a class-100 clean bench. The filtrates were then frozen at - 20 °C during the cruises of R/V "Dong Fang Hong 2" and were acidified to pH=2 by HCl in other cruises. Blanks were carefully prepared by filtering at sea a known volume of Milli-Q water with methods identical to the bulk sample sets.

1.2 Determination methods

The determination methods for arsenite and total dissolved inorganic arsenic (TDIAs) using a Hydride Generation-Atomic Fluorescence Spectrometry (HG-AFS) were described detailedly elsewhere [25]. In brief, Arsenite concentration was determined by generating hydride at pH 5.3 - 5.5 buffered by sodium citrate-HC1 solution, at which arsenate was not allowed to be reduced to arsenite. TDIAs concentration was determined by hydride generation at acidity of 1 mol/L HC1, after reducing arsenate into arsenite by thiourea-Vc mixed solution. The concentration of arsenate was calculated from the difference of TDIAs and As (III) assuming arsenic species other than arsenate and arsenite are

negligible in quantity. The detection limit for TDIAs and As (III) by HG-AFS are 0.11 nM and 0.02 nM, respectively. The precision of HG-AFS measurement for TDIAs was 6.8% at the concentration of 1.6 nM, while 3.1% at the concentration of 1.3 nM for As (III). The robust of the methods were tested by the inter-calibration experiments with the international standard reference sample NASS-4 and North Sea samples [25].

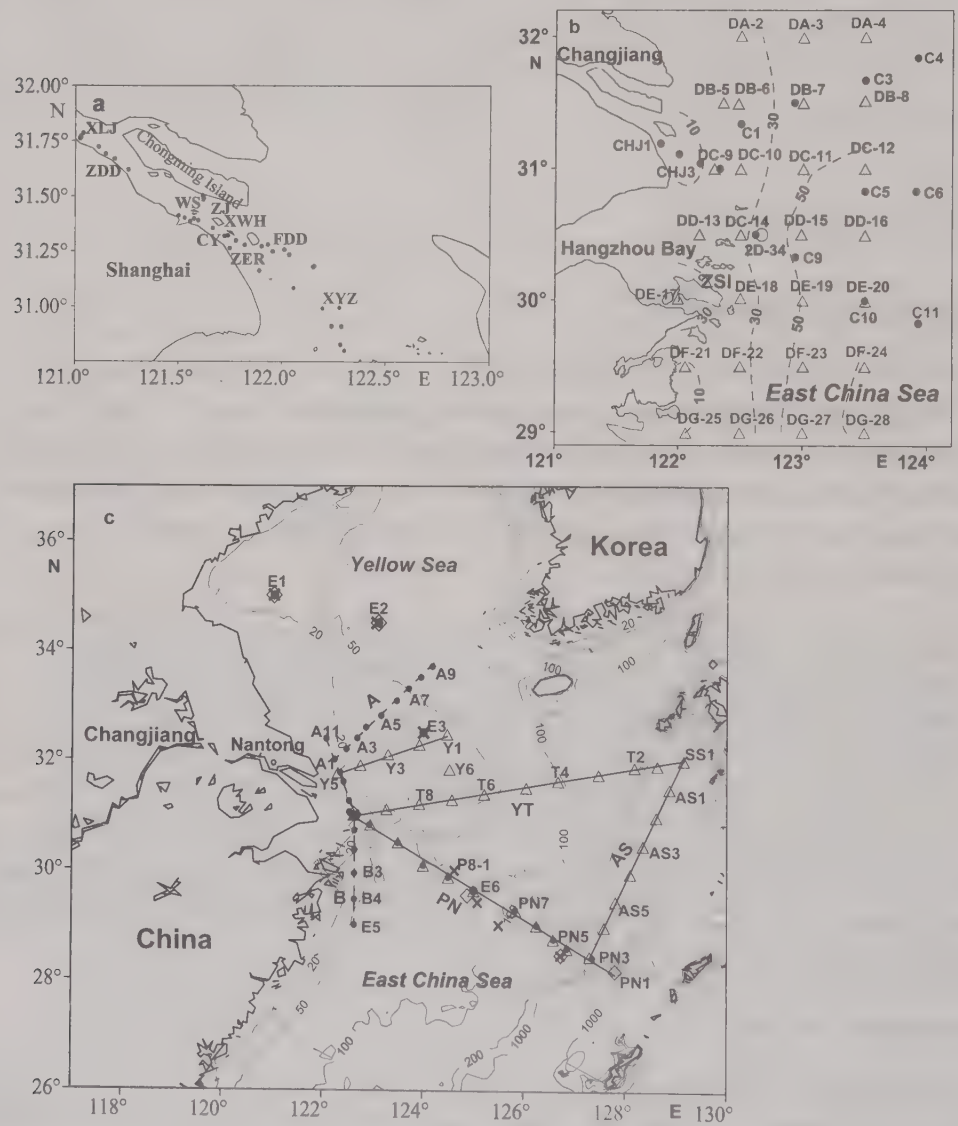

Fig. 1 Sampling locations of Changjiang Estuary

(a) adjacent area of the East China Sea (b) "Λ": cruises of August and November of 2002, and February and May of 2003 in the adjacent area of ECS; "•": represent the coastal stations of cruise of September 2003 in the YS and ECS) and Yellow Sea and East China Sea (c) "▲": September 2000; "■": May 2001; "◆": September 2002; "Δ": September 2003).

Tab. 1 Cruises information carried out in the YS and ECS Shelf

Time	Studied area	Research Vessel	TDIAs / nmol/L^{-1}	As^{3+} / nmol/L^{-1}	As^{3+}/ TDIAs	Reference
2000.10.21 - 2000.11.5	YS and ECS	R/V "Dong Fang Hong 2"	YS: 10.6 - 21.6 (16.7)	0.12 - 1.45 (0.50)	0.01 - 0.09 (0.03)	24
			ECS: 9.6 - 20.5 (14.9)	0.02 - 2.44 (0.31)	0.00 - 0.19 (0.02)	
2001.5.1 - 2001.5.10	YS and ECS	R/V "Dong Fang Hong 2"	YS: 16.8 - 20.5 (18.8)	0.12 - 2.36 (0.76)	0.01 - 0.12 (0.04)	24
			ECS: 12.9 - 23.2 (17.7)	0.01 - 9.52 (2.85)	0.00 - 0.87 (0.22)	
2002.9.11 - 2002.9.26	YS and ECS	R/V "Dong Fang Hong 2"	A: 8.1 - 21.1 (15.9)	0.06 - 1.84 (0.65)	0.00 - 0.23 (0.05)	25
			B: 8.2 - 18.1 (15.0)	0.20 - 2.21 (0.88)	0.01 - 0.27 (0.07)	
			PN: 9.0 - 21.1 (16.0)	0.05 - 1.38 (0.42)	0.00 - 0.15 (0.03)	
2003.9.4 - 2003.9.25	YS and ECS	R/V "Dong Fang Hong 2"	YT: 9.0 - 21.1 (13.8)	0.01 - 6.37 (1.31)	0.00 - 0.50 (0.10)	25
			AS: 10.8 - 19.4 (15.3)	BDL -2.91 (0.40)	0.00 - 0.16 (0.03)	
			PN: 10 - 24.3 (13.4)	BDL -6.37 (1.41)	0.00 - 0.50 (0.12)	
2001.7.17 - 2001.7.26	Changjiang Estuary	Small fishing boat	12.8 - 27.3 (20.7)	0.05 - 6.8 (1.79)	0.00 - 0.56 (0.14)	25
2002.8.26 - 2002.9.5	Changjiang Estuary	R/V "Jinxing 2"	9.27 - 23.90 (15.84)			26
2002.11.5 - 2002.11.10	Changjiang Estuary	R/V "Kexue 1"	18.27 - 30.47 (22.35)			26
2003.2.25 - 2003.3.19	Changjiang Estuary	R/V "Zhehaihuanjian"	13.74 - 24.66 (19.85)			26
2003.5.1 - 2003.5.11	Changjiang Estuary	R/V "Haijian 47"	3.78 - 29.66 (17.27)			26

BDL: Below detection limit

2 Results

2.1 Arsenic in the Changjiang Estuary and the coastal waters of ECS

In July 2001, field observation in the Changjiang Estuary started from the lower reaches of the river and crossed the coastal region to sites with salinity of ca. 30 psu were carried out using small fishing boat. There were another 5 cruises carried out in the coastal waters of ECS in different seasons from August 2002 to September 2003 (Tab.1, Fig.1). In the Changjiang Estuary, TDIAs concentrations in riverine end-member ranged from 15.0 to 27.8 nM. There was no obvious evidence that dissolved arsenic either increase or decrease with the distance from estuary within the data resolution [25]. In the adjacent coastal area, TDIAs showed considerable scatter in concentrations vs. salinity relationships in different cruises, with little differences between surface and near-bottom (Fig.2). During the mixing course between fresh and seawater end-members, TDIAs showed relative stable concentrations which indicated the conservative mixing profiles in the coastal area adjacent the Changjiang Estuary.

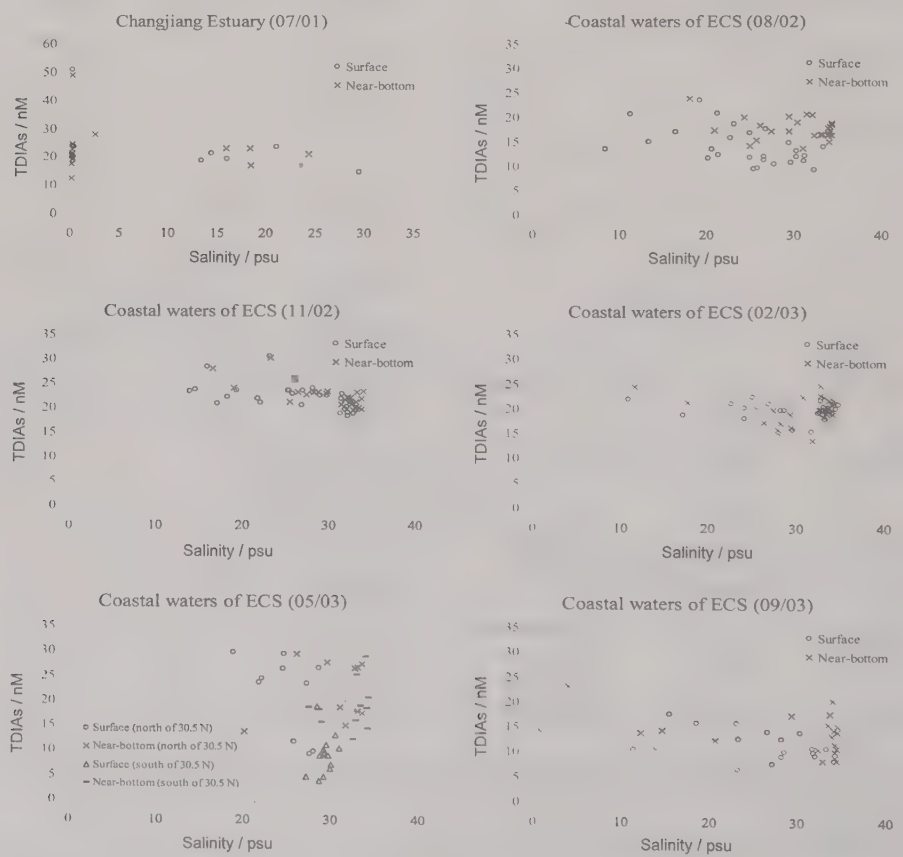
Changjiang Estuary (07/01)
Coastal waters of ECS (08/02)
Coastal waters of ECS (11/02)
Coastal waters of ECS (02/03)
Coastal waters of ECS (05/03)
Coastal waters of ECS (09/03)
TDIAs / nM
Salinity / psu
Surface
Near-bottom
Surface (north of 30.5 N)
Near-bottom (north of 30.5 N)
Surface (south of 30.5 N)
Near-bottom (south of 30.5 N)

Fig. 2 TDIAs plotted against salinity in the Changjiang Estuary and adjacent area of ECS in different seasons For comparison, samples form surface and near-bottom (i.e. 1 - 2 m above sea-bed) are selected to show the nutrient-salinity relationships.

The average concentrations of TDIAs in the coastal area of ECS in Jul. 2001, Aug. 2002, Nov. 2002, Feb. 2003, May 2003 and Sep. 2003 were 20.4 ± 3.0 nmol/L, 15.8 ± 3.4 nmol/L, 22.2 ± 2.5 nmol/L, 19.4 ± 3.8 nmol/L, 17.8 ± 5.0 nmol/Land 12.6 ± 3.4 nmol/L, respectively. The concentrations of TDIAs between wet and dry seasons in the coastal area of ECS were 16.9 ± 4.4 nmol/L and 20.8 ± 3.2 nmol/L, respectively. The Changjiang discharge is one of major sources of TDIAs in the coastal area of ECS. The average water discharge of Changjiang in July-August 2002 was 52.2×10^3 m^3 /s, while it was (15-20) $\times 10^3$ m^3 /s in January-February 2003 [27]. The variation of Changjiang discharge between dry and wet season caused the seasonal variations of arsenic in the coastal area of ECS.

2.2 Arsenic in the YS and ECS

The arsenic data obtained by "R/V Dong Fang Hong 2" in the YS and ECS from October 2000 to September 2003 covered various water masses, including the nutrient-rich and low salinity Changjiang Diluted Waters along the Chinese coasts (CDW); the warm and nutrient-poor Kuroshio Surface Water along the shelf edge (KSW); the cold and nutrient-rich Kuroshio Subsurface Water (KSSW) and Kuroshio Intermediate Water (KIW); the warm and nutrient-poor Taiwan Current Warm Water northward from the Taiwan Strait (TCWW) and Shelf Mixed Water (SMW) [25, 27]. In summer, the effluents from the Changjiang (CDW) dispersed eastward at the surface as far as 126°E based on the variations of Changjiang discharges, outlined by salinity=30 psu. The mid-shelf region was influenced by the TCWW and SMW with salinity of 30 - 34 psu. The shelf break region was influenced by KSW, KSSW and KIW [27]. The incursion of Kuroshio upward along the shelf can be tracked to water depths of ca. 30 m within a distance of 250 km from the Changjiang mouth [28].

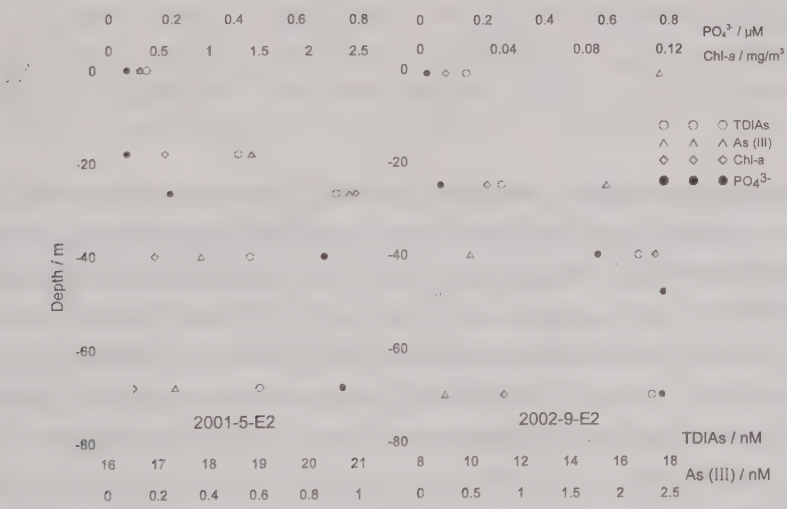

Fig. 3 Vertical profiles of TDIAs, arsenite, Chl-*a* and phosphate at Station E2 in May 2001 and September 2002 in the central Yellow Sea

The ranges and average concentrations for arsenic species at different sections of the cruises carried out in the YS and ECS are summarized in Tab. 1. The vertical distributions of TDIAs showed well mixed profiles in the coastal area, e.g. the Station E1 in the YS and stations in the adjacent area of the

ECS. However, TDIAs showed nutrient-like profile like phosphate in the central YS (e.g. Station E2, Fig. 3), the mid-shelf and shelf break of the ECS where the water column were stratified, with mild surface depletion and deep-water enrichment. As for the horizontal distributions of TDIAs, the concentrations of TDIAs were high in the coastal areas of the YS and ECS where influenced by the land-source input from the adjacent rivers, while depleted in the surface of the broad shelf. High concentrations of TDIAs also can be seen at the mid and near-bottom layer of shelf edge stations (e.g. Stations P3 and P1 in different cruises), with extremely low concentrations of SPM. This high concentration center of TDIAs in the shelf edge corresponded with the water mass with high salinity which indicated the incursion of Kuroshio across the shelf.

Arsenite, the reductive specie of arsenic, showed different profiles with TDIAs. The vertical distributions of arsenite were high in the surface layer and decreased with the water depth, which were opposite with the profiles of redox active species. The concentrations of arsenite were high in the surface of central YS, upwelling region at south of the Changjiang Estuary and mid-shelf of the ECS, where had relative high productivity.

3 Discussion

3.1 Arsenic regimes in the YS and ECS

The concentrations of TDIAs in the Changjiang Estuary and adjacent area are comparable to the less disturbed estuarine system (Gironde Estuary) [29] and lower than the estuaries polluted by the anthropogenic activities such as Pearl River Estuary in South China [30], Rhone Estuary in France [11] and Scheldt Estuary in Netherlands [17]. Concentrations of arsenite and TDIAs in the YS and ECS are comparable to those reported in open oceans, including the Atlantic [6-8], the Pacific[1] and the North Sea [9] (Tab. 1, 2).

TDIAs concentrations are higher in the shallow coastal waters of the YS and ECS (e.g. Changjiang Estuary), where receive large amounts of riverine input. The Changjiang brings huge amounts of fresh water and sediment into the YS and ECS, which is thought to be one of the major sources of TDIAs in the western boundary. TDIAs concentrations also show high level at the near bottom layer of Station P3, correspond to high salinity and extremely low SPM concentrations (< 2 mg/L), which indicate the incursion of Kuroshio onto the shelf. This high concentration center at the near bottom of shelf break region indicates that the Kuroshio waters are the other source of TDIAs in the eastern boundary. The freshwater discharges from Changjiang mainly affected the coastal area and the surface of the shelf region, whereas the incursion of Kuroshio Waters can be tracked in depth of 50 - 100 m of shelf region [28, 32]. The distributions of TDIAs in the shelf area are mediated by the circulation of different water masses. The annual variations of TDIAs in the study area are controlled by the relative importance of different water mass inputs. The nutrients like vertical profiles of TDIAs indicate that the cycle of arsenic in the shelf region is regulated by biological activities and will be discussed later.

Tab. 2 Comparison of arsenic species concentrations with other estuaries and open ocean

Region	period	TDIAs	As (III)	Reference
Huanghe Estuary	5/1985,1986	3.8 - 28.8		14
	8/1985,1986	17.8 - 38.8		
Pearl River Estuary	11/1992	26.7 - 36.0 (30.7)		30
Rhône Estuary, France	3/1984, 7/1987	14.7 - 50.7 (29.4)		11
	7/1988			
Scheldt Estuary, Belgium	7/1997 - 7/2001	25.6 - 53.4		17
Gironde Estuary, France	5/1994, 1995	14.2 - 20.2 (17.5)	0.2 - 3.9 (1.8)	29
North Atlantic (surface)	8 - 9/1993	(15.7 ± 1.3)	(0.45 ± 0.21)	6
Western Atlantic	5 - 6/1996	8.0 - 23.0 (16.3 ± 2.1)	0.1 - 2.0	7
Eastern Atlantic	3 - 5/1990	(12.9 ± 1.8) surface		8
		(20.9 ± 0.5) bottom		
North Pacific		(24.2 ± 0.4)	0 - 4.0	1
Central North Sea	8/1988	9.73 - 14.80 (11.39)		9
	9/1989	11.20 - 17.07 (13.1)		
Bohai	8/2003	(20 ± 4)		31

Arsenite show different horizontal and vertical distribution profiles with TDIAs in the YS and ECS, which indicate the different sources with TDIAs. The arsenite concentrations show high levels at the surface water of the central YS, Changjiang Estuary and mid-shelf of the ECS, correspond to the high levels of Chloraphyall-*a*. The distribution profiles of arsenite are similar with the results from other oceans [6, 7]. The ratios of As (III)/TDIAs follow the profiles of arsenite in the YS and ECS.

3.2 Seasonal and interannual variations of arsenic in the YS and ECS

In the Changjiang Estuary where mainly affected by the Changjiang Diluted Water, the average concentrations of TDIAs in the autumn and winter are higher than the spring and summer (Tab. 1, Fig. 2), which is corresponded to the seasonal variations of Changjiang runoff. The concentrations of TDIAs in the Changjiang River were monitored at Nantong (i.e. 180 km inland from the river mouth) every 3 months from July 1996 to September 2003, which showed minor high concentrations at the dry seasons (unpublished data). The average concentration of TDIAs in the cruise of July 2001 was exceptive higher than the other results from summer cruises, which was caused by the different sampling area with more riverine stations.

The seasonal and interannual variations of TDIAs concentrations in the YS and ECS were complicated compared to the coastal area, which were mediated by different water masses. PN Section (a southeast transect from the Changjiang Estuary to the Ryukyu Islands) was selected to discuss the seasonal and interannual variations of TDIAs in the East China Sea. Fig. 4 shows the T-S diagrams in the PN section at different seasons between 2000 and 2003, which clearly shows the impact of Changjiang

diluted water and the incursion of Kuroshio Waters. The water masses in the shelf region appear complicate mixing pattern according to different sampling time. Temperature at the shelf region in the spring was lower than the autumn, with relative similar salinity ranges between spring and autumn. If we compared the salinity ranges between three cruises carried out in autumn, the impact of the Changjiang in autumn 2002 was significant stronger than the other two years. Fig. 5 shows the variations of TDIAs and arsenite concentrations at the PN section between different seasons and years. The seasonal and interannual variations of TDIAs at the PN section were not statistically different, and with similar distribution patterns. However, the distributions of arsenite at the PN section show significant seasonal and interannual variations, with high concentrations appeared in spring 2001 and summer 2002. Based on the vertical distributions of arsenite at the PN section, the concentrations of arsenite were high in the euphotic layer of the mid shelf region [24, 25]. This distribution pattern indicated that arsenite may come from the local production rather than the inputs from Changjiang freshwater and/or Kuroshio incursion, and also shed light on the mediation of phytoplankton.

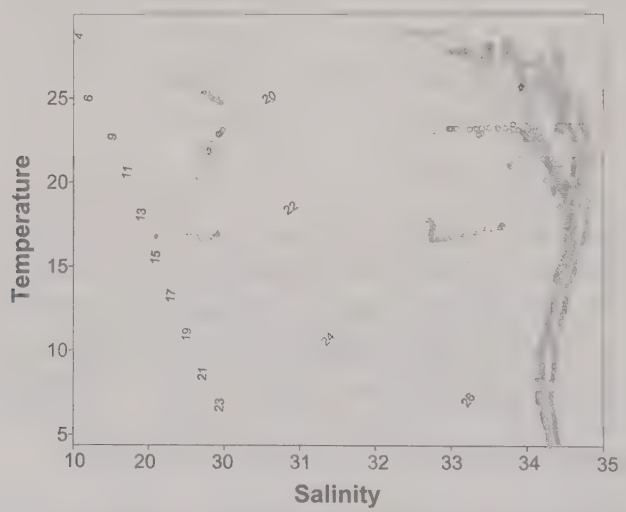

Fig. 4 Temperature-salinity plots for stations in the PN section

("□": October 2000; "□": May 2001; "□": September 2002; "■": September 2003)

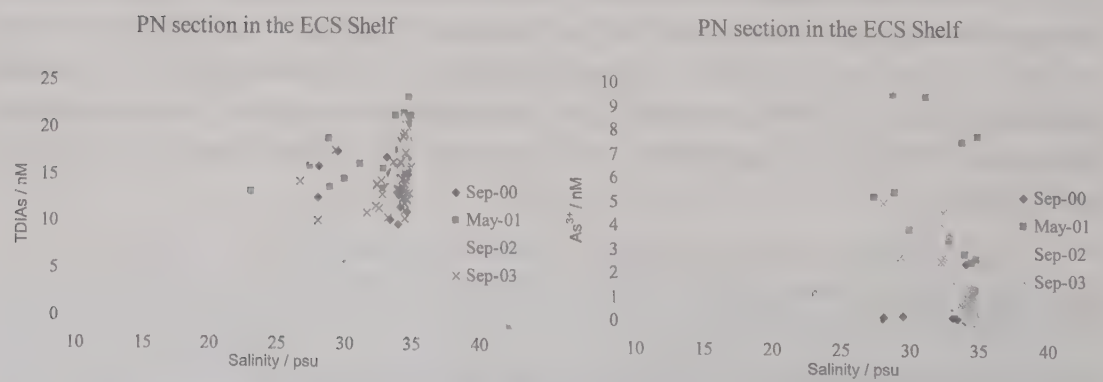

Fig. 5 Plots of TDIAs and arsenite as function of salinity in the PN section of the ECS Shelf

3.3 Biogeochemical cycling of arsenic in the YS and ECS

The vertical profiles of TDIAs were similar with phosphate in the YS and ECS shelf, with varying correlation coefficient (r) ranged from 0.11 to 0.99 in the PN Section and of 0.98 at Station E2 in the central YS (Fig. 3) [25], in agreement with previous studies in the North and South Atlantic [8]. Arsenite showed opposite vertical profile with arenate, with higher concentration in the euphotic layer following the variations of Chl-*a* which indicated the biological mediation of arsenic (Fig. 3) [25]. The concentrations of arsenite showed positive relationship with Chl-*a* in the PN section of the ECS in May 2001 and September 2003 when phytoplankton biomass were relatively high (Fig. 6a), which identified the biological source of arsenite in the surface water. This biological mediation of arsenate was also proved by the variations of TDIAs concentrations in the cruise of May 2003 in the adjacent area of Changjiang Estuary (Fig. 2). The observations were carried out in two separated periods by the interruption of epidemic SARS, algae bloom was erupted between that two periods. The concentrations of TDIAs after the algae bloom were significantly lower than before (Fig. 2).

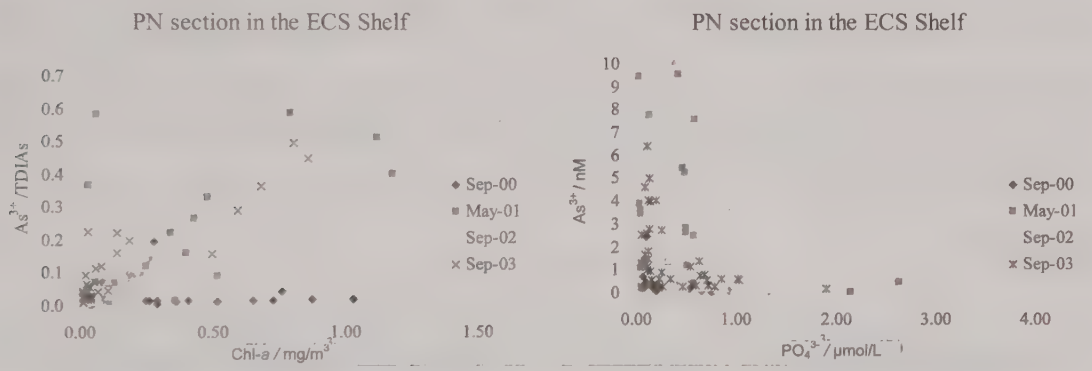

Fig. 6 Plots of arsenite as functions of Chl-*a* (a) and phosphate (b) in the PN section of the ECS Shelf.

Since the structure similarity of arsenate and phosphate, the depletion of arsenate and production of arsenite in the surface water is significant when phosphate level drops below ca. 0.05 μmol/L according to the results in the open oceans [7]. Fig. 6b shows the relationships between arsenite and phosphate concentrations in the PN section of the ECS shelf, arsenite concentrations increased dramatically when phosphate concentrations dropped below 0.5 μmol/L. The average stoichoimetric ratios of As to P in the biological assimilation were estimated to be about 2×10^{-3} at PN section of the ECS shelf in summer [25], which is consistent with the results from the North and South Atlantic Ocean (2.5×10^{-3}) [8] and the western Atlantic Ocean ($(2.6 \pm 0.4) \times10^{-3}$) [7].

4 Conclusion

Understanding the distributions of dissolved arsenate and arsenite in the Yellow Sea and East China

Sea provide opportunity to recognize the hydrological conditions and biological/chemical reactions that take place in this region. High levels of dissolved arsenate have been observed near the Changjiang Estuary and at the near bottom layer of the shelf edge of ECS, which indicate two major sources of arsenate comes from Changjiang diluted water and the intrusion of Kuroshio Subsurface water in the study area. The seasonal variation of TDIAs in the study area is controlled by the variations of Changjiang discharge and the incursion of Kuroshio Waters in the shelf region. Arsenite concentrations are relative higher in the euphotic layer of shelf region correspond to the higher phytoplankton activity. The seasonal variations of As^{3+} / TDIAs ratio follow the variations of arsenite. The predominant specie of arsenic was arsenate in the Yellow Sea and East China Sea. Concentrations of TDIAs in the YS and ECS are comparable to the other coastal areas and open oceans, but lower than the bays and estuaries where are polluted by anthropogenic activities.

Acknowledgements

This study was funded by National Science Foundation of China (No. 40606028) and National Basic Research Programs of China (No. 2006CB400601and 2001CB409703). The authors sincerely thank the captains and crew of R/V "Dong Fang Hong 2", "Jinxing 2", "Kexue 1", "Zhehaihuanjian", "Haijian 47", and all the members in the marine biogeochemistry laboratory of Ocean University of China for sampling and laboratory works. Drs. H. Wei, B. Q. Huang and Ms. R. X. Lv are acknowledged for providing us with hydrographic and Chl-*a* data. The anonymous referees are acknowledged for their critical comments which improve the quality of original manuscript greatly.

References

[1] Andreae M O. Arsenic speciation in seawater and interstitial waters: the influence of biological–chemical interactions on the chemistry of a trace element [J]. Limnology and Oceanography, 1979, 24: 440 - 452.

[2] Middelburg J J, Hoede D, van der Sloot H A, et al. Arsenic, antimony and vanadium in the North Atlantic Ocean [J]. Geochimica et Cosmochimica Acta 1988, 52: 2871 - 2878.

[3] Santosa S J, Wada S, Tanaka S. Distribution and cycle of arsenic compounds in the ocean [J]. Applied Organometallic Chemistry, 1994, 8: 273 - 283.

[4] Santosa S J, Mokudai H, Takahashi M, et al. The distribution of arsenic compounds in the ocean: biological activity in the surface zone and removal processes in the deep zone [J]. Applied Organometallic Chemistry, 1996, 10: 697 - 705.

[5] Santosa S J, Wada S, Mokudai H, et al. The contrasting behavior of arsenic and germanium species in seawater [J]. Applied Organometallic Chemistry, 1997, 11: 403 - 414.

[6] Cutter G A, Cutter L S. Metalloids in the high latitude north Atlantic Ocean: Sources and internal cycling [J]. Marine Chemistry, 1998, 61: 25 - 36.

[7] Cutter G A, Cutter L S, Featherstone A M, et al. Antimony and arsenic biogeochemistry in the western Atlantic Ocean [J]. Deep-Sea Research II, 2001, 48: 2 895 - 2 915.

[8] Cutter G A, Cutter L S. Behavior of dissolved antimony, arsenic and selenium in the Atlantic Ocean [J]. Marine Chemistry, 1995, 49: 295 - 306.

[9] Millward G E, Kitts H J, Comber S D W, et al. Methylated Arsenic in the Southern North Sea [J]. Estuarine, Coastal and Shelf Science, 1996, 43: 1 - 18.

[10] Froelich P N, Kaul L W, Byrd J T, et al. Arsenic, barium, geranium, tin, dimethylsulfide and nutrient biogeochemistry in Charlotte Harbor, a phosphors-enriched estuary [J]. Estuarine, Coastal and Shelf Science, 1985, 20: 239 - 264.

[11] Seyler P, Martin J M. Distribution of arsenite and total dissolved arsenic in major French estuaries: dependence on biogeochemical processes and anthropogenic inputs [J]. Marine Chemistry, 1990, 29: 277 - 294.

[12] Kitts H J, Millward G E, Morris A W, et al. Arsenic biogeochemistry in the Humber Estuary, UK [J]. Estuarine, Coastal and Shelf Science, 1994, 39: 157 - 172.

[13] Elbaz-Poulichet F, Garnier J M, Guan D, M et al. The conservative behavior of trace metals (Cd, Cu, Ni and Pb) and As in the surface plume of stratified estuaries: example of the Rhone River [J]. Estuarine, Coastal and Shelf Science, 1996, 42: 289 - 310.

[14] Zhang J. Geochemistry of arsenic in the Huanghe (Yellow River) and its delta region – A review of available data [J]. Aquatic Geochemistry, 1996, 1: 241 - 275.

[15] Millward G E. Kitts H J, Ebdon L, et al. Arsenic in the Thames Plume, UK [J]. Marine Environmental Research, 1997, 44, 51 - 67.

[16] Michel P, Chiffoleau J F, Averty B, et al. High resolution profiles for arsenic in the Seine Estuary seasonal variations and net fluxes to the English Channel [J]. Continental Shelf Research, 1999, 19: 2 041 - 2 061.

[17] Gieter M D, Elskens M, Baeyens W. Fluxes and major transport route of Arsenic in the Scheldt estuary [J]. Marine Chemistry, 2005, 95: 15 - 30.

[18] Yao Q Z, Zhang J, Qin X G, et al. The behavior of selenium and arsenic in the Zhujiang (Pearl River) Estuary, South China Sea [J]. Estuarine, Coastal and Shelf Science, 2006, 67: 170 - 180.

[19] Li Q S. Shen W R, Ma X N. Research of arsenic in the Bohai Bay. Journal of Shandong College of Oceanology, 1984, 14: 27 - 39.

[20] Li J, Chen S J, Yang S H, et al. Distribution and speciation of arsenic in the seawater of the Huanghe River estuary and adjacent areas [J]. Journal of Ocean University of Qingdao, 1989, 19(4): 87 - 96.

[21] Li J, Zhen G P, Yang Y P, et al. Variation characteristics of dissolved inorganic arsenic from surface seawater in Xiamen Harbor during the typhoon 'Bilis' [J]. Journal of Oceanography in Taiwan Strait, 2002, 21: 404 - 410.

[22] Meng W, Liu Z T, Fan W. Study on Pollutant Characters of Main Estuary of Bohai Bay [J]. Research of Environmental Sciences, 2004, 17(6): 66 - 69.

[23] Xiao H B, Zhao X D, Shi Z L. A preliminary study on the reduction of arsenate in Jiaozhou Bay [J]. Journal of Ocean University of Qingdao, 1995, 25: 338 - 342.

[24] Ren J L, Li D D, Zhang J, et al. Species and distribution of dissolved inorganic arsenic in the Yellow Sea and East China Sea [J]. Marine Environmental Science, 2007, 26(3): 211 - 216.

[25] Ren J L, Zhang J, Li D D, et al. Behavior of dissolved inorganic arsenic in the Yellow Sea and East China Sea [J]. Deep-Sea Research I, 2008, in press.

[26] Cheng Y, Ren J L, Li D D, et al. Distribution of dissolved inorganic arsenic and its seasonal variations in the

coastal area of the East China Sea [J]. Journal of Ocean University of China, 2006, 5(3): 243 - 250.

[27] Zhang J, Liu S M, Ren J L, et al. Nutrient gradients from the eutrophic Changjiang (Yangtze River) Estuary to oligotrophic Kuroshio Waters and re-evaluation of budgets for the East China Sea Shelf [J]. Progress in Oceanography, 2007, 74: 449 - 478.

[28] Ren J L, Zhang J, Li J B, et al. Dissolved aluminum in the Yellow Sea and East China Sea – Al as a tracer of Changjiang (Yangtze River) discharge and Kuroshio incursion [J]. Estuarine, Coastal and Shelf Science, 2006, 68: 165 - 174.

[29] Michel P, Boutier B, Herbland A, et al. Behaviour of arsenic on the continental shelf off the Gironde estuary: role of phytoplankton in vertical fluxes during spring bloom conditions [J]. Oceanologia Acta, 1997, 21: 325 - 333.

[30] Zhang Y Y, Zheng Q H, He Y Q, et al. An experimental study on the self purification of COD Mn, oil and As in the mixing area of saltwater and freshwater in the Zhujiang River Estuary [J]. Tropical Oceanology, 1995, 14: 67 - 74.

[31] Wang C Y, Wang X L. Spatial distribution of dissolved Pb, Hg, Cd, Cu and As in the Bohai Sea [J]. Journal of Environmental Sciences, 2007, 19: 1 061 - 1 066.

[32] Wu Y, Zhang J, Li D J, et al. Isotope variability of particulate organic matter at the PN section in the East China Sea [J]. Biogeochemistry, 2003, 65: 31 - 49.

黄、东海溶解态无机砷的分布及其季节变化

任景玲[1] 刘素美[1] 张 经[2]

（1. 中国海洋大学 海洋化学理论与工程技术教育部重点实验室，山东 青岛 266100；
2. 华东师范大学 河口海岸国家重点实验室，上海 200062）

摘 要：本文综合2000 ～ 2003年期间9个航次的研究结果，讨论了总溶解态无机砷、TDIAs，[TDIAs] = $[As^{5+}]+[As^{3+}]$）和亚砷酸盐（As^{3+}）在黄、东海的分布和季节性变化。调查海区覆盖了黄、东海不同水文和化学性质的区域，研究中点放在江河入海口、向东与流来群岛沿岛的PN断面以讨论陆源输运的物质对中国陆架边缘海的影响。利用氢化物发生原子荧光光谱法（HG - AFS）分析砷的不同形态，TDIAs，As^{3+}）。TDIAs受河流陆源输送的影响在近岸区域含量较高，并随着离岸距离的增加含量逐渐下降，在东海陆架坡折带的近底层水中也存在TDIAs的高值中心，此区域具有低温、高盐、低悬浮颗粒物含量的特征，显示出入侵陆架的黑潮水是陆架区TDIAs另一个主要的源。TDIAs的季节性变化趋势受到长江冲淡水水量及黑潮入侵陆架强度的季节及年际变化共同影响。研究区域中As^{3+}的分布特征与TDIAs相反，其含量、分布及季节性变化受到浮游植物活动的影响，表现出与叶绿素含量存在正相关关系。夏季东海陆架PN断面中As / P的化学计量比值约为2×10^{-3}。黄、东海溶解态砷的含量与同纬度其它海区相近，表明其未受到明显人为活动的影响。

关键词：溶解态砷；形态；黄东海；分布及季节变化

Regulatory Analysis of IPP Isomerase Gene in *Haematococcus pluvialis*

GAO Zheng-quan[1], MENG Chun-xiao[1], YE Nai-hao[2]

1. *School of Life Sciences, Shandong University of Technology, Zibo* 255049, *Shandong province, China;*
2. *Yellow Sea Fishery Research Institute, CFAS, Qingdao* 266071, *Shandong province, China*

Abstract: The unicellular green alga *Haematococcus pluvialis* uniquely accumulates carotenoids in the cytoplasm and in late developmental stages turns deep-red in color because of accumulation of astaxanthin in the cytosol. The enzyme, isopentenyl pyrophosphate (IPP) isomerase, plays a key role in astaxanthin biosynthesis of *H. pluvialis*. In this paper, two separate 5'-flanking regions (1.8 kb and 2.5 kb) of IPP isomerase gene was cloned through walking upstream firstly. Results of sequence analysis showed that two separate 5'-flanking regions of IPP isomerase gene might have similar putative *cis*-acting elements such as ABA (abscisic acid)-responsive element (ABRE), drought-responsive element (DRE/C-repeat), light-responsive element (G-box, GAG-motif, I-box and ATC-motif), heat-shock element (HSE), wound-responsive element (WUN-motif), SA (salicylic acid)-responsive element (TCA-element), auxin-responsive element (TGA-element), MeJA (methyl jasmonate)-responsive element (TGACG-element), enhancer-like element involved in anoxic specific inducibility (GC-motif) and MYB binding sites (MBS and MRE), except for typical TATA box or CCAAT box, which exhibit diversiform transcriptional patterns of IPP isomerase gene in astaxanthin biosynthesis of *Haematococcus pluvialis*.

Keywords: astaxanthin; *cis*-acting elements; 5'-flanking region; *Haematococcus pluvialis*; IPP isomerase gene

Introduction

The ketocaronoid astaxanthin (3, 3'-dihydroxy-beta, beta-carotene-4, 4'-dione) is produced by a number of microorganisms including the green alga *Haematococcus pluvialis* and the heterobasidiomycetous yeast *Phaffia rhodozyma* [1]. Astaxanthin is responsible for imparting the pinkish color to the flesh of many marine animals such as salmonids and crustaceans, and to the feathers of some birds, i.e. flamingoes. Animals cannot synthesize astaxanthin but must acquire it from their diets. Astaxanthin has been shown to be an extremely efficient antioxidant that provides protection against oxygen free radicals [2, 3], acts as an anti-cancer agent [4] and stimulates the immune system [5]. The unicellular fresh-water green alga *Haematococcus pluvialis* reveals the highest astaxanthin accumulation (up to 4% by dry weight) when exposed to unfavorable growth conditions, seems to be the most suitable

Received on April 27, 2007

microbial source for commercial production of natural astaxanthin [6-8].

The enzyme isopentenyl pyrophosphate (IPP) isomerase catalyzes the revisible isomerization of IPP to produce dimethylallyl pyrophosphate, the initial substrate leading to the biosynthesis of carotenoids and many other long-chain isoprenoids. The differential expression of two IPP isomerases after exposure to high illumination and two highly similar cDNAs encoding IPP isomerase, ipiHp1 and ipiHp2, were identified in *H. pluvialis* [9], which implied the possible existence of two separate 5'-UTRs. However, there is little information about regulatory 5'-regions of IPP isomerase gene in astaxanthin biosynthesis of *H. pluvialis*. This research reported the cloning of two separate 5'-flanking regions (1.8 kb and 2.5 kb) of IPP isomerase gene in *H. pluvialis* through walking upstream. Moreover, difference in transcriptional patterns of two 5'-flanking regions were discussed by sequence analysis.

1 Materials and methods

Haematococcus pluvialis (strain 712) were grown in a liquid medium [10] under a light density of 25 μmol photon m^{-2} /s (12h: 12h) at 25 °C.

A Universal GenomeWalker (Clontech, California, USA) kit was used to isolate 5'-flanking regions of IPP isomerase gene. According to manufacturer's instructions, total genomic DNA was digested with four kinds of restriction endonucleases (*Dra* Ⅰ, *Eco*RⅤ, *Pvu* Ⅱ, *Stu* Ⅰ) respectively, then ligated with a GenomeWalker adaptor before used as each template for nested PCR. The adaptor primer AP1 (5'-GTAATACGACTCACTATAGGGC-3') provided by this kit and a gene-specific primer GSP1 (5'-GTGAGGCCTCTGAGCAACGAACGAAGCA-3') designed based on the data from GenBank No. AB019034 were used in the primary PCR amplification. Moreover, the other nested adaptor primer AP2 (5'-ACTATAGGGCACGCGTGGT-3') and a nested gene-specific primer GSP2 (5'-CGGACTGCCGCCGGGCCAGGTTCCAAGT-3') designed based on the same data as above were used in the secondary PCR amplification. The PCR product was cloned into TA vectors and sequenced by custom service of CA Sarray Co., Ltd. (Shanghai, China). Moreover, software (CLUSTAL 1.8) [11] and Internet tool (http://oberon.fvms.ugent.be:8080/PlantCARE/) [12] were used to perform sequence analysis including prediction of putative *cis*-acting elements.

2 Results and discussion

Through walking upstream, two different fragments (No. AY786410 and AY786411) were shown to be part of the 5'-flanking regions of IPP isomerase gene (Fig. 1). Computer analysis using *PlantCARE* for potential regulatory elements revealed that both might have similar putative *cis*-acting elements such as ABA (abscisic acid)-responsive element (ABRE), drought-responsive element (DRE/C-repeat), light-responsive element (G-box, GAG-motif, I-box and ATC-motif), heat-shock element (HSE), wound-responsive element (WUN-motif), SA (salicylic acid)-responsive element (TCA-element), auxin-responsive element (TGA-element), MeJA (methyl jasmonate)-responsive element

(TGACG-element), enhancer-like element involved in anoxic specific inducibility (GC-motif) and MYB binding sites (MBS and MRE), except for typical TATA box or CCAAT box, as described in our previous works about cloning of 5′-flanking regions of beta-carotene ketolase gene and carotenoid hydroxylase gene in *H. pluvialis* [13-15], which suggested that lack of typical TATA box or CCAAT box in 5′-flanking regions of major genes involved in astaxanthin biosynthesis in *H. pluvialis* be common.

Fig. 1 Alignment of two separate 5′-flanking regions (1.8 kb and 2.5 kb) of IPP Isomerase Gene in *H. pluvialis* using CLUSTAL 1.8.

(The information of start codon ATG is derived from the data on Genbank No.AB019034.)

Many drought- and cold-inducible genes contain both DRE/C-repeat and ABRE motifs in their promoters. The DRE/C-repeat was shown to have a role in the cold-inducible gene *cor15a* from *Arabidopsis* [16] and ABRE is a major *cis*-acting element in ABA-responsive expression of the *Arabidopsis* gene *RD29B* [17]. Moreover, ERE [18], HSE [19], WUN-motif [20], GC-motif [21], MBS [22] and TCA-element [23] have also been reported to be involved in stress-inductive gene expression. Nevertheless, the 1.8 kb 5′-region had its specific regulatory elements such as ethylene-responsive element (ERE), and the 2.5 kb 5′-region had its specific regulatory elements such as auxin-responsive element (AuxRR-core) and gibberellin-responsive element (P-box). Therefore, we conclude that there might be two separate 5′-flanking regions with similar regulatory patterns to regulate transcription of IPP isomerase gene in astaxanthin biosynthesis of *H. pluvialis*.

Although IPP isomerase catalyzes the interconversion of IPP a DMAPP, the equilibrium is in favor of DMAPP production, and suggestions have been made that this isomerization reaction is a crucial rate-limiting step for carotenoids biosynthesis [24 25]. IPP isomerase activity was stimulated by high light intensity in differentiation chloroplasts of maize etioplasts [24], unlike in differentiation cytoplasm of the green alga *Haematococcus*. Sun et al. [9] have reported the differential expression of two IPP isomerases and identified two cDNAs encoding IPP isomerase gene with two polypeptides of 34 and 32.5 kDa. They suggested that the 32.5 kDa form was involved with the carotenoid accumulation in the cytoplasm, since this polypeptide was preferentially up-regulated by high light preceding the carotenoid increase. We conclude that these two cDNAs (No. AF082326 and No. AF082869) encoding IPP isomerase gene, having two separate 5'-UTRs, showed the possible existence of multiple IPP isomerase genes in *H. pluvialis*. Consistent with our previous studies was the existence of multiple carotenoid ketolase genes in *H. pluvialis* [14].

Although our study is elementary, the prediction of putative *cis*-elements in two separate 5'-flanking regions of IPP isomerase gene provides the basis for deep study on its transcriptional regulation.

Acknowledgements

The research were supported by the National Natural Science Foundation in China (NO. 30671126; 40706050 and 40706048); National Key Technology R&D Program (No. 11200602); The Special Foundation of State-level and Public Interest Research Institute (No. 2060402/2); Natural Science Foundation in Shandong University of Technology (No. 4040306017) and Start-up Foundation for Ph.D in Shandong University of Technology (No. 4041-405017 and 4041-405016).

References

[1] Andrewes A G, Phaff H J, Storr M P. Carotenoids of *Phaffia rhodozyma*, a red-pigmented fermenting yeast [J]. Phytochemistry, 1976, 15:1 003 - 1 005.

[2] Palozza P, Krinsky N I. Astaxanthin and canthaxanthin are potent antioxidants in membrane model [J]. Arch Biochem Biophys, 1992, 297: 291 - 295.

[3] Miki W. Biological functions and activities of animal carotenoids [J]. Pure Appl Chem, 1991, 63: 141 - 146.

[4] Tanaka T, Morishita Y, Suzui M, et al. Chemoprevention of mouse urinary bladder carcinogenesis by the naturally occurring carotenoid astaxanthin [J]. Carcinogenesis, 1994, 15: 15 - 19.

[5] Jyonouchi H, Sun S I, Gross M. Effect of carotenoid on *in vitro* immunoglobulin production by human peripheral blood mononuclear cells: astaxanthin, a carotenoid without vitamin A activity, enhances *in vitro* immunoglobulin production in response to a T-dependent stimulant and antigen [J]. Nutr Cancer, 1995, 23: 171 - 183.

[6] Kobayashi M, Kakizono T, Nagai S. Enhanced carotenoid biosynthesis by oxidative stress in acetate-induced cyst cells of a green unicellular alga, *Haematococcus pluvialis* [J]. Appl Environ Microbiol, 1993, 59: 867 - 873.

[7] Boussiba S, Wang B, Yuan P P, et al. Changes in pigments profile in the green alga *Haematococcus pluvialis*

exposed to environmental stresses [J]. Biotechnol Lett, 1999, 21: 601 - 604.

[8] Boussiba S. Carotenogenesis in the green alga *Haematococcus pluvialis*: cellular physiology and stress response [J]. Physiol Plant, 2000, 108: 111 - 117.

[9] Sun Z, Francis X. Cunningham J. et al. Differential expression of two isopentenyl pyrophosphate isomerases and enhanced carotenoid accumulation in a unicellular chlorophyte [J]. Proc Natl Acad Sci USA, 1998, 95: 11 482 - 11 488.

[10] Boussiba S, Vonshak A. Astaxanthin accumulation in the green alga *Haematococcus pluvialis* [J]. Plant and Cell Physiol, 1991, 32: 1 077 - 1 082.

[11] Thompson J D, Higgins D G, Gibson T J. Improving the sensitivity of progressive multiple sequence alignment through sequence weighting, position-specific gap penalties and weight matrix choice [J]. Nucleic Acids Res, 1994, 22: 4 673 - 4 680.

[12] Lescot M, Dehais P, Thijs G, et al. PlantCARE: a database of plant cis-acting regulatory elements and a portal to tools for in silico analysis of promoter sequences [J]. Nucleic Acids Res, 2002, 30: 325 - 327.

[13] Meng C X, Teng C Y, Jiang P, et al. Cloning and characterization of beta-carotene ketolase gene promoter in *Haematococcus pluvialis* [J]. Acta Biochim Biophys Sin, 2005, 37: 270 - 275.

[14] Meng C X, Liang C W, Jiang P, et al. There are two 5'-flanking regions of *bkt* encoding beta-carotene ketolase in the *Haematococcus pluvialis* [J]. Phycologia, 2006, 45: 218 - 224.

[15] Meng C X, Wei W, Su Z, et al. Characterization of carotenoid hydroxylase gene promoter in *Haematococcus pluvialis* [J]. Indian J Biochem Biophys, 2006, 43: 284 - 288.

[16] Barke S S, Wilhelm K S, Thomashow M F. The 5'-region of *Arabidopsis thaliana cor15a* has *cis*-acting elements that confer cold-, drought- and ABA-regulated gene expression [J]. Plant Mol Biol, 1994, 24: 701 - 709.

[17] Uno Y, Furihata T, Abe H, et al. *Arabidopsis* basic leucine zipper transcription factors involved in an abscisic acid-dependent signal transduction pathway under drought and high-salinity conditions [J]. Proc Natl Acad Sci USA, 2000, 97: 11 632 - 11 637.

[18] Ohem-Takagi M, Shinshi H. Ethylene-inducible DNA binding proteins that interact with an ethylene- responsive element [J]. Plant Cell, 1995, 7: 173 - 182.

[19] Newton E M, Knauf U, Green M, et al. The regulatory domain of human heat shock factor 1 is sufficient to sense heat stress [J]. Mol Cell Biol, 1996, 16: 839 - 846.

[20] Ni M, Cui D, Gelvin S B. Sequence-specific interactions of wound-inducible nuclear factors with mannopine synthase 2' promoter wound-responsive elements. Plant Mol Biol, 1996, 30: 77 - 96.

[21] Manjunath S, Saches M M. Molecular characterization and promoter analysis of the maize cytosolic glyceraldehyde 3-phosphate dehydrogenase gene family and its expression during anoxia [J]. Plant Mol Biol, 1997, 33: 97 - 112.

[22] Sugimoto K, Takeda S, Hirochik A H. MYB-related transcription factor NtMYB2 induced by wounding and elicitors is a regulator of the tobacco retrotransposin *Ttol* and defense-related genes [J]. Plant Cell, 2000, 12: 2 511 - 2 528.

[23] Goldsbrough A P, Albrecht H, Stratford R. Salicylic acid-inducible binding of a tobacco nuclear protein to a 10bp sequence which is highly conserved amongst stress-inducible genes [J]. Plant J, 1993, 3: 563 - 571.

[24] Albrecht M, Sandmann G. Light-stimulated carotenoid biosynthesis during transformation of maize etioplasts is

regulated by increased activity of isopentenyl pyrophosphate isomerase [J]. Plant Physiol, 1994, 105: 529 - 534.

[25] Ramos-Valdivia A C, van der Heijden R, Verpoorte R. Isopentenyl diphosphate isomerase: a core enzyme in isoprenoid biosynthesis [R]. A review of its biochemistry and function. Nat Products Rep, 14: 591 - 603. 1997.

雨生红球藻中 IPP 异构酶基因表达调控机制的初步研究

高政权[1]，孟春晓[1]，叶乃好[2]

（1. 山东理工大学 生命科学学院，山东 淄博 255049； 2. 中国水产科学院 黄海水产研究所，山东 青岛 266071）

摘 要：单细胞淡水绿藻 — 雨生红球藻能够在一定条件积累一种次生类胡萝卜素 — 虾青素，因而在生长后期藻体变为深红色。其中，IPP 异构酶在雨生红球藻中的虾青素合成过程中发挥了重要作用。在本研究中，我们首次通过基因组上游步移克隆到了雨生红球藻中 IPP 异构酶基因的两个不同 5′ 上游侧翼序列，大小分别是 1.8 kb 和 2.5 kb。利用生物信息学方法分别对这两个不同 5′ 上游侧翼序列进行了序列分析，结果发现，二者具有某些相同的顺式作用元件，如可能的脱落酸反应元件（ABRE）、干燥或低温反应元件（DRE/C-repeat）、几种光反应元件（G-box, GAG-motif, I-box and ATC-motif）、热激反应元件（HSE）、机械伤害反应元件（WUN-motif）、水杨酸反应元件（TCA-element）、生长素反应元件（TGA-element）、茉莉酸甲酯反应元件（TGACG-element）、缺氧特异反应中的增强子类似元件（GC-motif）和反式作用因子 MYB 蛋白的结合位点（MBS and MRE），但是二者并不具有典型的 TATA 框和 CCAAT 框。上述研究预示了雨生红球藻虾青素合成中 IPP 异构酶基因转录调控方式的多样化。

关键词：虾青素；顺式作用元件；5′上游侧翼学列；雨生红球藻；IPP 异构酶基因

Distribution of Biogenic Silica Content in Surface Sediments from the Southern South China Sea and Its Environmental Dignificance

ZHANG Lan-lan[1,2], CHEN Mu-hong[1], XIANG Rong[1], LU Jun[1], ZHANG Li-li[1,2]

1. Key Laboratory of Marginal Sea Geology, South China Sea Institute of Oceanology, CAS, Guangzhou 510301, *Guangdong province, China;*

2. The Graduate School of the Chinese Academy of Sciences, Beijing 100039, *China*

Abstract: Biogenic silica content was determined in 25 surface sediment samples from the southern South China Sea to study its distribution and its modern oceanic environmental significance, which may provide further scientific evidence for paleoceanography explaination. This study showed that biogenic silica content in surface sediments and its water depth have evidently positive correlation, and the correlation coefficient was up to 0.782. Biogenic silica content was very low in continental shelf shallows and could not reflect the productivity of siliceous micropaleontology in surface waters, which may be affected by sedimentary types and terrigenous matter dilution. Distribution of biogenic silica content in surface sediments from deep water areas showed that it could not only reflect the paleoproductivity of siliceous micropaleontology in surface waters, but also indicate the strong or feeble upwelling. Thus, it was further confirmed that using biogenic silica content in sediments to trace upwelling and its change was effective and reliable. The analyzed result showed that radiolaria and poriferous specula have more contribution for biogenic opal, comparing with diatom in surface sediments from the northern studied area, probably owing to the diatom dissolved easily away and eaten by other organisms with little effort. In the upwelling areas, radiolarian, diatom and poriferous specula all approximately showed high abundance, which was consistent with high biogenic silica content.

Keywords: southern SCS; surface sediments; biogenic silica; upwelling

The South China Sea (SCS) with a unique geographical location and the monsoon-ocean circulation, has become the hot spot for the research of paleoceanology and paleoclimate. Biogenic silica is also called as biogenic opal or opal. Diatom and radiolarian with the siliceous shell are the main components. The biogenic silica content in the sediments has become an important indicator to reflect the primary productivity and paleo-upwelling development activity [1, 2]. In the SCS, study about biological silicon began to develop only in recent years [3 - 8], mainly using the biogenic silica in the core samples to reflect the paleoproductivity distribution from several millions of years, and is lacking in the biogenic silica research of modern surface sediment. This job aims to study the distribution pattern of biogenic silica in the 25 surface sediments sampling in the Multidisciplinary Oceanographic Investigation of the Nansha Sea Area cruises,

Received on January 4, 2008

and to explore the relationship between the distribution of biogenic silica and modern ocean environment in order to provide a reference for the future to reflect the paleoproductivity level using the biogenic silica from the regional sea sediments. At the same time, this paper also discussed the relationship between the biogenic silica content and the siliceous organism abundance of radiolarian, diatom and poriferous specula.

1 Material and methods

The analyzed samples in this paper were collected at 25 surface stations in the southern SCS during the Multidisciplinary Oceanographic Investigation in the Nansha Sea Area during May - June 2002 and 2004 by RV "*Experiment III*" of the South China Sea Institute of Oceanology, Chinese Academy of Sciences (Surface sediment samples were taken from the uppermost 0 cm - 2 cm sediment to ensure that the samples for the formation of modern deposition) (Fig. 1). The span of longtitude and latitude of sampling stations is for 5°18 ´ - 12°02 ´ N, 108°29 ´ - 116°24 ´ E, and sampling water depth ranges from 107 m to 2 900 m. The sediment samples were collected by grab or box corer. Tab. 1 shows the specific locations and water depths of sampling stations in two cruises.

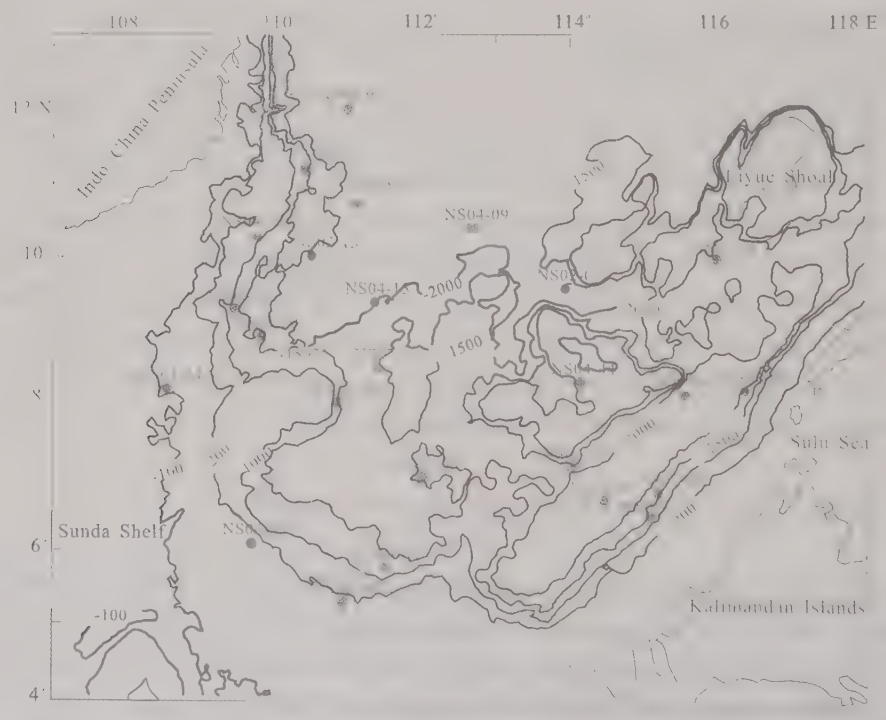

Fig. 1 Locations of 25 surface sediment samples in the southern South China Sea

The biogenic silicon content was determined by a simple method for the rapid determination of biogenic opal [9], namely silicon-molybdenum blue colorimetry. Its basic principle is to remove the organic matter and carbonate from the samples with hydrogen peroxide and hydrochloric acid, then to extract the

biogenic silica from the sediment sample with an alkaline solution of 2 M Na_2CO_3, and then react with ammonium molybdate solution formatting silicon-molybdenum yellow, and react with ascorbic acid solution formatting silicon-molybdenum blue, followed by spectrophotometer measured by the absorbance of color and calculated opal content with absorbance numeral through this regression equation.

2 Results and discussion

2.1 Depth distribution of biogenic silica in the sediments

The water depth span of 25 surface sediment samples collected in the research sea area is large, ranging from the shallow waters of the continental shelf to deep-water areas. Their corresponding biogenic silicon content ranged from 0.33% to 9.00% (Tab. 1). Jia et al. (2000)[4] determined the biogenic silica content in core samples at station 17 962 with water depth of 1 968 m from the southern SCS and reported that the biogenic silica content in the surface sediments was about 3.38%, which is in accordance with the determination numeral of 3.94% at station NS02-33 with the same position. Fig. 2 shows the relationship between the biogenic silica content in modern sediments from the southern SCS and its water depth.

Tab. 1 Locations, depths, biogenic silica contents, radiolarian abundance and poriferous spicule abundance of 25 surface sediment samples in the southern SCS

Station	Longitude / E	Latitude / N	Depth / m	Biogenic silica content / %	Radiolarian abundance / $\times10^4$ ind/g	Poriferous specula abundance / $\times10^3$ ind/g
NS02-01	110.98	12.02	2 898	9.00	2.76	13.08
NS02-07	113.96	9.58	2 260	8.40	13.53	23.20
NS02-12	111.10	10.72	2 460	5.28	7.99	1.40
NS02-13	110.48	10.02	2 300	3.77	2.92	2.08
NS02-16	111.39	8.49	1 572	3.97	4.90	17.60
NS02-20	109.81	8.92	1 716	4.22	6.18	3.10
NS02-21	109.42	9.29	1 316	4.21	2.53	4.18
NS02-30	110.90	5.30	136	1.37	0.03	0.02
NS02-33	112.01	7.01	2 040	3.94	2.46	1.37
NS02-40	115.22	6.80	1 514	5.26	3.45	2.04
NS02-42	114.04	7.16	1 700	5.18	4.58	3.60
NS02-50	116.40	8.20	1 741	6.83	2.79	5.32
NS02-54	116.02	9.99	1 751	6.56	2.27	8.72
NS04-09	112.69	10.40	2 350	8.39	2.75	2.60
NS04-12	110.39	11.21	1 562	4.99	3.33	0.33
NS04-13	109.73	10.26	940	3.62	2.50	0.92
NS04-15	111.35	9.39	1 750	5.72	3.02	1.46
NS04-18	110.84	8.01	1 894	4.81	2.65	3.03
NS04-24	108.49	8.20	107	0.33	0.03	0.05
NS04-29	109.67	6.08	153	1.86	0.06	0.12
NS04-31	111.51	5.79	1 297	3.39	1.65	0.32
NS04-39	115.11	6.49	1 367	5.28	8.35	3.72
NS04-41	114.49	6.70	2 900	6.56	3.73	6.80
NS04-44	114.17	8.31	1 652	5.86	2.65	10.05
NS04-47	115.60	8.13	2 865	5.27	12.83	15.07

From Fig. 2 we can see that there is some correlation between the biogenic silica content in the surface sediments from the southern South China Sea and the water depth: in the shallow waters of the continental shelf with less than 200 m water depth, biogenic silica content in the sediments is very small, and the correlation coefficients rang from 0.37% - 1.86%; in the surface sediment area with more than 1 000 m depth-water, biogenic silica content is relatively high, and the correlation coefficients rang from

3.39% - 9.00% with the majority between 4% - 6%. According to Wu and Luo[10] on the information of sedimentary types in the Nansha Islands and its adjacent waters, the shallow-water shelf deposition at station NS04-24 belongs to the continental shelf of modern clastic deposition of land-based sources, accompanied by the Mekong terrigenous material impact significantly, and a large number of terrigenous material input will greatly dilute biogenic silica content in the sediment; the shallow stations NS02-30 and NS04-29 of the continental shelf lie in the junction region of the relict and modern sediments, of which the relict sedimentary region is found to be in the late of significant transformation effect. So the biogenic silica content in the surface sediments at two stations may also be affected by terrigenous material dilution. However, the effect of terrigenous material dilution on two stations is low comparing with the effect on station NS04-24. In the continental slope and deep-sea areas with depth of more than 1 000 m, the biogenic silica content of the surface sediment is larger, which may be related to the weak effect of terrigenous material dilution, and mainly to siliceous biological productivity in waters, nutrient salt and sea currents and so on.

The result of correlation analysis on the biogenic silica content in the modern sediment and the water depth shows that the correlation coefficient is 0.782 with the significant level for 0.01, suggesting that there is the significantly positive correlation between biogenic silica content in modern sediment and the water depth in the study area. However, the study of Leinen [11] found that the biogenic silica accumulation rate in the sediment of the central equatorial Pacific had no correlation with the paleo-depth of samples. There is a lot of terrestrial inputs in surface sediment of the shallow shelf area from the marginal sea, and the terrestrial inputs would have a very significantly dilute effect on the biogenic silica content. So, as derived from the correlation analysis, the biogenic silica content in the surface sediments of marginal sea area has a certain relevance to the water depth; however, the terrigenous material has no effect on the biogenic silica content in the sediment of the open ocean which may be only related to the siliceous biological productivity in overlying waters, water masses and ocean currents and so on. This is also the unique difference between the marginal sea and the open ocean.

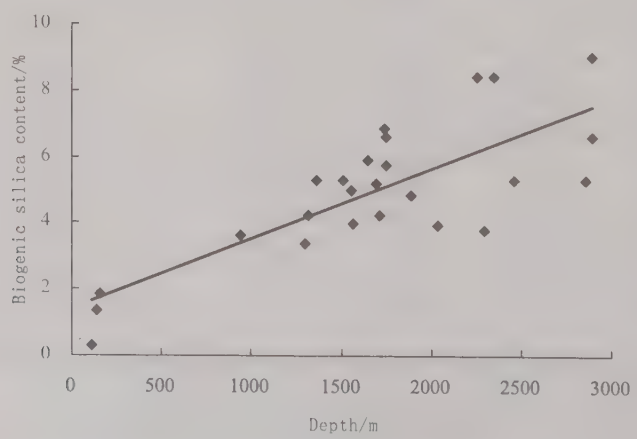

Fig. 2 Relation between the biogenic silica content in modern sediment and water depth

2.2 Relation between the biogenic silica content and modern marine environment

The distribution of biogenic silica content in the surface sediment of the southern SCS is shown in Fig. 3. The biogenic silica content in the surface sediment increases from the continental shelf to the continental slope. Lower biogenic silica content distributed in the shallow continental shelf of the southwest SCS and in the continental slope with water depth of 1 500 m - 3 000 m area, the biogenic silica content is relatively high.

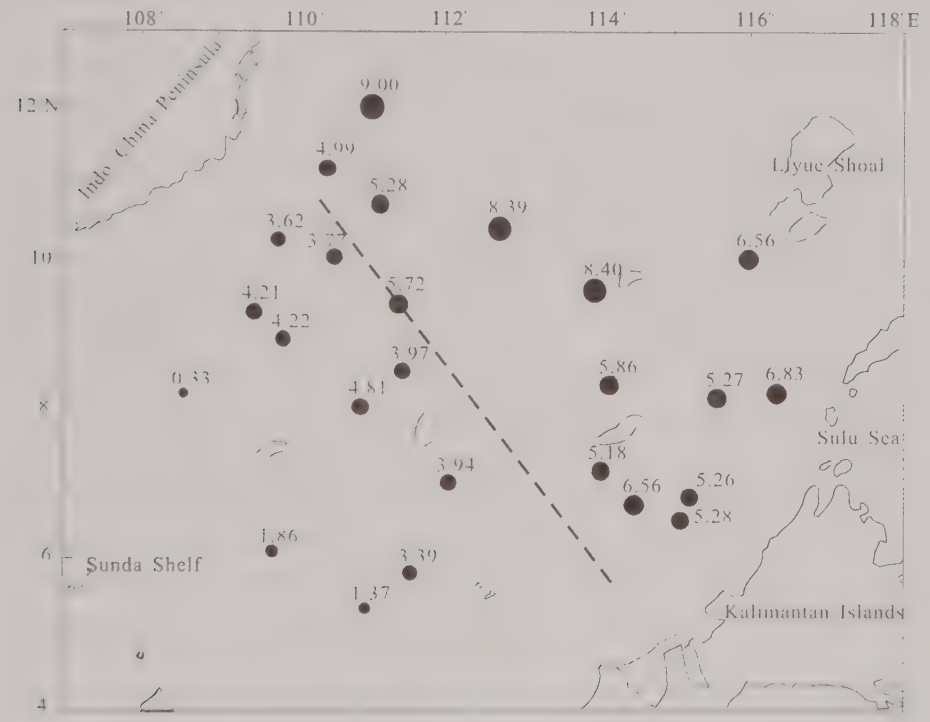

Fig. 3 Distribution of biogenic silica contents of surface sediments in the southern SCS

The ocean circulation in the study area is significantly affected by the monsoon. During the summer monsoon, there is a strong offshore upwelling forming beyond the southestern coast of Vietnam, and during the winter monsoon, there is a weak anti-cyclone circulation in the Nansha trough area [12], namely, a weak upwelling. Generally, the upwelling area is rich in nutrients, and siliceous biological flux is correspondingly comparatively high. Abelmann [13] in 1997 proved this point that radiolarian abundance was low in the subtropical region with poor nutrition and increased evidently in the upwelling development zone. Fig. 3 shows that the biogenic silica contents in the surface sediment of the upwelling areas beyond the Vietnam southestern coast and in the Nansha trough are significantly higher than those in the surrounding area, and the biogenic silica content in the strong upwelling beyond the Vietnam southestern coast (maximum biogenic silica content for 9.00%) is obviously higher than that in the weak upwelling of the Nansha trough (maximum biogenic silica content for 6.56%). Thus, the distribution of biogenic silica

content in the sediment can better reflect the activities of upwelling oceanographic conditions, and the upwelling is an important oceanographic index to the monsoon climate. Therefore, the upwelling development and change of the biogenic silica records in the sediment could be used to trace the paleo-monsoon information, which thus becomes an important means to the paleoclimate study.

The central north of the study water area (more than 2 000 m depth) lies in the summer upwelling (that is, offshore upwelling formed in the southeastern coast of Vietnam) development region [14], having the obviously high density of siliceous biological radiolarian [15]. Thus, it may be conjectured that there is comparatively high level of siliceous biological productivity in this water area. In this region, biogenic silica content in the surface sediment is also obviously high, with maximum value for 8.40%. Therefore, the biogenic silica content in the surface sediment at deep water area from the southern SCS could better reflect the paleoproductivity level of siliceous biology in overlying waters.

The shallow continental shelf in the southwest is a part of the Sunda Shelf, not more than 200 m water depth. There is high chlorophyll and primary productivity, because of different water mass, mixed intersection and bottom water upwelling existing in this sea area [16]. The siliceous biological radiolarian and diatom have very high densities in upper water column in this area, due to the obviously high nutrient concentration [15, 17, 18]. Although there is very high biological productivity level in waters of the shallow southwestern area, the biogenic silica content in the surface sediment of this region is quite low, less than 2%. Hence, the high productivity level of siliceous biology can't be reflected in the sediment, which may be related to the sediment type and terrigenous material input. The surface sediment at station NS04-24 belongs to the modern terrigenous clastic deposition. The biological deposition composition is significantly diluted by the large amount of terrigenous material carried by the Mekong, and the sediment type consisting mainly of sand makes biological shells is difficult to be buried and preserved. The stations NS02-30 and NS04-29 locate in the junctional area between the relict and modern sediments, and the relict sediment belongs to the continental shelf deposition during low sea level in the glacial period, most of which have been transformed in the late period, not a completely closed system, with the material inevitably joining in and out [10]. Therefore, the biogenic silica content in the surface sediments in this region can be more difficult to accurately reflect the productivity level of siliceous biology in the overlying waters.

Clearly, the biogenic silica content in the surface sediment with deep water area of the southern SCS is mainly related to the upwelling, nutrient and productivity level of siliceous biology, and the biogenic silica content in the shallow shelf sediment is significantly affected by the terrigenous material input and sediment type and so on. Therefore, when the biogenic silica content in the sediment is used to indicate the volatility of paleo-productivity, it is necessary to consider the then sea-level change, water depth and sediment type and so on.

2.3 Biogenic silica content distribution and its siliceous biology sources

Biogenic silica in the sediment comes mainly from the siliceous skeleton shells of diatom and

radiolarian, and the siliceous spicule of poriferans there is a certain contribution. The author determined the biogenic silica in 25 surface sediments from the southern SCS, at the same time, with the quantitative statistics about the radiolarian and poriferous spicule (Tab.1); the diatom data cited identification results published [18]. This study aims to preliminarily analyse and explore the distribution relationships between the biogenic silica content and its main sources of siliceous materials (diatom, radiolarian and poriferan) in the sediment of the tropical marginal sea.

Correlation analysis between biogenic silica and its sources in 25 surface sediments from the study area shows that there is the moderate correlation between biogenic silica and its sources of radiolarian and poriferan with a correlation coefficient, 0.431 and 0.538, respectively. Thus, the biogenic silica content in the surface sediments of the study area can basically reflect the productivity level of siliceous biology. Correlation analysis between diatom abundance in 10 surface sediments of the southern SCS from Lu et al. [18] and corresponding biogenic silica content data shows the weak correlation with a correlation coefficient only for 0.326. This may be due to be easily eaten off and dissolved during the sedimentation or other reasons. If the abundances of diatom, radiolarian and poriferous spicule and the biogenic silica content undergo a horizontal distribution analysis (see Fig. 4), the influence degree of three sources on the biogenic silica content distribution can be comparatively intuitive to see

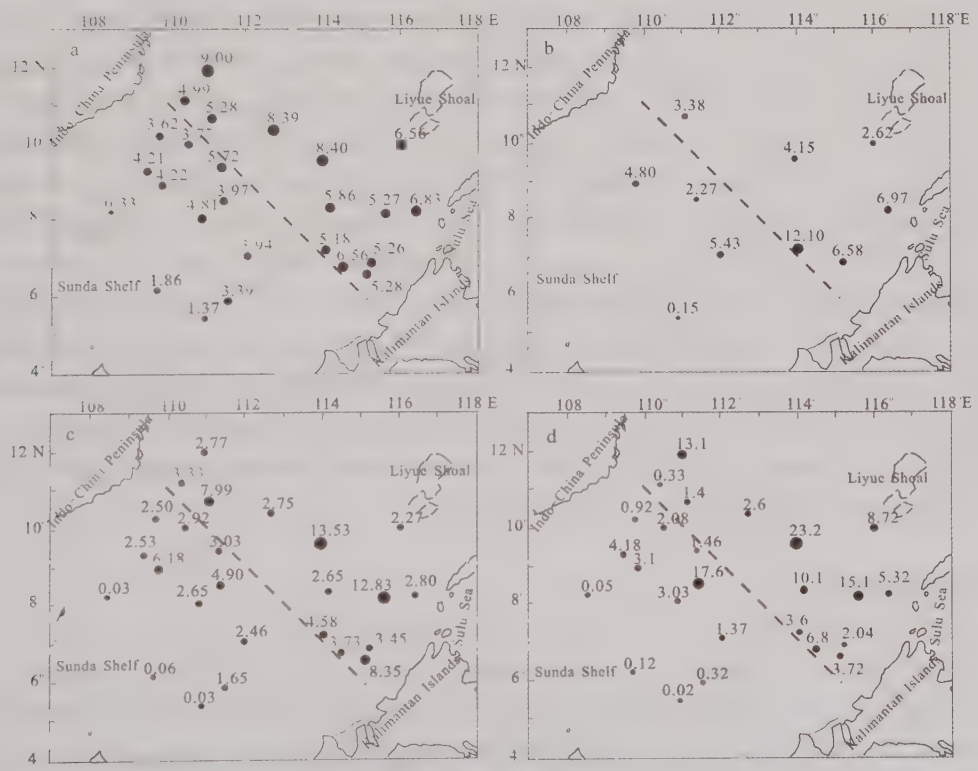

Fig. 4 Distributions in the surface sediment samples in the southern SCS

(a) for biogenic silica content (%), (b) for diatom abundance (ind. $\times 10^6$/g), (c) for radiolarian abundance (ind. $\times 10^4$/g) and (d) for poriferous specula abundance (ind. $\times 10^3$/g)

Fig. 4 shows that the abundances of radiolarian and poriferous spicule and biogenic silica content have great values, but diatom abundance of smaller value, at station NS02-07 which lies in the central sea area far from the mainland with a weak impact of the terrigenous material input. Ragueneau et al. [19] found that in the sea area with relatively low deposition rate, radiolarian of biogenic silica is more significant than diatom. Therefore, deposition rate of siliceous biology in the central and northern of the study area may be comparatively low. The distribution trend of biogenic silica content in all 25 surface sediments of the southern SCS is similar to that of radiolarian and poriferous spicule abundances, with low values locating at the Sunda Shelf and high values at the sea area north to the dotted line. From the existing data distribution of diatom abundance, there is a larger difference between diatom abundance distribution and biogenic silica content distribution comparing to the radiolarian and poriferous spicule. The biogenic silica content and abundances of radiolarian and poriferous spicule have relatively high values in the surface sediments with upwelling development of Nansha trough and outside of Vietnam bank, and diatom has high abundance in Nansha trough area with insufficient data in Vietnam offshore area. This is consistent with the high content of biogenic silica.

3 Conclusion

The analysis results of biogenic silica content in 25 surface sediments of the southern SCS shows that biogenic silica content in surface sediments and its water depth have evidently positive correlation, and the correlation coefficient was up to 0.782. Biogenic silica content was very low in continental shelf shallows and could not reflect the productivity of siliceous micropaleontology in surface waters, which may be affected by sedimentary types and terrigenous matter dilution. Distribution of biogenic silica content in surface sediments from deep water areas showed that it could not only reflect the paleoproductivity of siliceous micropaleontology in surface waters, but also indicate the strong or feeble upwelling. Thus, it was further confirmed that using biogenic silica content in sediments to trace upwelling and its change was effective and reliable. The analyzed result showed that radiolaria and poriferous specula have more contribution for biogenic opal comparing with diatom in surface sediments from the northern studied area, probably owing to the diatom dissolved easily away and eaten by other organisms with little effort. In the upwelling areas, radiolarian, diatom and poriferous specula all approximately showed high abundance, which was consistent with high biogenic silica content.

Acknowledgements

We are grateful to the captain crew, technicians, and scientists on board involved in the Multidisciplinary Oceanographic Investigation of the Nansha Sea Area cruise, for their efforts in collecting the plankton samples. We thank Dr. Gao Jiangtao of Mississippi College for English editing of the manuscript. This study was funded by the following research programs: National Natural Science Foundation of China (No. 40476024), National Key Technology R&D Program (No. 2006BAB19B03) and supported by Key Laboratory of Marginal Sea Geology, Chinese Academy of Sciences (No. MSGL0613)

and the Knowledge Innovation Program of the Chinese Academy of Sciences (No. SQ200808).

References

[1] Chen M, Huang L, Tu X, et al. Radiolarian transfer function for paleo-primary productivity in the South China Sea [J]. Chinese Science Bulletin, 1999, 44 (13): 1 232 - 1 237.

[2] Brewster N A. Cenozoic biogenic silica sedimentation in the Antarctic Ocean [J]. Geological Society of America Bulletin. 1980, 91: 337 - 347.

[3] Huang W, Wang P X. Sedimentation rates of deep water areas from the late glaciation in the South China Sea [J]. Science in China (Series D), 1998, 28(1): 13 - 17.

[4] Jia Guo-dong, Jian Zhi-min, Peng Ping-an, et al. Biogenic silica records in core 17962 from southern South China Sea and their relation to paleo-ceanographical events [J]. Geochimica, 2000, 29(3): 293 - 296.

[5] Wang R J, Fang D Y, Shao L, et al. Oligocene biogenic siliceous deposits on the slope of the northern South China Sea [J]. Science in China (Series D), 2001, 31(10): 867 - 872.

[6] Li J R, Wang R J, Li B H. Variations of opal accumulation rates and paleoproductivity over the past 12 Ma at ODP Site 1143, southern South China Sea [J]. Chinese Science Bulletin, 2002, 47(3): 235 - 237.

[7] Wang R J, Li J. Quaternary high-resolution opal record and its paleoproductivity implication at ODP Site 1143, southern South China Sea [J]. Chinese Science Bulletin, 2003, 48(1): 74 - 77.

[8] Li J, Wang R J. Paleoproductivity variability of the northern South China Sea during the Past 1 Ma: the opal record from ODP site 1144 [J]. Acta Geologica Sinica, 2004, 78(2): 228 - 233.

[9] Mortlock R A, Froelich P N. A simple method for the rapid determination of biogenic opal in pelagic marine sediments [J]. Deep-Sea Research, 1989, 36(9): 1 415 - 1 426.

[10] Wu S G, Luo Y L. The relict sediments in the south shelf of South China Sea [J]. Tropic Oceanology, 1994, 13(3): 47 - 53.

[11] Leinen M. Biogenic silica accumulation in the central equatorial Pacific and its implications for Cenozoic paleoceanography: Summary [J]. Geol S Am B, 1979, 90: 801 - 803.

[12] Fang W, Fang G, Shi P, et al. Seasonal structures of upper layer circulation in the southern South China Sea from in situ observations [J]. Geophys Res, 2002, 107(C11), 3202. doi: 10.1029/2002JC001343.

[13] Abelmann A, Gowing M M. Spatial distribution pattern of living polycystine radiolarian taxa-baseline study for paleoevironmental reconstructions in the southern ocean (Atlantic sector) [J]. Marine Micropaleontolgy, 1997, 30: 3 - 28.

[14] Xie S P, Xie Q, Wang D X, et al. Summer upwelling in the South China Sea and its role in regional climate variations [J]. Journal of Geophysical Research, 2003, 108(C8), 3261, doi: 10.1029/2003JC001867.

[15] Zhang L L, Chen M H, Lu J, et al. Living polycystine radiolarian fauna in upper water column of southern South China Sea and its distribution [J]. Journal of Tropical Oceanography, 2005, 24(3): 55 - 64.

[16] Huang L M, Chen Q C. Distribution of Chlorophyll-a and estimation of primary productivity in winter of Nansha Islands [R]. Research on ecological process in Nansha Islands. Beijing: Science Press, 1997. 1 - 11.

[17] Zheng Z Z, Tu X, Cai H M, et al. Sedimentary organism [A]. Comprehensive investigation report on Nansha Islands and it's adjacent waters, Next Volume [R]. Beijing: Science Press, 1989. 774 - 801.

[18] Lu J, Chen M H, Chen Z. Distribution of diatoms in the water and surface sediments of southern South China Sea [J]. Chinese Science Bulletin, 2006, 51(Supplement Ⅱ): 66 - 70.

[19] Ragueneau O, Tréguer P, Leynaert A, et al. A review of the Si cycle in the modern ocean: recent progress and missing gaps in the application of biogenic opal as a paleoproductivity proxy [J]. Global and Planetary Change, 2000, 26: 317 - 365.

南海南部表层沉积物中生物硅的分布及其环境意义

张兰兰[1,2]，陈木宏[1]，向荣[1]，陆钧[1]，张丽丽[1,2]

（1. 中国科学院南海海洋研究所 中国科学院边缘海地质重点实验室，广东 广州 510301；

2. 中国科学院 研究生院，北京 100039）

摘 要：对南海南部 25 个表层沉积样进行了生物硅的测定分析，试图揭示南海南部表层沉积生物硅的分布及其对现代海洋环境的指示意义，以便为古海洋学研究提供进一步的科学依据。研究发现，表层沉积物中生物硅含量与其所处水深呈显著正相关关系，相关系数达到 0.782。陆架浅水区表层沉积物中生物硅含量非常低，不能反映表层水体中硅质生物生产力情况，这可能与沉积类型和陆源物质输入影响有关。深水区表层沉积物中生物硅的含量分布表明，其不仅能反映出表层水体中硅质生物的古生产力水平，而且还能指示上升流的强弱，从而进一步证实了利用沉积物中生物硅含量来追踪上升流发育和变化的有效性与可信度。研究结果还显示，在研究区域中北部表层沉积生物硅中放射虫和海绵骨针较硅藻占有更大的比重，这可能是由于硅藻易被溶解并易被其他生物体摄食的缘故。在有上升流发育的海域，放射虫、硅藻和海绵骨针基本上均表现出较高的丰度，这与高的生物硅含量相一致。

关键词：南海南部；表层沉积；生物硅；上升流

Growth Strategy of Seagrass *Thalassia hemprichii* in Xincun Bay near Hainan Island of China

XU Zhan-zhou[1, 2], HUANG Liang-min[1], HUANG Xiao-ping[1], ZHU Ai-jia [1, 2] ZHANG Si [1,3]

1. *LMB, LED of South China Sea Institute of Oceanology, CAS, Guangzhou* 510301, *Guangdong province, China;*
2. *Graduate School of the Chinese Academy of Science, Beijing* 100049, *China;*
3. *Tropical Marine Biological Research Station in Hainan, CAS, Sanya* 572200, *Hainan province, China*

Abstract: A compilation of data on biomass and growth allowed an examination of the intraspecific plasticity in *Thalassia hemprichii* which played key roles to develop site-specific growth strategies for this species in Xincun Bay. The results showed the difference in rhizome elongation rates which explained most of the variation of biomass and growth within species. The seagrass *T. hemprichii* in Xincun Bay adjusted its vertical and horizontal rhizome elongation rates alternatively in response to light level and temperature changes, resulting in the variation of shoot densities and above biomass in return. The vertical and horizontal rhizomes elongated at rates of 2.38 and 24.4 cm yr^{-1} in summer while 1.87 and 29.2 cm yr^{-1} in winter respectively. The shoot density ranged from 822 to 941 shoots m^{-2} with a peak in summer and a trough in winter which was similar to that of biomass. The growth strategy enabled *T. hemprichii* to minimize the negative effects of desiccation in summer as well as light reduction in winter.

Keywords: *Thalassia hemprichii,* intraspecific variation, rhizome elongation rates

Seagrasses are valuable coastal resources characterized by a relative taxonomic and architectural uniformity and represented by few species (Den Hartog 1970; Stevenson 1988). Yet, the biomass and turnover rates of different seagrass species differ by orders of magnitude. Attempts to explain differences in seagrass biomass and production have focused primarily on the influence of habitat conditions, particularly on temperature, light and nutrient availability (Short 1987; Duarte 1991). Duarte and Marbà have succeeded in using an extensive compilation of data on architecture and growth of different seagrass species to examine the implications of differences in module size to account for differences in productivity among seagrass species (Duarte 1991; Marbà and Duarte 1998). Duarte (1991) founded a close scaling of the size of leaves, shoots, and fruits to rhizome diameter, as well as strong relationships between shoot size and the dynamics (e.g. turnover rate, plastochrone interval, and longevity). Although much (between 40% and 173%) of the variability of seagrass horizontal rhizome and clonal growth programmes is species-specific and largely (21% to 63% of the variance) associated with differences in size among species, seagrasses also show important intraspecific variability (Marbà and Duarte 1998). The considerable intraspecific plasticity in seagrass module size suggests that it may have an important adaptive value, therefore, an important component of the capacity of seagrasses to cope with changes

Received on January 7, 2008

and heterogeneity in the environment. In turn, the plasticity of seagrass modules may also respond to the availability of resources, reducing the construction cost when resources are scare (Hemminga and Duarte 2000). In another word, the intraspecific plasticity has formed the base for seagrass populations to develop site-specific growth strategies which play a key role in the population survive and expansion (Vermaat et al.1997).

Seagrass *Thalassia hemprichii* is among the most widely-distributed seagrass species in an Indo-Pacific flora, dominating in many mixed meadows (den Hartog 1970; Brouns 1987; Vermaat et al. 1995). The biomass and growth of *T. hemprichii* have been widely researched in Southeast Asia, especially in the Philippines (Agawin et al. 2001; Brouns 1985; Estacion and Fortes 1998; Erftemeijer and Herman1994; Lanyon and Marsh 1995), southern Taiwan of China (Lin and Shao 1998), Kenya (Uku and Bjork 2005), Mozambique (Paula et al. 2001) and Arabian sea (Jagtap 1998). However, no study on the site-specific growth strategy of this species was reported. Here, we conducted a study to examine these growth characteristics for *T. hemprichii*. We also compiled all the growth and biomass data from the available literature as points of comparison. Our study area near Hainan Island is located at the intersection of the tropical southern Indo-Pacific flora. The published data combined with our results will allow us to better examine the site-specific growth strategy of this species, a factor important in the disturbance and recovery dynamics of this species and therefore the management.

1 Materials and methods

1.1 Study sites

The present study was performed at Xincun Bay (18°24′34″N - 18°24′42″N, 109°57′42″E - 109°57′58″E) located in south of Hainan province, China (Fig. 1). Xincun Bay (22.6 km^2 water surface) is a nearly closed lagoon with only one narrow entrance in the southwest, by which it exchanges water with South China sea. According to the surveys performed in 2002, a mixed seagrasss meadow with an area of about 200 ha inhabits in the southern shallow waters of Xincun Bay (Huang et al. 2006). All the seagrass species presented at this meadow were *Thalassia hemprichii*, *Enhalus. acoroides*, *Halophilas ovalis*, *Halodule uninervis* and *Cymodocea rotundata*. *Enhalus acoroides* was dominant species followed by *Thalassia hemprichii*.

1.2 Environmental parameters

We measured seawater surface temperature daily with a seawater surface thermometer. Salinity was determined by a hand-held refractometer. Measurements of photosynthetically active radiation (PAR) at the seagrass canopy level were collected during 1 - 3 h at noon (daily maximum of incoming of irradiance) with a LI-193SA spherical quantum sensor. The content of nitrate, nitrite, ammonium and phosphate of the water samples were then determined with methods described by Parson et al. (1984).

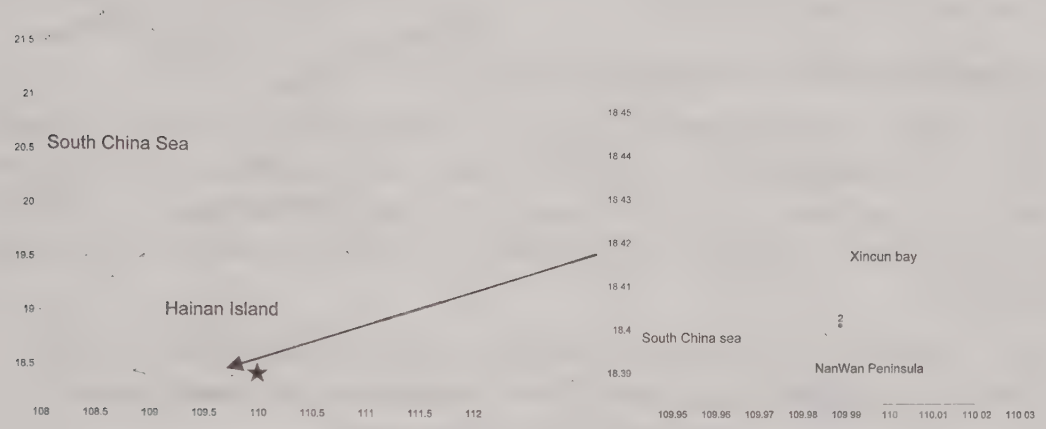

Fig. 1 Map of the Xincun Bay, showing the sampling sites

1.3 Biomass and growth of *T. hemprichii* in Xincun Bay

From November 2004 to January 2006, sampling of plant biomass was made seasonally within an area of 50 m × 50 m (central point was at 18°24′3.6″N 109°59′20.4″E） during low tide periods with a depth between 0.3 and 1.0 m. Sampling was conducted within intertidal monotypic stand of *T. hemprichii* which was exposed into air during low tide periods. Biomass samples were collected randomly using an aluminium frame (surface area 0.0 625 m^2) by 6 replicates. All the plant material within the frame was harvested and transported on ice to a laboratory and stored in a refrigerator at 4 °C. At the laboratory, samples were rinsed with tap water and divided into different plant parts (leaves, rhizomes, roots). Epiphytes were removed by careful scraping of the leaves. The plant were dried at 80 °C for 24 hours and weighed.

Leaf growth was measured in Jul 2005 and Jan 2006 respectively, corresponding to the highest and lowest level of the PAR and seawater surface temperature during a year. Leaf growth was obtained by the hole punch methods described by Dennison (1990) and Zieman (1974). A minimum of 50 shoots were punched and have been harvested after 10 days. We estimated the leaf plastochrone interval (leaf PI) by the methods described by Brouns (1985).

Vertical rhizome elongation was calculated by regressing the length of vertical rhizomes against shoot age. The slope of the regression equation represented the vertical elongation rate. The growth rate of the horizontal rhizome may be obtained by dividing the length of the rhizome between 2 consecutive shoots by the difference in the ages of the 2 shoots (Duarte et al. 1994). The production of roots in the vertical shoots can be estimated by regressing the number of roots formed against shoot ages, and the production of roots in the horizontal rhizomes can be calculated as the product of the root numbers per unit rhizome biomass and the production of horizontal rhizomes (Duarte et al. 1994).

Shoot age was estimated as the product of the total number of leaves produced during the shoot life-span (i.e. number of standing leaves plus number of leaf scars on the vertical rhizome supporting the

shoot) multiplied by the leaf PI (in days).

1.4 Intraspecific plasticity in biomass and growth of *T. hemprichii*

We compiled from the published literature (Tab. 1) available data on leaf weight, aboveground biomass, leaves numbers per shoot, leaf PI, rhizome elongation rate and shoot density of *T. hemprichii*. We consider individual seagrass stands as the units of this study. We use the coefficient of variation (CV) to quantify the intraspecific variability of biomass and growth of *T. hemprichii* (Marbà and Duarte 1998; Hemminga 2000).

Tab. 1 Sources of data on 1(1) leaves numbers per shoot, (2) leaf productivity, (3) leaf PI, (4) aboveground biomass, (5) vertical rhizome elongation rate, (6) horizontal rhizome elongation rate and (7) shoot density.

Source	Site	Variables	Number of stands examined	Habitats
Vermaat et al.(1995)	The Philippines	7	3	reef flat
Agawin et al.(2001)	The Philippines	2	1	lagoon
Rollon et al. (2001)	The Philippines	5	1	reef flat
Gacia et al.(2003)	The Philippines	2	5	reef flat
Uku and Bjork (2005)	Kenya	3	4	lagoon
Jagtap (1998)	India	3	7	lagoon
Huang et al. (2006)	China	2	2	lagoon
This study	China	8	1	lagoon

2 Results

2.1 Environmental parameters of the study areas

The PAR level revealed a distinctly unimodal seasonality with a maximum of 1 861 ± 69 μmol /s m^{-2} in Jul 2005 and a minimum of 1 438 ± 42 μmol /s m^{-2} in Jan 2006. The sea surface temperature showed a similar seasonal variation coincided with the PAR during the sampling periods. The water column at study sites were of low level of nutrients with mean concentrations of 3.1 μmol/L dissolved inorganic nitrogen (a sum of nitrate, nitrite and ammonium) and 0.28 μmol/L phosphate, respectively.

2.2 Biomass and growth of *T. hemprichii* in Xincun Bay

The biomass of *T. hemprichii* varied seasonally (Fig. 2a). The whole plant biomass (a sum of dry weight of leaves, rhizomes and roots) ranged from 284.3 ± 84.2 g DWm^{-2} in autumn to 409.6 ± 75.5 g DWm^{-2} in winter. The biomass of rhizomes and roots increased from spring to autumn and decreased sharply during winter while the opposite pattern was observed in the variation of leaves biomass. Leaves biomass ranged from a minimum of 59.2 g DWm^{-2} in summer to a maximum of 115.2 g DWm^{-2} in winter. The root shoot ratio also varied from 0.24 in summer to 0.33 in winter with an average of 0.30(Fig. 1b).

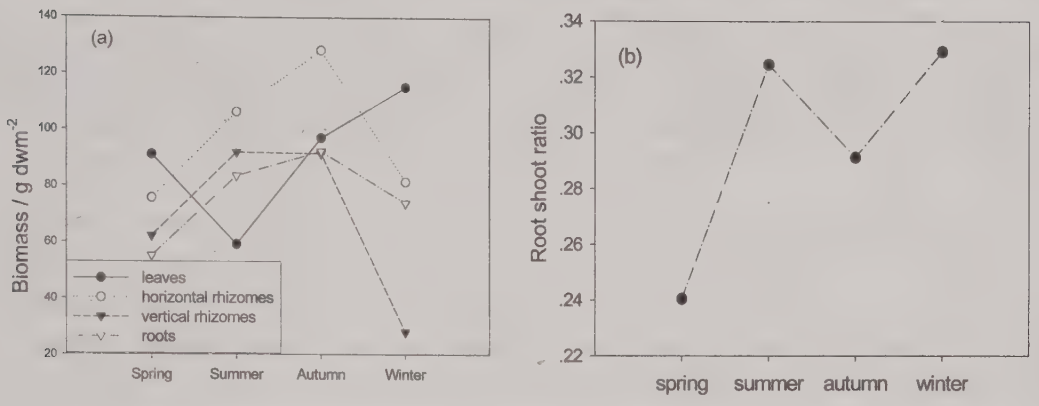

Fig. 2 Temporal variation of (a) the biomass of leaves, rhizomes and roots, (b) root shoot ratio of *T. hemprichii* in Xincun Bay

The leaf plastochrone interval was 10.6 days. The leaf elongation rates were 2.8 ± 1.3 mm leaf^{-1}/d and 2.6 ± 1.6 mm leaf^{-1}/d in summer and winter respectively. The shoot density ranged from 822 to 941 shoots m^{-2} with an average of 884 shoots m^{-2}. The maximum of shoot density was recorded in summer and the minimum in winter.

The vertical rhizome growth was significantly correlated with shoot age, which allowed the calculation of vertical rhizome elongation rates. The vertical rhizome growth rates were 2.38 cm/yr in summer ($R^2 = 0.59$, $p < 0.01$, $n = 97$) and 1.87 cm/yr in winter ($R^2 = 0.64$, $p < 0.01$, $n = 148$). The horizontal rhizome growth rates reached the values of 24.40 and 29.20 cm/yr in summer and winter respectively. As we can see, the seasonality of the vertical rhizomes was quite different from that of horizontal ones. The vertical rhizome extended at a 27.3% greater rate in summer than in winter, while the horizontal rhizome elongation rate in winter was 20% greater than that in summer.

The formation rate of roots on horizontal rhizomes (19.6 roots yr^{-1}) was almost one times greater than that on vertical rhizomes(10.8 roots yr^{-1}), which indicated faster lateral growth of horizontal rhizomes than vertical ones in winter.

The shoot age structure was characterized by a high abundance of shoots younger than 1.7 yr old followed by an exponential decline in shoot abundance for older shoots. Most of the shoot aged from 20 PIs (212 d) to 60 PIs (636 d).

2.3 Intraspecific plasticity in biomass and growth of *T. hemprichii*

The variation of shoot density ranked the first within specie variation of *T. hemprichii* followed by rhizome elongation rates. The minimal variation occured in the leaf plastochrone interval followed by leaves number per shoot, showing much more conservative traits within this species (Tab. 2). The shoot densities of the populations inhabited in lagoons were significantly greater than those in reef flats ($P < 0.01$) while no obvious differences are found between the aboveground biomass ($P > 0.05$), suggesting the

greater shoot size of reef flat populations than lagoon ones.

Tab. 2 Data on leaves number per shoot (LN), leaf productivity (LP, in g DW m^{-2} / day), aboveground biomass (AB, in g DW m^{-2}), leaf plastochrone interval (PI, in days), vertical rhizome elongation rate (VE, in cm $shoot^{-1}$/ yr), horizontal rhizome elongation rate (HE, in cm/yr) and shoot density (Den, in shoots m^{-2})

Site	LN	LP	AB	PI	VE	HE	Den
Philippine	3.9	4.14	250.2	10.9	3	20.6	548
		4.08					533
			148	9.19	2.14	56	1 358
			167.9		1.65	36	1 853
				10.9			335
				10.9			65
				11			325
Kenya	4.05	5.4					653
	3.8	2.85					733
India	3		25.3				300
	3						270
	3						300
	4		109.2				270
	4		258.3				1 300
	4		231.6				1 000
	3		34.2				150
China		4.07					1 508
		2.76					1 024
	4.6	2.02	154	10.6	2.12	26.8	884
Within species CV / %	15.42	35.21	56.20	7.35	25.26	44.35	72.61

3 Discussion

3.1 Extent of intraspecific plasticity in biomass and growth of *T. hemprichii*

The bio-geographic researches of *T. hemprichii* indicated a relative wide distribution of this species. As showed in Tab. 2, a considerable extent of intraspecific plasticity in biomass and growth of *T. hemprichii* was observed. This was one of the most important reasons for which it dominated in many seagrasses meadows. In fact, the plasticity in the architecture of seagrasses was an important component of their capacity to adapt to disturbance or resource heterogeneity. The horizontal rhizomes have an exploratory capacity, being responsible for the extension of the clone into new areas and recruitment of new shoots, while vertical rhizomes have the capacity to use resources, deploying leaves and roots at the same position to use the local resources (Hemminga and Duarte 2000). The diameter of seagrass

rhizomes are most conservative traits within individual species (Duarte 1991, Marbà and Duarte 1998). So the intraspecific plasticity in biomass and growth of *T. hemprichii* was mainly attributed to the within-species variation of rhizome elongations. For instance, the populations in reef flats developed less dense but greater size of shoots responding to greater water dynamical power than those in lagoons.

3.2 Site-specific growth strategy of *T. hemprichii* in Xincun bay

The leaf and vertical rhizomes grew vertically while the horizontal rhizomes occupied the sediments by lateral elongation and branching. In general, these two aspects of the seagrass growth compete for resources and respond to the disturbances directly. In summer, most of the leaves biomass lost caused by desiccation and the herbivorous fishes, resulting in the leaves grew at a higher rate in order to recover as soon as possible. Although the gross leaf productivity was enhanced, the respiration rates of leaf segments might be unnaturally high due to high temperature and wound effects (Hemminga and Duarte 2000). As a result, the net leaf productivity was even lower than that in winter (1.85 and 2.80 mg DW $shoot^{-1}/d$, respectively). So the elongation of horizontal rhizomes was restrained by the reduced material flux from leaves to horizontal rhizomes and roots. And shoot density reached a maximal value of 941 shoots m^{-2} in summer. On the contrary, the light intensity and temperature decreased in winter. The vertical growth of *T. hemprichii* reduced and more material was transported and stored in horizontal rhizomes and roots indicated by the increase of root shoot ratio from spring to winter (Fig. 2b). The lateral growth was strengthened which caused the shoot density decreased in return to avoid the shading effects. The courses discussed above can be illustrated as Fig. 3.

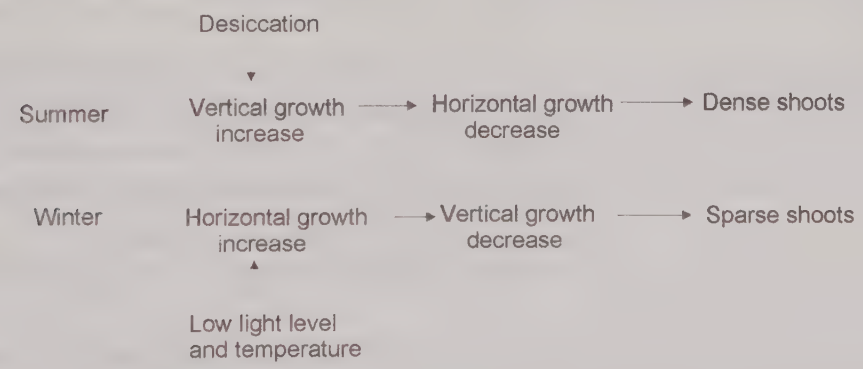

Fig. 3 Courses regulating the growth and biomass of *T. hemprichii*

The average and the maximum shoot ages of *T. hemprichii* in Xincun Bay were smaller than those reported in previous studies carried out in the Philippines (453 and 1 455 days, respectively), so did the horizontal and vertical rhizome elongation rates. This suggests the population in Xincun Bay was younger and more sensitive to disturbances than did those in the Philippines. As a result, it would recover more slowly after disturbances which emphasized the important of protecting the rhizomes in the efforts to retain the seagrasses meadow in this lagoon. And the activities endangering the growth of rhizomes (e.g. digging and raking shells, fishing by benthic trawling, Huang et al. 2006) should be forbidden as soon as

possible.

Acknowledgements

We are grateful to associated professor Wang Han-kui for supplying convenience on lab use. Huang Dao-jian, Hu You-mu and Liang Ji-lin offered much help at field work. This paper is supported by UNEP and Global Environment Foundation (No. UNEP/GEF/SCS/Chi/MoU2c), the Key Innovation Project of Chinese Academy of Science ((No. KSCZ2-SW-132), the National Natural Science Foundation of China (No. 40576052 and No. U0633007).

References

[1] Agawin NSR, Duarte CM, Fortes MD, et al. Temporal changes in the abundance, leaf growth and photosynthesis of three co-occuring Philippine seagrasses [J]. J. Exp. Mar. Biol. Ecol. 2001, 260: 217 - 239.

[2] Brouns JJWM. A comparison of the annual production and biomass in three monospecific stands of the seagrass *Thalassia hemprichii* (Ehrenb) [J]. Achers. Aquat. Bot. 1985, 23: 149 - 175.

[3] Brouns JJWM. Growth patterns of some Indo-West-Pacific seagrasses [J]. Aquat. Bot. 1987, 28: 39 - 61.

[4] Duarte CM. Allometric scaling of seagrass form and productivity [J]. Mar. Ecol. Prog. 1991, Ser.77: 289 - 300.

[5] Duarte CM, Marbà N, Agawin NSR, et al. Reconstruction of seagrass dynamics: age determinations and associated tools for the seagrass ecologist [J]. Mar. Ecol. Prog. 1994, Ser. 107: 195 - 209.

[6] Den Hartog C. *The seagrasses of the world* [M]. Amsterdam, Netherland: North Holland Publishing House, 1970.

[7] Dennison WC. Leaf production. In: Phillips RC and McRoy CP, eds. Monographs on Oceanographic Methodology 9: Seagrass Research Methods [J]. UNESCO, Paris. 1990, 77 - 79.

[8] Erftemeijer PLA, Herman PMJ. Seasonal changes in environmental variables, biomass, production and nutrient contents in two contrasting tropical intertidal seagrass beds in South Sulawesi Indonesia [J]. Oecologia. 1994, 99: 45 - 59.

[9] Estacion JS, Fortes MD. Growth rates and primary production of *Enhalus acoroides* L.f. Royle and its epiphytes [J]. Aquat. Bot. 1998, 29: 347 - 356.

[10] Huang Xiao-ping, Huang Liang-min, Li Ying-hong, et al. Main seagrass beds and threats to their habitats in the coastal sea of South China [J]. Chinese Science Bulletin 51(Supp. II), 2006, 136 - 142.

[11] Hemminga MA, Duarte CM. Seagrass Ecology [M]. Cambridge, UK: Cambridge University Press, 2000.

[12] Jagtap TG. Structure of major seagrass beds from three coral reef atolls of Lakshadweep, Arabian Sea, India [J]. Aquat. Bot. 1998, 60: 397 - 408.

[13] Lanyon JM, Marsh H. Temporal changes in the abundance of some tropical intertidal seagrasses in North Queensland [J]. Aquat. Bot. 1995, 49: 217 - 237.

[14] Lin Hsing-Juh, Shao Kwang-Tsao. Temporal changes in the abundance and growth of intertidal *Thalassia hemprichii* seagrass beds in southern Taiwan [J]. Bot. Bull. Acad. Sin. 1998, 39: 191 - 198.

[15] Marbà N, Duarte CM. Rhizome elongation and seagrass clonal growth [J]. Mar. Ecol. Prog. 1998,Ser.174: 269 -

280.

[16] Parson TR, Maita Y, Lalli CM. A manual of chemical and biological methods for seawater analysis [M]. Oxford UK: Pergamon Press, 1984.

[17] Paula J, Fidalgo e Costa P, Martins A, et al. Patterns of Abundance of Seagrasses and Associated Infaunal Communities at Inhaca Island, Mozambique [J]. Estuarine, Coastal and Shelf Sci. 2001, 53: 307 - 318.

[18] Rollon RN, Cayabyab NN, Fortes MD. Vegetative dynamics and sexual reproduction of monospecific *Thalassia hemprichii* meadows in the Kalayaan Island Group [J]. Aquat. Bot. 2001, 71: 239 - 246

[19] Stapel J, Manuntun R, Hemminga MA. Biomass loss and nutrient redistribution in an Indonesian *Thalassia hemprichii* seagrass bed following seasonal low tide exposure during daylight [J]. Mar. Ecol. Prog. 1996, *Ser.* 134: 251 - 262.

[20] Stevenson JC. Comparative ecology of submerged grass beds in freshwater, estuarine, and marine environment. Limnol [J]. Oceanogr. 1988, 33: 867 - 893.

[21] Short FT. Effects of sediment nutrients on eelgrass: literature review and mesocosms experiment [J]. Aquat. Bot. 1987, 27: 41 - 57.

[22] Uku J, Bjork M. Productivity aspects of three tropical seagrass species in areas of different nutrient levels in Kenya [J]. Estuarine, Coastal Shelf Sci. 2005, 63: 407 - 420.

[23] Vermaat JE, Agawin NSR, Duarte CM, et al. Meadow maintenance, growth and productivity of a mixed Philippine seagrass bed [J]. Mar. Ecol. Prog. 1995, *Ser.* 124: 215 - 225.

[24] Vermaat JE, Agawin NSR, Fortes MD, et al. The capacity of seagrasses to survive increased turbidity and siltation: the significance of growth form and light use [J]. *Ambio* 1997, 26(8): 491 - 496.

[25] Zieman JC. Methods for the study of the growth and production of turtle grass [J]. *Thalassia testudinum konig. Aquaculture* 4, 1974, 139 - 143.

新村湾海黾草（*Thalassia hemprichii*）的生长策略研究

许战洲[1,2], 黄良民[1], 黄小平[1], 朱艾嘉[1,2], 张偲[1,3]

（1. 中国科学院 南海海洋研究所 热带海洋环境动力学重点实验室，广东 广州 510301；
2. 中国科学院 研究生院，北京 100049；3. 中国科学院 热带海洋生物研究站，三亚 海南 572200）

摘 要: 海草的种内差异是它在特定环境中形成生长策略的关键因素。本研究通过将现场实测数据和文献记录进行类比以探讨新村湾海黾草（*Thalassia hemprichii*）的生长策略。研究结果表明海黾草地下茎伸长速率的差异可以解释该海草生物量和生长的大部分种内差异；新村湾海黾草垂直地下茎和水平地下茎的伸长速率在夏季分别为 2.38 cm/yr 和 24.4 cm/yr，在冬季分别为 1.87 cm/yr 和 29.2 cm/yr。海黾草茎枝密度的变化范围是 822 shoots m^{-2} 至 941 shoots m^{-2}，最大值出现在夏季而最小值出现在冬季，生物量的季节变化与此类似。新村湾海黾草通过交替调节垂直地下茎和水平地下茎的伸长速率以适应光照强度和温度的季节变化，从而导致茎枝密度和地上生物量的相应变化。通过这样的生长策略，海黾草可以把夏季干旱和冬季光照强度下降对其生长造成的消极影响降低到最小程度。

关键词: 海黾草（*Thalassia hemprichii*）,种内差异, 地下茎伸长速率

Influence of Microstructure Change of Seafloor Sediments on the Sound Velocity in them in the Course of Stress-strain

LI Gan-xian, LU Bo, HUANG Shao-jian

Key Laboratory of Marginal Sea Geology, South China Sea Institute of Oceanology, Chinese Academy of Sciences, Guangzhou 510301, *Guangdong province, China*

Abstract: Test tools and methods for synchronizing acoustic measurements in the course of stress-strain for seafloor sediment are elaborated and the test data of 45 sediment samples from the seafloor in the South China Sea are analysed. The result shows that the coarser the sediment grains are, the smaller the porosity is and the larger the unconfined compression strength is, the higher the sound velocity is. In the course of stress-strain, the sediment sound velocity varies obviously with the stress. Acoustic characteristics of sediment in different strain phases and the influence of sediment microstructure change on its sound velocity are discussed. This study will be of important significance for surveying wells of petroleum geology and evaluating the base stabilization of seafloor engineering.

Keywords: seafloor sediment, stress-strain, microstructure features, sound velocity, compression strength

Sound velocity of seafloor sediment is an important basic parameter needed in the fields of seafloor acoustics, seafloor engineering and research on marine petroleum geology and marine acoustic field. To propose the method of accurately predicting seafloor sound velocity, our predecessors have made constant experimental researches and achieved rather beneficial results (Biot 1956, Anderson 1974 and Hamilton 1982 et al.). In recent years, more and more scholars have found that besides porosity, an important factor affecting the sound velocity in seafloor sediment, there are some other factors that can also affect the sound velocity in seafloor sediment, such as shape and structural features of sediment pores, mechanical coupling state of sediment grain contact as well as unconfined compression strength, etc.(Yuanbo Liang and Bo Lu 1984,1985). To further study the relationship between the microstructural characteristics of sediment and its sound velocity change, we have carried out synchronizing acoustic measurements in the course of stress-strain for seafloor sediment so as to discuss the influence process of the internal microstructural changes of sediment in different strain phases under the action of stress on its sound velocity.

Received on January 7, 2008

1 Samples collection and experimental methods

The controlled stress-strain process used in this paper is an unconfined compression strength experiment without confining pressure and drainage. Additional acoustic transducers are at both ends of the compressed sediment, and the acoustic wave meter and the computer constitute the stress-strain/ sound velocity measuring system, the latter being used for data processing and spectral analysis.

Among the seafloor sediment samples, 22 are collected from the continental shelf and 23 from the continental slope of the South China Sea. The types of sediments include silty clay, clayey silt, silty sand and sandy silt.

When they are brought to the laboratory from the sea, the columnar samples must be kept vertical and sealed so as to prevent the samples from disturbation and evaporation and loss of water. After the sample is dissected, its central part is taken for this experiment while other parts are used in the analysis and measurement of other parameters such as grain size, water content, wet density, etc. The treatment and measurement of samples are carried out in accordance with the requirement of the national standard (The China National Standard Method GBJ 138 - 88). The diameter of the sample is 3.8 cm and the ratio of height to diameter is 2.0 - 2.5. The measurement of each sample is completed within 10 mins, and the sound velocities in sediment samples in various data measurements in the course of stress-strain are calculated (the precision of the sound-wave meter $\leq \pm$ 0.5%). The sound velocity curve and the stress-strain curve in the course of stress-strain are plotted, and the unconfined compression strength of the sample is computed by using the method given by the national standard.

2 Data and results

Tab. 1 lists the mean values of various physical-mechanical and acoustic parameters of three typical seafloor sediments in the South China Sea. The types of sediments include silty clay, clayey silt and silty sand. These three types of sediments are the ones most extensively distributed in the seafloor of the South China Sea and the numbers of samples measured can reflect the basic condition of the various types of sediment (the numbers of samples: 15 of silty clay, 11 of clayey silt and 10 of silty sand).

From the Tab. 1, a few very distinct regularities can be found. With the increase of the grain size of the sediment grains from silty clay to clayey silt and then to silty sand (According to the unified international grading criteria, $\Phi = -\log_2 d$, with mm as unit of d, so the smaller the Φ value is, the larger the grain is), the sediment density increases; the pores reduce and become smaller; the water content drops; the unconfined compression strength increases and the sound velocity becomes larger, which is in accordance with the analytical results of data in the related documents(Yuanbo Liang and Bo Lu 1985). It can thus be seen that besides the porosity, there are related variations between other physico-mechanical factors and the sound velocity of marine sediment, while these factors are directly or indirectly affected by

the microstructural characteristics of sediment.

Tab. 1 Mean Values of acoustic and physical-mechanical parameters of the seafloor sediment in the South China Sea

Parameter	Φ	ρ	Gs	ω	LL	PL	I_l	Ip	n	q_u	Cp
Silty clay	8.24	1.33	2.59	152.2	90.9	48.6	3.34	42.2	79.9	3.47	1 355
Clayey silt	7.12	1.43	2.62	127.5	61.1	35.9	3.74	25.3	74.3	4.15	1 364
Silty sand	3.60	1.58	2.66	52.3	33.7	21.5	2.98	12.2	58.4	12.18	1 446

Note:Φ= Median grain size, ρ= wet density / g/cm^3; Gs = grain specific gravity;ω= water content / %;LL= liquid limit / %; PL=plastic limit / %; I_l = liquid index; Ip =plastic index; n= porosity / %; q_u = unconfined compression strength / kPa; Cp = longitudinal wave velocity / m/s.

In order to better analyse and study the law of the variations of sediment sound velocity with the microstructure, we have made synchronous measurements of sound velocity for all types of sediment samples in the course of stress-strain. The results show that whatever seafloor sediment is, its sound velocity follows the pattern of changing with the stress-strain process, with the sound velocity generally in the range of 1 300 - 1 500 m/s and the magnitude of sound velocity change generally above 20 m/s, which is obviously not caused by the insufficient precision of instrumental measurements. The typical results of experimental measurements are shown in Fig. 1, 2 and 3, which are the result diagrams superimposed by the stress-strain sound velocity measuring curves of three types of sediments respectively, ie., silty clay, clayey silt and silty sand. It can be seen from these diagrams that the stress-strain/sound velocity curves, the three types of sediment have an approximately consistent change rule. In the whole course of strain, the various sediment types have all undergone the process that their stress and sound velocity change from small to large and then to small again. When the strain is within about 3%, the sound velocity increases rapidly with the increase of the stress; when the strain is between 3% and 10%, the stress and sound velocity of all types of sediment fluctuate to varying degrees. The stress presents a distinct process of becoming larger and then tending to be smaller while the sound velocity shows a more complicated change, i.e., rising to the high level, then dropping and finally rising again. When the strain is between 10% and 20%, the sound velocities in the three types of sediments all drop constantly with the increase of strain and the decrease of stress. This is the situation when the sediment is fragmented under the action of stress. This basically consistent regular change indicates that in the course of stress-strain, the microstructural change of sediment is closely related to the change of sound velocity.

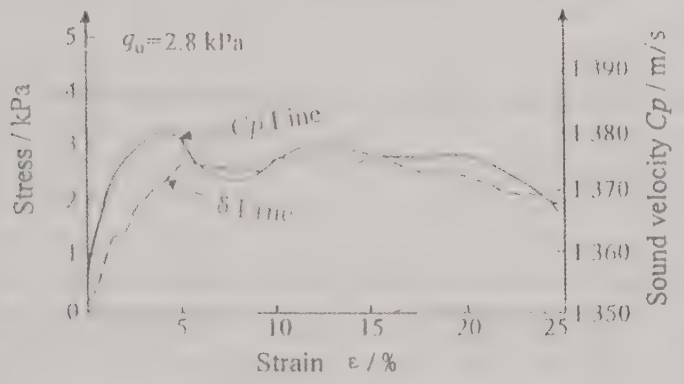

Fig. 1 Stress-strain/sound velocity measuring curve for silty clay sample

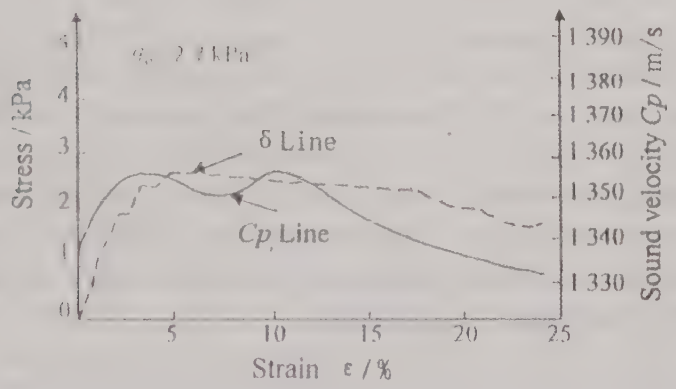

Fig. 2 Stress-strain/sound velocity measuring curve for clayey silt sample

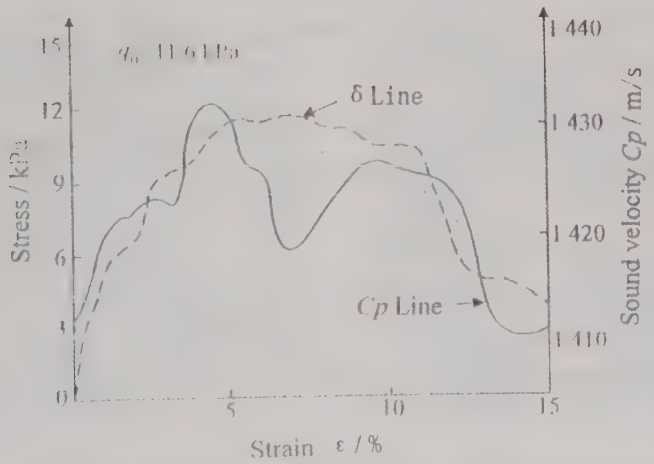

Fig. 3 Stress-strain/sound velocity measuring curve for silty sand sample

3 Analysis of the influence of microstructural change of sediments on the sound velocity in them

3.1 Stress is an important factor affecting the sound velocity of sediment.

The seafloor sediment in natural state is not, as presumed by the Wyllie model, suspended in the fluid medium with the solid grains not being contacted and cemented, but there are different ways of accumulation and mechanical coupling states between grains (LIANG Yuan-bo and LU Bo 1985). For the sediments with the same degree of porosity, the different shapes of grains and ways of grain accumulation, different statistically preferential orientations of various primary and secondary structural planes, such as microbedding, microfissure and long axes of pores, will result in quite different sound velocities. In recent years, the gradual development and in-depth application of the microtechniques in the study of the physical properties of sediment have made it possible to understand the microstructures of sediment. Toksoz cited the concept of pore shape spectrum. Zhu Zhengya introduced the pore structure factor K and Liang Yuanbo et al. used the sediment compression strength *qu* to represent the integrated factors that affect the sound velocity, such as the microscopic pore structure, grain accumulation pattern and mechanical coupling state, etc., of the sediments. These researches have demonstrated that the microstructure of sediment is an important factor affecting sound velocity and that, if there exists cementation between grains, the influence of microstructure on sound velocity is more obvious(LU Bo and LI Gan-xian et al. 1998). The experimental research in this study indicates that under the action of stress, the different microstructure states within the same sediment sample in different phases of the strain would result in the corresponding changes of sound velocities.

In order to probe the correlation between the stress and the sound velocity of seafloor sediment, a correlated regression analysis has been made for the corresponding changes between the stress and the sound velocity of part of the experimental samples. The result shows that the sound velocity in the seafloor sediment changes correlatively with the stress added on it. For the three typical sediment samples mentioned above, the results of correlated regression analysis are as follows:

For the silty clay, the regression equation is not generated because of the lower correlation coefficient between the stress and the sound velocity:

For the clayey silt, Cp=1 528.67+1.048 6 δ (R=0.800 5 F=39.251 6),

For the silty sand, Cp=1 409.38+1.626 5 δ (R=0.708 0 F=17.085 4)

Where Cp is the sound velocity of longitudinal wave; δ, the stress; R, the related coefficient; and F, the standard deviation.

It can be seen from the results of stress-sound velocity regression analysis of three typical sediment samples that for the silty clay which has the lowest mean values of sound velocity, the stress is poorly

correlated with the sound velocity, so the correlation regression equation cannot be got. For the silty sand and the clayey silt samples which have relatively higher sound velocities, the stress and the sound velocity are significantly correlated, and the higher the initial sound velocity is before the stress is applied, the better the correlation between the stress and the sound velocity is. This shows that the higher initial sound velocity indicates a closer contact between sediment grains and a good contact angle between them, and the contact plane between grains becomes larger as the stress increases, which would have effect especially on the closer contact of grains, leading to a higher degree of correlation between stress and sound velocity.

3.2 Analysis of the effect of microstructural change of the sediment on its sound velocity

As the bulk modulus of seawater is much larger than the sediment grains, the sound wave velocity of the sediment strongly depends on the quantity of pore water on the acoustic line, i.e., the void ratio on the acoustic line. But the mode of contact between sediment grains directly determines the void ratio in the acoustic propagation path. Obviously, the closer the grain contact on the acoustic line is, the higher the sound velocity is.

Observation and scanning have been made for the experimental samples under a 2 000-time electron microscope before and after loading of the stress (Fig. 4 and 5). It is found that under the electron microscope at the same scope, the internal grain structure of the same sediment has changed significantly after loading of the stress as compared with that before. After the stress loading, within 3% of the strain, the grains are closer, and the pores become less and smaller, and the small grains fill into the pores among large grains and the contact between grains changes from the point-side form to the side-plane form. And within 3% - 10% of the strain, the local compression within the sediment and the local hybrid fissure make the sound velocity fluctuation complicated, while after the stress passes the maximum value and the strain is larger than about 10%, the sound velocity drops along with the fracturing of sediment and decrease of stress.

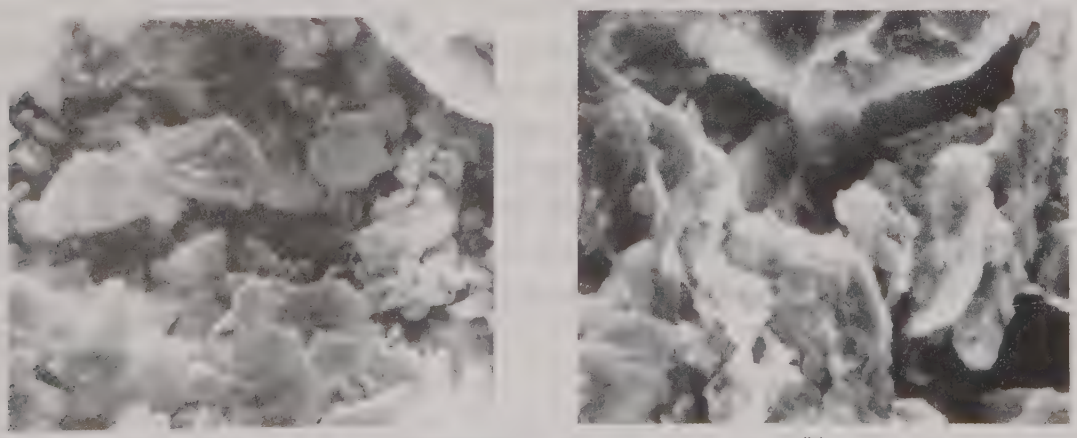

(a) (b)

Fig. 4 An electron microscope photo of the seafloor sediment microstructure before stress loading (x 2000)

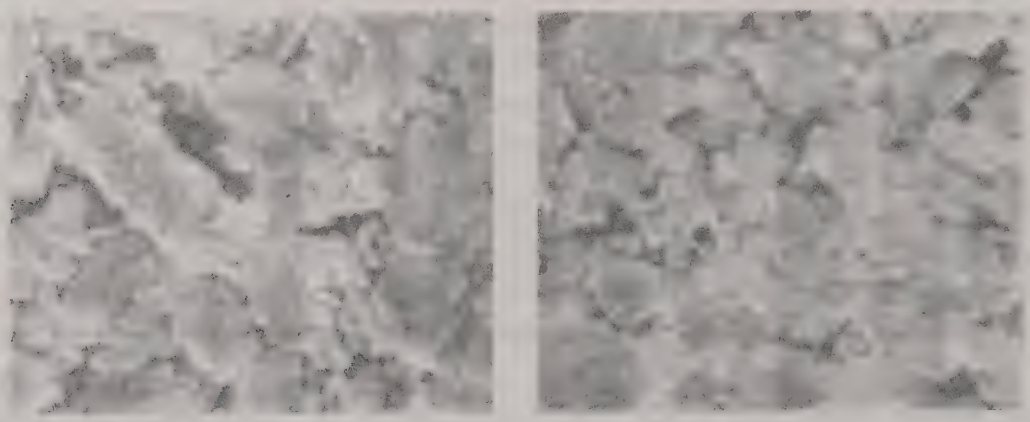

(a) (b)

Fig. 5 An electron microscope photo of the seafloor sediment microstructure after stress loading (x 2000)

5 Summary

It can be clearly seen from the theoretical analysis in this paper that the microstructural features of the seafloor sediment is an important factor affecting the sound velocity in it. It has been demonstrated by the synchronous measuring experiment on the stress-strain/ sound velocity of various typical seafloor sediment samples that the stress acting on the sediment affects its sound velocity by changing the contact modes between grains and their mechanical coupling states. The same seafloor sediment has different sound velocities in different stress states and strain phases. This research is of important significance both in theory and practice. In fact, the ground stress exists everywhere in the crustal surface including the seafloor and, in individual regions, the strong accumulation of ground stress may result in the stratigraphic inclination, fold or even fracture, and, corresponding to the microstructural change of sediment under the action of ground stress, its sound velocity also changes. Especially when the seafloor sediment is used as the basement of engineering carrier, e.g., in the case of oil platform and pipeline laying, etc., it would be subjected to a stronger stress and changes in its microstructure and sound velocity would occur accordingly. Under such circumstances, sound velocity should be take into careful consideration as an important parameter on which the seafloor engineering design is based. Therefore, it is essential to collect more specimens in the future research and make in-depth studies so as to develop a set of effective acoustic methods for telemetering the stress-strain state and phases of the seafloor engineering basement and serve the seafloor engineering construction and evaluation of its stability.

Acknowledgements

This article is funded by the Key Laboratory of Marginal Sea Geology, South China Sea Institute of Oceanology, Chinese Academy of Sciences (No. MSGL0606) and the China National Natural Science Fundation (Ratification No. 40876018, 40476020).

References

[1] Biot M A. Theory of propagation of elastic waves in a fluid-saturated porous solid [J]. J Acoust Soc Am, 1956, (28): 179 - 191.

[2] Wyllie M R J. Elastic wave velocities in heterogeneous and porous media [J]. Geophysics, 1956, 21(1-4): 41 - 70.

[3] Zhou Zhi-yu, Meng Jing-sheng. Acoustic estimations of porosity and thickness for thin soft surface layer of sea floor [J]. Marine Geology, 1988, (7): 211 - 219.

[4] Anderson R S. Statistical correlation of physical properties and sound velocity in sediments. Hampton L, ed. Physics of Sound in Marine Sediments [M]. New York: Plenum Press, 1974. 481 - 518

[5] Hamilton E L, Buchman R T. Sound velocity and related properties of marine sediments [J]. J Acoust Soc Am, 1982, (72): 1 891 - 1 904.

[6] Liang Yuan-bo, Lu Bo. On the effect of physico-geotechnical characteristics upon sound velocities of sea floor sediments [J]. Acta Oceanologica Sinica, 1984, 9(3): 313 - 320.

[7] Liang Yuanbo, Lu Bo. Physical mechanism of the mechanical property of seafloor sediment affecting its sound velocity [J]. Acta Oceanologica Sinica, 1985, 7(1): 111 - 117.

[8] Lu Bo, Li Gan-xian, Huang Shao-jian. Acoustic-physical property of submarine calcium soil in the South China Sea and its engineering geological implications [J]. Scientia Sinica, 1998, 28 (6): 518 - 522.

应力-应变过程中海底沉积物微结构变化对其声速的影响

李赶先，卢博，黄韶健

(中国科学院 南海海洋研究所 边缘海地质重点实验室，广东 广州 510301)

摘 要：本文阐述了对海底沉积物样品在应力-应变过程中进行同步声学测量的实验工具和方法，分析了采自北部湾45个站位的海底沉积物样品的实验数据资料，结果表明，沉积物颗粒越粗、孔隙越小、侧限抗压强度越大，声速越高。沉积物样品在受力变形过程中，声速具有明显的随应力变化的特征。进一步探讨了不同应变阶段沉积物的声学特征以及应力所导致沉积物微结构变化对其声速的影响过程，这一研究将在石油地质勘探和海底工程基底稳定性评价等方面具有重要的应用意义。

关键词：海底沉积物；应力-应变；微结构特征；声速；抗压强度

Fractal Analysis of Spatial Fault Distribution in the Southern South China Sea

YAO Yan-tao[1, 2], ZHAN Wen-huan[1]

1. *CAS Key Laboratory of Marginal Sea Geology, South China Sea Institute of Oceanology, Chinese Academy of Sciences, Guangzhou* 510301, *Guangdong province, China*
2. *Graduate University of Chinese Academy of Sciences, Beijing* 100049, *China*

Abstract: Fractal geometry can effectively quantify naturally nonlinear or much complicated phenomena, and fractal dimension is the quantitative parameter. In this paper, we applied fractal geometry to analyze spatial fault distribution of the southern South China Sea. Calculation results indicate that the spatial fault distribution of this area have remarkable fractal features in a non-scale interval of 25 - 250 km, with fractal dimensions of 1.660 1, 1.387 5, and 1.269 3 for all faults, NE-trending faults and NW-trending faults, respectively. These dimensions (capacity dimensions), obtained by box-counting method, represent well the characteristics of spatial fault distribution. Displayed by isoline-maps of fractal dimensions, faults in the study area arrange symmetrically along the spreading axis of the Southwest Sub-basin, and density of the NE-trending faults supplements to that of the NW-trending faults, revealing a property of mutual restriction between these two groups of faults. At last, by correlating the fractal features of spatial fault distribution with the evolution of the South China Sea and the distribution of oil or gas basins, we tried to reveal their relationships.

Keywords: fractal, box-counting method, faults, southern South China Sea

1 Introduction

Researches on the distribution, activity and formation mechanism of faults help greatly to understand crustal structure, tectonic evolution, minerogenesis, et al. [1], and thus become the basis of studies on geotectonics, geodynamics, perambulation and exploitation of mineral resources, engineering geology, and such like.

The South China Sea is a marginal sea formed by the interaction of three major plates, i.e. the Eurasian, Pacific and Indian-Australian plates. Faults are extremely developed, which have recorded the interaction process of these three plates and the evolution of the South China Sea. Basins bearing oil or gas are also widespread, whose types, structures and sub-tectonic units' distribution are controlled by faults [2]. Therefore, studies on faults, always regarded as one of the most crucial investigations of geology, has not only theoretical implication but also applied significance for the South China Sea. However, most previous researches focused on qualitative analysis, such as trending direction, structural characteristic

Received on January 17, 2008

and activity property. Quantitative researches were few, and mainly dealt with fault length, displacement and slip velocity.

Fractal geometry, introduced by Mandelbrot in 1975, provides a useful tool to study naturally nonlinear and complicated phenomena, and it has been widely applied to earth sciences [3-8]. With its continual development in theory, a new method for quantitative research on faults is available and has been successfully applied to this field [9-12]. Furthermore, many fractal analyses of fracture traces confirmed that distribution of various fractures appears to be self-similar. And, spatial fault distribution is not out of the case, with fractal dimension as a multi-indicator for its characteristics, including faults' quantity, assemble pattern, and even dynamic mechanism. As a result, fractal dimension can be a quantitative parameter representing the complexity level of fault structures [13].

Based on box-counting method, we probed into the fractal properties of spatial fault distribution of the southern South China Sea. It was the first time to apply fractal geometry to fault research in this area, so it was tentative and enriched the content of studies on faults of the South China Sea.

2 Methods

As to the orientation of faults in the South China Sea, different researchers will make different classifications. On the whole, however, it is dominated by two groups in strike (northeast and northwest). Therefore, in this paper we performed the calculations for this research in three cases, i.e. all faults of the area (AF), faults trending NE (NEF), and faults trending NW (NWF). Based on the first-scale and second-scale faults (including the spreading centers and transform faults of the South China Sea Basin) (Fig. 1) from the report of Qiu et al. [1], using box-counting method, fractal analyses of spatial distribution of AF, NEF and NWF in the southern South China Sea were carried out respectively, and corresponding isoline maps of fractal dimensions were plotted. As a result of making groups, faults trending NNE and NEE were operated as NEF, and faults trending NNW and NWW as NWF.

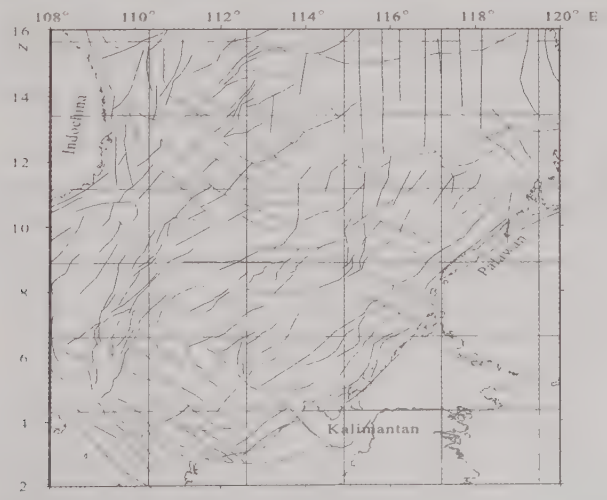

Fig. 1 Distributions of faults (from [1]) and square boxes (250 × 250 km^2)

2.1 Box-counting method

Box-counting method, also called covering method, is one of the most common techniques for calculating fractal dimension of a self-similar object, and the dimension obtained by this method is called capacity dimension (D_0). Calculation based on box-counting method will not be valid unless the fractal dimension is under or around 2 [14]. Generally, fractal dimension of spatial fault distribution is within a range of 1 to 2, so it can be obtained by the method discussed here. In this method, a grid of square boxes with side length r is superimposed on the investigated object, and then the number of boxes that are not empty $N(r)$ is counted. This procedure is repeated for as large a range of r-values as possible. If the investigated object is a fractal, a power-law relationship between $N(r)$ and r will come into existence.

$$N(r) = Cr^{-D}$$

here, C is a constant, and D is the fractal dimension of the object.

2.2 Calculating the fractal dimension of spatial fault distribution

Take AF for example, first covered the studied area with square boxes of side length 250 km from the left lower corner to the right upper corner (Fig. 1) and deleted those less than one box in the marginal areas; then, counted the number of occupied boxes; next, changed the side length into 125, 62.5, 50, 31.25 and 25 km, and counted the corresponding numbers respectively; at last, plotted the numbers $N(r)$ of the occupied square boxes versus the side lengths (r) in a double-logarithmic graph, and used straight line to fit their relation by least-square method. Finally, the slope of the straight line was the fractal dimension of AF that we aimed to obtain. When calculating those of NEF and NWF, just follow the same process described above.

2.3 Plotting the isoline map of fractal dimensions

In order to plot the isoline map of fractal dimensions, the studied area has to be divided into many small sections, and fractal dimension of each section will be calculated, which is regarded as the value of the central point. The isoline map can be achieved by interpolation. When dividing the studied area, section size should not be too big or too small. If too big, the isoline map would be poor in precision; while, if too small, it would be very difficult to calculate all the fractal dimensions. In this research, we used square boxes with side length of 200 km to cover the studied area and chose 33 sections with numbers from 1 to 33 (Fig. 2). Fractal dimension of each section was calculated also by the method discussed in 2.2. Side lengths for covering each section were 100, 50, 40, 25 and 20 km. In this part, the calculation was operated respectively under three cases, i.e. AF, NEF and NWF.

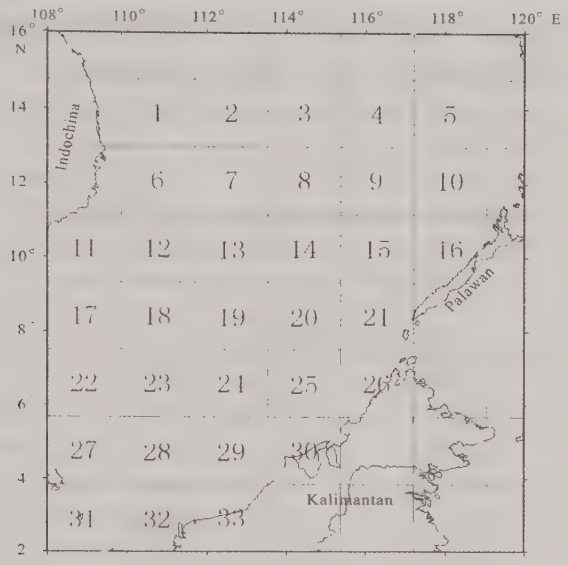

Fig. 2 the 33 dividing sections

3 Results and discussions

3.1 Fractal characteristics of spatial fault distribution

Statistical data about the studied area covered with full square boxes of 250 km × 250 km are listed in Tab. 1. From the data, we can see that spatial distributions of AF, NEF and NWF are remarkably self-similar or scale-invariant in the scale interval of 25 - 250 km. Thus, they are fractals with dimensions of 1.660 1, 1.387 5 and 1.269 3, respectively. Fig. 3 is the double-logarithmic graph showing the degree of linear fitting.

Tab.1 Statistical data about the studied area

r / km	N / r			Correlation coefficient			D_0		
	AL	NEF	NWF	AL	NEF	NWF	AF	NEF	NWF
250	28	27	23						
125	102	85	62						
62.5	357	234	161	0.996 7	0.995 2	0.997 6	1.660 1	1.387 5	1.269 3
50	506	321	202						
31.25	970	537	340						
25	1222	639	424						

As AF include faults striking NE, NW, S—N and E—W, the amount of AF is consequentially larger than those of NEF and NWF. When in fractal dimension, its value is accordingly higher than those of the later two. This positive correlation also exists between NEF and NWF. Thus, with extrapolation fractal dimension of spatial fault distribution is an indicator for fault density. The higher, the denser.

Specially, we should point out that the statistical area includes some regions lacking fault data, like the Indochina, Kalimantan, and Sulu Sea.

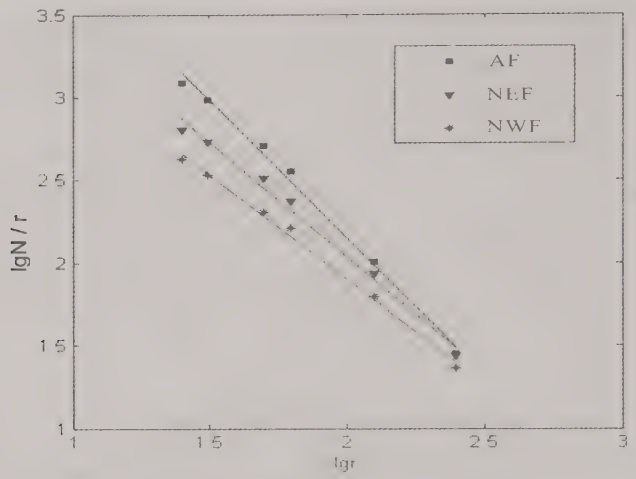

Fig. 3 double-logarithmic graph of spatial fault distribution

As a result, the fractal dimensions we obtained are a little bit lower than their actual values. Therefore, the fractal dimensions of spatial distributions of AF, NEF and NWF in the southern South China Sea should be higher than 1.660 1, 1.387 5 and 1.269 3, respectively.

3.2 Characteristics of isoline maps

3.2.1 All faults

From Tab. 2, we can see that the distribution of AF in each section is statistically self-similar within the scale interval of 20 - 100 km. All correlation coefficients are above 0.98 with 29 ones above 0.99, and all fractal dimensions are above 1.1 with 17 ones above 1.5. Shown in Fig. 4, there are three visable characteristics of the isoline map: (a) High values mainly center in the Zhongjiannan Basin—Wan'an Basin. Influenced by the western marginal fault zone, large numbers of sub-faults striking NNE—SN—NNW developed in this area and ranged along the fault zone. (b) Low values mainly center in the South China Sea Basin. In this basin most faults are composed of the spreading axis and its perpendicular transform faults. Particularly, low values in northwest of the Kalimantan are attributed to section 30, 31 and 33 which lie in the marginal area with most fault data absent. (c) Along the spreading axis of the Southwest Sub-basin, isolines arrange symmetrically. Influenced by the spreading and thermal subsidence of the South China Sea Basin, extensional faults trending NE and strike-slip faults trending NW were formed on both sides along the spreading axis.

3.2.2 NE-trending faults

Except that section 4, 5, 31 and 32 are empty and that correlation coefficient of section 1 is under 0.9, correlation coefficients of other sections are all above 0.9 (Tab. 2). However, this doesn't mean that distributions of NEF in these sections bear remarkable properties of self-similarity. In fact, most fractal

dimensions are low in value. Even some are under 1, suggesting that the NEF traces in the corresponding sections are not statistically self-similar in the scale interval of 20 km - 100 km or this interval is not a non-scale interval for the sections. Therefore, those isolines with values under 1 hadn't been plotted in Fig. 5.

Tab. 2 Statistical data about the 33 sections

Section number	AF		NEF		NWF	
	Correlation coefficient	D_0	Correlation coefficient	D_0	Correlation coefficient	D_0
1	0.993 9	1.633 1	0.882 9	0.676 1	0.986	1.289
2	0.993 7	1.669 9	0.992 5	1.462 4	0.995 1	0.938 9
3	0.997 7	1.425 7	0.967 5	0.877 6	0.996 4	0.938 3
4	0.990 9	1.222	0	0	0	0
5	0.993 4	1.276 8	0	0	0.959	0.9 41 4
6	0.991 4	1.581 6	0.997 7	1.185 7	0.989 5	1.159 9
7	0.991 7	1.521 4	0.995 9	1.126 5	0.965 3	1.194 2
8	0.993 4	1.366 3	0.990 3	1.181	0.991 5	0.964 4
9	0.992 3	1.422	0.984 1	0.967 5	0.978 9	0.764 7
10	0.998 9	1.435 5	0.996 5	1.231 2	0.993 8	1.358 3
11	0.989 4	1.469 6	0.980 6	1.331 4	0.831 1	0.418 6
12	0.998 7	1.631	0.994 3	1.420 7	0.995 7	1.077
13	0.993 6	1.3 20 9	0.976 3	1.079 4	0.994 4	1.121 2
14	0.992 6	1.409 2	0.990 2	0.955	0.835	0.294 1
15	0.993 9	1.597 4	0.993 8	1.274 7	0.992 6	1.235
16	0.990 7	1.514 7	0.979 4	1.3438	0.610 3	0.3
17	0.987 7	1.530 2	0.981 4	1.412	0.902 4	0.701 3
18	0.994 3	1.584 5	0.993 1	1.497 7	0.976 7	0.695 4
19	0.989 2	1.489	0.994 2	1.176 9	0.994	1.140 1
20	0.998 6	1.477 9	0.998 5	1.234 1	0.988 4	1.205 4
21	0.993 1	1.525 5	0.983 7	1.192 3	0.994 8	1.078 2
22	0.996 7	1.697 6	0.997 5	1.189	0.991	0.971 3
23	0.995 5	1.515	0.972 7	1.151 4	0.986 7	1.492 9
24	0.993 4	1.558 1	0.992 7	1.391 7	0.979 3	1.138 9
25	0.997 7	1.500 9	0.995 9	1.452 5	0	0
26	0.997 8	1.583 7	0.993 6	1.493 9	0.963	0.737 5
27	0.995 3	1.463 8	0.991 2	0.865	0.991 6	1.248 8
28	0.994 4	1.379 2	0.932 8	0.696 3	0.985 5	1.274 3
29	0.987 7	1.457 9	0.989 4	1.073 8	0.990 8	0.982 6
30	0.999 6	1.129 7	0.977 9	1.016 6	0.991 7	0.999 5
31	0.997 3	1.181 6	0	0	0.997 8	1.167 5
32	0.998 4	1.535 7	0	0	0.996 4	1.508 4
33	0.999 2	1.506 5	0.997 3	1.178 3	0.993 4	1.43

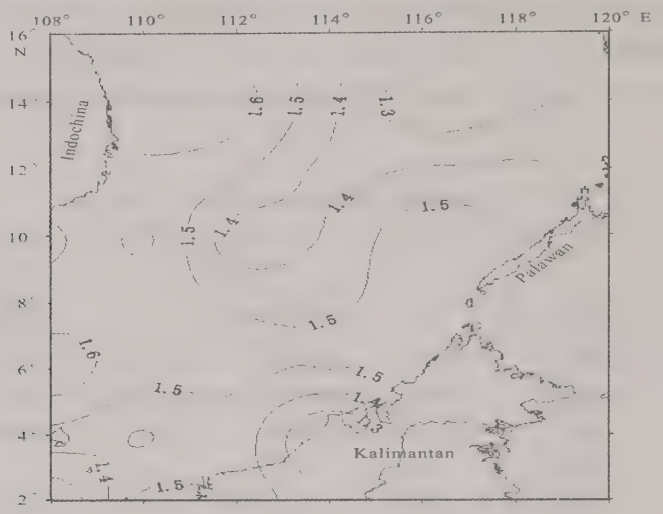

Fig. 4 Fractal dimension isolines of AF

Comparing Fig. 5 with Fig. 4, it would be found that the isoline arrangements of these two figures have much in common, especially in the South China Sea Basin. This indicates that the NE-trending faults, among all faults, are the most developed. Characteristics of the isoline map of NEF can be summed up as follows: (a) High values, up to 1.4, mainly center east of the Indochina and in the eastern Wan'an Basin—Sabah Basin. Influenced by the western marginal fault zone, a series of NNE—NE trending faults developed in the eastern Zhongjiannan and Wan'an basins. On the other hand, subduction of the Nansha Trough led to a range of reverse thrusts in the Sabah Basin, with some extensional and strike- slip faults in addition [1]. (b) Low values mainly center in the South China Sea and Zengmu basins. As the Zengmu Basin lies in the southwestern end of the South China Sea, most faults in this area strike NW. (c) Isolines arrange symmetrically along the spreading axis of the South China Sea Basin.

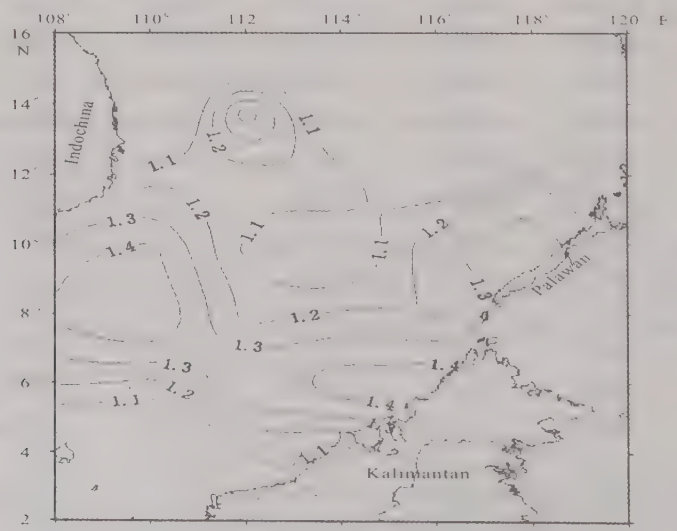

Fig. 5 Fractal dimension isolines of NEF

3.2.3 NW-trending faults

Except section 4, 11, 14, 16 and 25, correlation coefficients of other sections are all above 0.9 (Tab. 2). Since the NWF is not so well as the NEF both in development degree and in distribution homogeneity, fractal dimensions of the NWF in most sections are much lower than those of the NEF. Besides two empty sections, 14 sections have dimensions under 1 and only 9 ones are above 1.2. The isolines with values under 1 also hadn't been plotted in Fig. 6. As a result, Fig. 6 shows very thin isolines. Its features are as follows: (a) High values mainly center in the Zengmu Basin, where a great deal of second-scale faults trending NW were formed because of being sandwiched by the Lupar and Tinjar faults. (b) High and low values in Fig. 6, on the whole, correspond respectively to the low and high values in Fig. 5, revealing a relationship of mutual restriction between the NEF and the NWF during their development process.

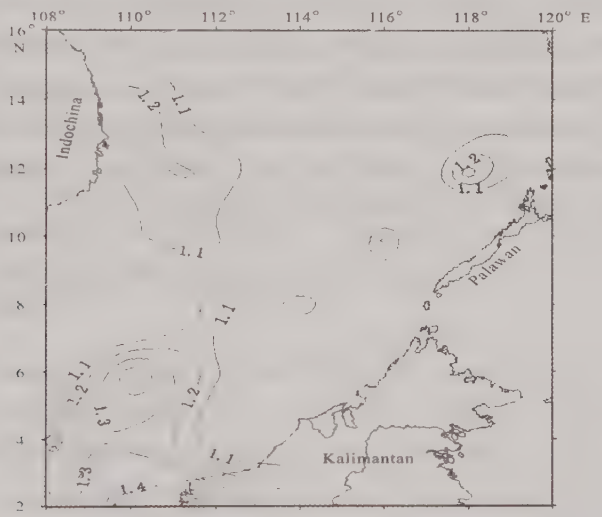

Fig. 6 Fractal dimension isolines of NWF

3.3 Relationship between fractal characteristics and tectonic evolution of the South China Sea

Systematic analysis of faults in the studied area can provide important insight into the formation and evolution of the South China Sea. The fractal dimension of all faults in the southern South China Sea, up to 1.66, implies the intensive interaction of the Eurasian, Pacific and Indian-Australian plates. Since the NE-trending faults are the most developed in this area, its fractal dimension up to 1.39 is relatively high. Among this group, extensional faults are dominant, and reverse thrusts next which resulted from the subduction of the southern margin. As showed in Fig. 5, high dimension values center around southeast of the Indochina and in the eastern Wan'an Basin—Sabah Basin, which mainly attributes to the continental-margin-spreading faults on both sides of the South China Sea Basin. Since the Cretaceous, as the Pacific Plate subducted toward the Eurasian Plate, back-arc spreading had resulted in a series of marginal rifts and NE—NNE trending faults [15], whose activities were inherited and cyclical. Obviously, the

formation and evolution of the South China Sea Basin have been controlled by these faults. In contrast, the NW-trending faults, with fractal dimension of 1.27, are not so developed as the NE-trending faults. Due to the restriction from the NE-trending faults formed earlier, the NW-trending faults formed later mostly developed in the area with few or no pre-existing faults. As a result, high fractal dimension values of the NWF mainly center in the Zengmu Basin, tectonic structure of which was controlled by the collision of the Zengmu Block with the Borneo Block and the combined actions of the Lupar and Tinjar faults. During the Miocene, as the spreading of the Southwest Sub-basin getting weakened, the Zengmu Block pressed southward by the Indochina Block, and the Sabah accretion zone thrusting northwestward, the Tinjar Fault turned to be dominated by sinistral movement and, at last, resulted in many NWW-trending faults and NE-trending folds [16].

3.4 Relationship between fractal characteristics and basins bearing oil or gas

According to available publications, some preliminary studies about the relationship between fractal characteristics of spatial fault distribution and mineral deposits or hydrocarbon basins have been carried out. However, their relationship is still being questioned, because there are so many factors have to be put into consideration. As to this between fractal characteristics and hydrocarbon basins, it relates to the formation order of faults and basins, the conditions of source and reservoir, and cap rocks. Therefore, to understand their relationship demands concrete and systematic analysis.

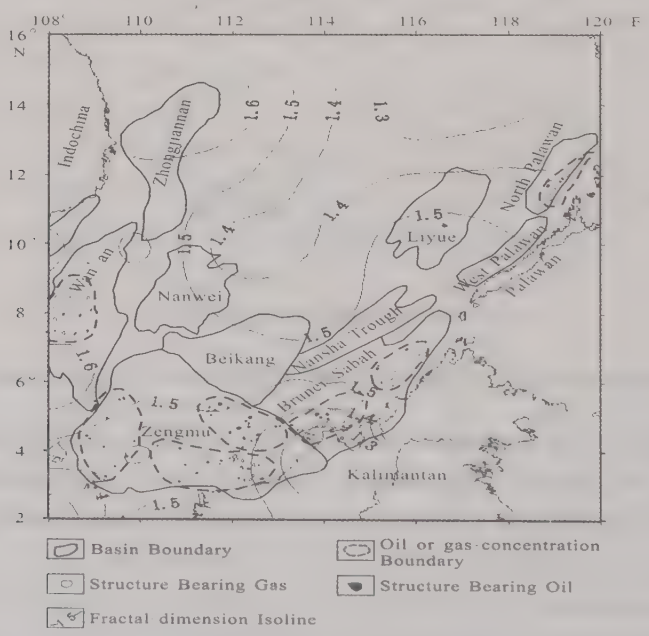

Fig. 7 Distributions of hydrocarbon basins (from [17]) and fractal dimension isolines

Displayed by Fig. 7, the accumulation zones of oil or gas in the southern South China Sea correspond more or less to the areas of high fractal dimension values, but still more work has to be done to know the exact relation and, further, the mechanism.

4 Conclusions

Faults are extremely developed in the South China Sea. They are information media for the interaction of the Pacific, Eurasian and Indian-Australian plates and the evolution of the South China Sea. This paper focuses on the fractal properties of spatial distribution of the first-scale and second-scale faults in the southern South China Sea. Results show:

(a) Fractal dimension of fault traces obtained by box-counting method can well represent the development degree of faults; isoline map of fractal dimensions can reflect not only the development degree but also the distribution homogeneity of faults. Thus, fractal dimension is a quantitative indicator for spatial fault distribution.

(b) Spatial fault distributions in the southern South China Sea are statistically self-similar within the scale interval of 25 km - 250 km. The fractal dimension 1.66 of all faults suggests that faults develop quiet well in this area, and the fractal dimension 1.39 of the NE-trending faults larger than 1.27 of the NW-trending faults reflects that the former group is more developed than the later one.

(c) High and low fractal dimension values of the NE-trending faults correspond respectively to low and high values of the NW-trending faults, showing certain mutual complementation between these two groups of faults in spatial distribution, and consequently revealing a relation of mutual restriction during their development process.

(d) Fractal characteristics of spatial fault distribution, to a certain extent, help to understand the tectonic evolution of the South China Sea. From the distribution map of dimension isolines and hydrocarbon basins, accumulation zones of oil or gas correspond more or less to high fractal dimension values.

To sum up, this research confirms that the application of fractal geometry to spatial fault distribution is feasible. It is an advanced method for quantitative research on faults and has vast prospect. However, there are still some problems in the process of application. For instance, no criterion is available for researchers to count the occupied box, and fractal dimension of the same investigated object would vary with different scale interval. Further questions, such as the relation of fractal dimension with stress field and dynamic mechanism, also need to be probed into.

Acknowledgements

This study is supported by the National Natural Science Foundation of China under contract No. 40476026 and the Guangdong Natural Science Foundation under contract No. 04001309.

References

[1] Qiu Y, Zeng W J, Li T G. Fracture systems and their tectonic significance in the central and southern parts of the South China Sea [J]. Geotectonica et Metallogenia, 2005, 29(2): 166 - 175.

[2] Wei X. Fault-system control to hydrocarbon-bearing basins in Nansha sea area of the South China Sea [J]. Marine Sciences, 2005, 29(6): 66 - 68.

[3] Xie H P, Wang J A, Kwaśniewski M A. Multifractal characterization of rock fracture surfaces [J]. International Journal of Rock Mechanics and Mining Sciences, 1999, 36: 19 - 27.

[4] Han X Q, Li J B, Wang Y, et al. Application of fractal theory to distribution of polymetallic nodules from the Pacific Ocean [J]. Acta Oceanologica Sinica, 2001, 23(3): 142 - 146.

[5] Jia Y G, Fu Y B, Xu G H, et al. The fractal characteristic change in the Huanghe River Estuary due to the hydrodynamic conditions' variation [J]. Acta Oceanologica Sinica, 2003, 22(2): 191 - 200.

[6] Volland S, Kruhl J H. Anisotropy quantification: the application of fractal geometry methods on tectonic fracture patterns of a Hercynian fault zone in NW Sardina [J]. Journal of Structural Geology, 2004, 26: 1 499 - 1 510.

[7] Xu J D, Huang J F, Wei F Q, et al. Correlation fractal and multifractal characteristics of seismic activity in the Taiwan area, China [J]. Acta Geologica sinica, 2005, 79(2): 225 - 232.

[8] Dai Z J, Li C C, Wang W J, et al. Research on stability and fractal of arc-shaped coast in South China [J]. Acta Geologica sinica, 2006, 28(1): 176 - 180.

[9] Shi Z J, Luo Z T, Peng D J, et al. Multifractal characteristics of fault spatial distribution in Sichuan area [J]. Geoscience, 1995, 9(4): 467 - 474.

[10] Nanjo K, Nagahama H. Fractal properties of spatial distributions of aftershocks and active faults [J]. Chaos, Solitons and Fractals, 2004, 19: 387 - 397.

[11] Pérez-López R, Paredes C, Muñoz-Martín. Relationship between the fractal dimension anisotropy of the spatial faults distribution and the paleostress fields on a Variscan granitic massif (Central Spain): the *F*-parameter [J]. Journal of Structural Geology, 2005, 27: 663 - 677.

[12] Ding S J. Fractal analysis on fault system in central and western Hainan gold metallogenic province [J]. Earth Science Frontiers, 2004, 11(1): 189 - 194.

[13] Xie Y S, Tan K X. Fractal research on fracture structures and application in geology [J]. Geology-Geochemistry, 2002, 30(1): 71 - 77.

[14] Chen Y, Chen L. Fractal Geometry [M]. Beijing: Seismology Press. 2005.

[15] Ding W W, Chen H L, Yang S F, et al. Geological and geophysica analysis of the Southwestern and Eastern sub-basins, South China Sea [J]. Geological Journal of China Universities, 2002, 8(3): 268 - 279.

[16] Zhong G J, Wu J M, Wang L L. Characteristics of strike-slip system and its relation to oil and gas in the south-west area of the South China Sea [J]. Journal of Ocean University of Qindao, 1995, 25(4): 495 - 502.

[17] Liu Z H. Distribution of sedimentary basins and petroleum potential in southern South China Sea [J]. Geotectonica et Metallogenia, 2005, 29(3): 410 - 417.

南海南部断裂的分形研究

姚衍桃[1,2]，詹文欢[1]

（1. 中国科学院 南海海洋研究所 中国科学院边缘海重点实验室，广东 广州 510301；
2. 中国科学院 研究生院，北京 100049）

摘 要：分形几何作为定量描述自然界中复杂非线性现象的强有力工具，将其应用于南海南部断裂体系的研究中，通过数盒子法计算了断裂分布的分维值。研究结果表明这种方法是可行的，断裂分布的分维值能有效地描述断裂的空间分布特征。南海南部断裂体系在标度区间 25 ～ 250 km 内具有很好的统计自相似性，全部断裂的分维值为 1.660 1，北东向断裂的为 1.387 5，北西向断裂的为 1.269 3。根据断裂分维等值线，沿西南海盆扩张轴，两侧断裂呈对称展布；北东向的与北西向的在空间上有一定的互补性，这反映了两组断裂在发育过程中的相互制约性。结合南海的构造演化及南海南部油气盆地的分布，初步探讨了断裂分形特征与南海的构造演化及断裂分形特征与油气盆地分布之间的关系。

关键词：南海南部；断裂；分形；数盒子法

Research on the Model of Coastline Demarcation and Management

LIN Ning[1], HUANG Nan-yan[1], XU Wen-bin[1, 2]

1. National Marine Data and Information Service, Tianjin 300171, *China*

2. Ocean University of China, Qingdao 266003, *Shandong province, China*

Abstract: The coastline demarcation and announcement models in China are outlined in this paper. The issues related to the coastline revision system, coastline zoning, coastline usage and the coastline information management are put forward. The concreted research and discussion on these issues are made which are valuable for the coastline management in our country.

Keywords: Coastline; Demarcation; Management; Models

1 Introduction

The Law of the People's Republic of China on the Administration of the Use of Sea Areas and the Law of Land Administration of the People's Republic of China form the basic system of management ownership in our country sovereignty domain. From the geographical scope, the two laws take the coastline as a dividing line. Together they cover the whole sovereignty area of China. But in the real world, due to the effects of natural factors and the human activities' interference, it is difficult to demarcate the coastline.

The difficulty of determination of the coastline leads to the different understanding of the coastline, which results in the unclear management of land and sea authority and triggers the conflict of interest. Thus, our country pays much attention to the job of demarcation of the coastline. In 2002, the Office of the State Department issued "The Circular of the Office of the State Department on Certain Issues Regarding Developing the Provincial and Country Level Sea Area Administrative Boundary Survey". The Circular makes it clear that the coastline demarcation is the basic job of provincial and country level sea area administration boundary survey.

2 Patterns of coastline demarcation

The coastline demarcation is an important foundation and technical work to demarcate the coastline and identify the land and sea management boundaries. At present, the technical methods, theory systems and reference models concerning the coastline demarcation have not been formed yet. National and local administrative departments in charge of marine administration pay much attention to the coastline demarcation, and have launched the researches and pilot projects of the coastline demarcation.

Received on September 18, 2008

2.1 In situ measurement

According to the actual situation, the location of the various types of coastline is identified and determined, and the in situ measurement using GPS technology is applied. The advantages of the in situ measurement are that the data are accurate and in line with the actual situation at the scene. The disadvantage of taking in situ measurement is that it involves many human and financial resources.

2.2 Remote sensing information extraction

Using remote sensing to extract coastline information means acquiring coastline information through computer analyzing on the satellite image data by using image processing software, GIS and the remote sensing image of multi-satellite observations and multi-space scale according to the spectrum features of coastal ground objects. The advantage of using remote sensing to extract coastline information is that the information processing speed is fast. People can survey and map the coastline rapidly and quasi-synchronously. The disadvantages are that more input is needed to ensure the high resolution remote sensing data with high-resolution, and the acquisition of remote sensing data is subject to restrictions on certain weather conditions.

2.3 Amendment on the topographic map

Amendment on the topographic map means the measurement is based on the coastline in the latest version of 1:50 000 or 1:10 000 basic scale topographic maps. The topographic map is mapped in accordance with the law and is published in accordance with established procedures. The topographic map has the force of law. The advantages of amendment on the topographic map are that it is easy to do and the amendment takes less time. Due to the long update cycle, some changes of coastline during the publication period could not be taken into consideration, it is difficult to make the real up-to-date maps to mark the coastline.

2.4 Combination of different patterns

In the practical work of coastline demarcation, the different patterns should be taken to get the complementary advantage according to the actual situation. Practical and feasible solution is to mainly take in situ measurement in the area where it is easy to measure and where there are larger changes in the coastline. And where there is not easy to take in situ measurement and where there is few changes in the coastline, people can mainly take the other two kinds of methods of remote sensing information extraction or amendment on the topographic map.

3 The principles of the coastline demarcation

The scientific character should be taken into consideration in the job of the coastline demarcation. The coastline demarcation should accord with the scientific definition of the coastline. The historical

perspective of the coastline should also be taken into consideration. The principles, methods and the results of the coastline demarcation are universal through the country. The principles, methods and the results of the coastline demarcation should accord with the fact. The demarcated coastline should have the stability and the operation ability in the practice. The principles to be followed during the coastline demarcation are as follows:

3.1 Principle of science

The coastline demarcation should strictly follow the relevant national laws and regulations and relevant technical standards.

3.2 Principle of inheritance

The coastline which was formed historically and did not have changes keeps invariable.

3.3 Principle of common use

The principles, methods and the results of the coastline demarcation are universal.

3.4 Principle of applicability

The coastline demarcation should accord with the fact and be beneficial to the management, protection and the sustainable development of the marine and land resources.

3.5 Principle of stability

The demarcated coastline should have the relative stability, be easy to figure out and have the operation ability in the actual working.

Based on the above principles, the special principles should be observed according to the characters of the different types of the coastline and the local conditions. For example, for the estuarine coastline, which is an important part of the continental coastline, we should take into account our national interests, uphold the scientific approach of seeking truth from facts, and adhere to such principles as fairness, justice and publicity during its demarcation. Also the principle should be carried out about all benefits covered to ensure the estuarine coastline demarcated reasonably. In the demarcation of estuarine coastline, while sticking to the basic principles of the coastline demarcation, consideration to comprehensive principle, economic principle, ecological principle and the principle of easy resolution should be given for the estuarine specificity.

4 The technique of the coastline demarcation

4.1 The technique of the demarcation of the natural coastline

4.1.1 The rock coastline

The rock coastline is usually a coastline which is formed naturally and locates where mountains or

hills extend to adjoin the ocean. The demarcation of this kind of coastline is suggested to demarcate along the side of the natural coastline which faces the ocean.

4.1.2 The estuarine coastline

The demarcation of the estuarine coastline is a complicated job. The actual situation interlacing natural, social and economic development determines the multi-sided influencing factors which affect the demarcation of the estuarine coastline. When the natural factors such as estuarine coastline morphology, geology, geomorphology, hydrology and biology are the main control factors, these natural factors should be the basis of the demarcation of the estuarine coastline. Under this circumstance, there are the approaches of topography, geomorphology, hydrology and biology, et al.

4.1.3 Other kinds of natural coastline

As for other kinds of natural coastline such as sandy coastline, muddy coastline and biological coastline, the demarcation should demarcate along land-sea trace line of the mean high water. Further special judge is necessary according to the abrasion terrace, beach deposit or shore plants.

4.2 The technique methods of the demarcation of the artificial coastline

4.2.1 Sea embankment

The sea embankment is one of the major measurements which prevent the sea waves from damaging the coastal areas. It is divided into main embankments and common embankments. The structures mainly include the vertical style, slope style and mixed style. For the sea embankments, The seaward boundary of the embankments can be the demarcation line.

4.2.2 Ports and docks

The outer margin of the harbor basin could be the demarcation line. The seaward of marginal quay could be the coastline. As for bridge dock and trestle wharf, the legato of the docks which connects the lands can be the demarcation line.

4.2.3 Estuarine coastline

Generally, with the high social and economic development level, the estuarine areas are under the influence of the artificial factors. There are many artificial coastlines. Under these circumstances, the social factors such as the administration, transportation, shipping, water conservancy, fishery and economy should be taken into consideration. The social factors may decide the demarcation of the coastline.

4.2.4 Other kinds of artificial coastline

According to the definition of the coastline and the principles of the coastline demarcation, other kinds of artificial coastline can be demarcated according to actual situation with references to above

artificial coastlines demarcation techniques.

5 Models of coastline announcement

The demarcation of the coastline is a kind of complicated technical job, and a kind of management which involved multi-departments. During the process of the demarcation of the coastline, the government plays a very important role. The local governments take different models to announce the coastline at the management level after finishing the demarcation of the coastline technically.

5.1 In the form of government documents

Longhai city, Fujian province approved "The Advices about the Definition of the Sea Area Range of the Longhai City" on October 30, 2002, which identify the coastline of Longhai city in principle in the form of people's government documents.

5.2 In the form of orders

This kind of model is represented by the demarcation of Jiangsu province coastline. "The Orders of Jiangsu Province on the Administration of the Use of Sea Areas (Draft)" was deliberated and approved in principle by the Jiangsu province government executive meeting on March 17, 2005. There are regulations in the Article 2 of the order, "For the purpose of this order, the sea areas refer to the sea surface, water volume, seabed and subsoil of the inland waters and territorial seas extending from the coastline side of Jiangsu province to the sea. According to the national standardization, the coastline in Jiangsu province is demarcated by the municipal government which is divided into districts along the sea side. The plans should be submitted to the competent province administrative department in charge of marine administration for the record."

5.3 Approved by the government after taking measurement by the technical support department

This kind of coastline announcement model is represented by the Tianjin coastline demarcation. The result of the Tianjin coastline measured by the technical support department and calibrated by the survey and mapping department was approved by the Tianjin municipal government on August 5, 2007. The result of the Tianjin coastline demarcation is used as a basis of the land and natural resources and marine resource management of Tianjin.

6 Research on the coastline management

The dynamic management of the coastline will be a new important part of the sea area management as soon as the demarcation and announcement of the coastline is finished. The demarcation of the coastline transforms the coastline from a theoretically mean high water line into a sea-land demarcation line which acts as the demarcation line of sea-land management. But in the real management, it is not a simple line to manage.

6.1 Establishment of the revision system

The location and the length of the coastline are in dynamic change. Most of the natural coastline change relatively slow under the natural circumstances. But the human developments such as reclamation from the sea, damming the streams, sand and coral reef excavation, mangrove logging and ports construction usually lead to the change of the coastline in short time. Thus, the revision system of the coastline should be established in coastline management, in which the work procedure, work method, time and revision of the coastline should be included. The revision system will promote the dynamic management of coastline.

In the concrete work of coastline demarcation, different revision models can be adopted according to the actual situation. The first model is that the national administrative departments in charge of marine administration provide the comprehensive services. According to concrete conditions of coastline changes, the administrative departments in charge of marine administration are in charge of the implementation of the revision of coastline. The second model is that the revision is led by administrative departments in charge of marine administration, and the concrete organization of revision is implemented by the enterprises or individuals who use the coastline. The third model is that after receiving the submission of the application from the enterprises or individuals, the administrative departments in charge of marine administration organize the job of the coastline revision. The concrete works are completed by the technological support units which own the surveying and mapping qualification certification. The revision results should be submitted to the administrative departments in charge of marine. They are going to come into force after being audited by the administrative departments in charge of marine administration which will make a uniform management.

6.2 Paying more attention to coastline zoning

With the economic and social development, the coastline which used to be a kind of natural resource being free for use has gradually became a kind of shortage resources or rare natural resources. Without well protection and ordered utilization, the coastline is going to be the bottleneck which is barrier of economic development and thus does harm to the sustainable development. Therefore, based on the marine functional zoning, the coastline zoning should be made according to the natural and social characters of the coastline. According to the location condition, nature environment, natural resources, the status of protection and development and the needs of social economic development, the coastline could be divided into different function zones which have different usages or different function zones which need different environmental quality according to the function standard of the coastline. The coastline zoning should be according to the coastline function standards. The coastline zoning aims to control and lead the usage direction of specific coastline function zone, protect and improve the marine ecological environment, and promote the sustainable use of the marine resources.

Based on the coastline zoning, the coastline regional utilization planning should be formulated. This

planning should be involved in the planning systems of the sea area uses. The strategic targets of the coastline development and utilization, management planning, the main problems needed to be solved, action plan and specific measures should be involved in the coastline regional utilization planning.

6.3 Enhancing the coastline use management

There are the regulation in the Article 18 of Law of the People's Republic of China on the Administration of the Use of Sea Areas, "Use of sea areas for the following projects shall be subject to examination and approval by the State Council: (1) a project that involves filling of more than 50 ha. of the sea area; (2) a project that involves enclosure of more than 100 ha. of the sea area; (3) a project that involves the use of more than 700 ha. of the sea area without altering the natural attributes of the area; (4) major national construction projects; and (5) other projects specified by the State Council". In this article, the area of the project is mentioned, but this article does not figure out the coastline length which the project occupies. Given the same area of the sea area, the longer the coastline is occupied, the less utilization of the coastline we can get.

To better use and protect the coastline, a series of supporting systems which are related to the coastline use management should be established. The standard of the length of the coastline occupied by the project should be designed according to the article 18 of Law of the People's Republic of China on the Administration of the Use of Sea Areas. In order to prevent the waste and the unreasonable utilization of the coastline, the project of which the length exceeds the standard of the length of the coastline should be submitted to the State Council, and the project of which the length is below the standard of the length of the coastline should be submitted to the sectors of the government of the province, autonomous region and municipality directly under the Central Government.

6.4 Implementation of coastline information management

With the change of the coastline and the time passing by, information management of the coastline with the utilization of the 3S (GIS, GPS and RS) technology and the information technology would be the important ways to develop, utilize, protect and manage the coastline.

In the dynamic management of the coastline, spatio-temporal data management model could be used to divide the coastline into the history coastline and the current status of coastline. By researching the relationship between the history coastline and the current status of coastline, the functions of dynamic management such as the history reconstruction of the coastline, the backtracking of the change of the coastline usage, and the spatial overlay analysis of coastline usage can be made.

7 Discussion

The demarcation of coastline transforms the coastline from a theory mean high water line into a sea-land demarcation line in a scientific sense, also the demarcation of coastline solves the unclear management or the overlap of land and sea authority in a management sense. The demarcation of

coastline is beneficial to the effective implementation of relevant laws and regulations. It is the effective method to achieve the marine sustainable development.

The demarcation of coastline means a new beginning in the sea area management. After the research on the demarcation of the coastline and the management models, the authors hold that there exists some large difference for the job between the demarcation of coastline and its management. It is needed to do further research to achieve the effective coastline management, make it quantitative and institutional, and make it have the operational value.

References

[1] Sun Shu-xian. Determine the Sea-land Management Line Reasonably, Totally Fulfill the Basic System of Management Ownership of Sea Area [N]. China Ocean News, 2003-06-20.

[2] Sun Mei-xian, Zhang Wei. Study on Coastline Remote Sensing Survey and Application in Fujian Province [J]. Journal of Oceanography in Taiwan Strait, 2004, 23(2):213 - 218.

[3] Lin Ning, Wang Jiang-tao, Xu Wen-bin. Research on the Spatio-temporal Data Management Model of the Sea Area Use [J]. Ocean Technology, 2005, 24(1):82 - 85.

[4] Technical Report on Tianjin Coastline Demarcation, 2005.

[5] The Law of the People's Republic of China on the Administration of the Use of Sea Areas, 2002.

[6] The Orders of Jiangsu Province on the Administration of the Use of Sea Areas, 2005.

我国海岸线确定和管理模式研究

林 宁[1]，黄南艳[1]，徐文斌[1,2]

(1. 国家海洋信息中心，天津 300171；2. 中国海洋大学，山东 青岛 266003)

摘 要：文章归纳总结了我国海岸线确定和公布的模式．提出了海岸线确定后的海岸线修订、海岸线区划、海岸线使用和海岸线信息化管理等方面的问题．并对其进行了具体的研究和探讨，为我国海岸线的管理提供了有益的参考。

关键词：海岸线；确定；管理；模式

Development and Management Status of Voluntary Observing Ships in China

LIU Jia-yi

China Institute for Marine Affairs, Beijing 100860, *China*

Abstract: Voluntary observing ship (VOS) observations are international obligations that must be fulfilled by China. Currently, the number of Chinese VOSs is showing a decreasing trend, which has decreased from more than one hundred ships in the past to the current number of thirty something ships. Moreover, the observation capabilities have many existing problems, such as relatively outdated observation measures, simple observation parameters, and lack of observation data. Fundamentally speaking, the operation mechanism of VOSs lacks effective systematic assurance and protection. Consequently, these VOSs are unable to have sufficient operational capabilities and cannot effectively fulfill their international obligations.

Keywords: voluntary observing ship (VOS), marine observations, ship monitoring

Introduction

Observation made by voluntary observing ships (VOSs) is an obligation fulfilled by merchant ships, transport ships, fishing boats, and other vessels engaged in marine activities. These ships are equipped with adequate meteorological instruments for making oceanographic observations in shore and high seas. Development of VOS observations can compensate for the lack of real-time monitoring capabilities. Accessing valuable information regarding marine scientific researches, maritime transport security, and national defense has major significance scientifically and is important for the purpose of national security as well.

VOS observations are not only to obtain a country's own marine meteorological data for its own climate services but also, more importantly, to serve all international ships navigating in the region, which is considered as an international obligation. International VOS observations scheme has already been implemented internationally, which is coordinated by the Joint WMO-IOC Technical Commission on Oceanography and Marine Meteorology (JCOMM). The JCOMM is an intergovernmental body of experts jointly established by the World Meteorological Organization (WMO) and Intergovernmental Oceanographic Commission (IOC). For the purpose of international coordination, regulation, and management, this administrative body is established to undergo oceanographic and marine meteorological observations and data management and services. As a member of the WMO and IOC member as well as one of the permanent members of the United Nations, China is obligated to fulfill its international responsibilities. Hence, development of Chinese VOS observations system is very

Received on August 20, 2008

necessary.

1 Origin of international VOS scheme

As an important component of the three-dimensional monitoring of the marine environment, the role and significance of ship observations have already been well recognized internationally. Ocean voyages have to face many dangers, such as storm surges, rough sea waves, and icebergs. Lieutenant Matthew Fontaine Maury of the U.S. Navy was the first man to realize the scientific and commercial value of meteorological information collected from ships. Under his proposal, the first session of the International Climate Conference was held in 1953 in Brussels. The aim of this conference was to overcome these navigation difficulties and to establish maritime meteorological observations scheme. Moreover, international cooperation was considered to construct a unified system of ocean observations, with these meteorological observations providing important support for weather forecasts and reports. After the conference, the marine meteorological agencies worldwide have made arrangements for ships to dock periodically. As a result, the meteorological observations carried by these ships are transmitted ashore at no cost. With the development of the radio communication in the early 20th century, transmission of the observed data from ships in real-time became possible, which allowed ships to transmit these data to meteorological agencies. Warnings of dangerous situations could be issued to ships from the shore also. Shipping companies usually have volunteered to provide free meteorological observation data in exchange for services on navigation guidance and weather forecasts and warnings from meteorological agencies.

In the 1990's, in response to the demand of more accurate weather forecasts resulting from the increase of abnormal weather changes and the rapid economic development, the WMO and the IOC of the United Nations Educational, Scientific, and Cultural Organization (UNESCO) and the maritime groups strengthened cooperation for the development of VOS observations activities. In 1990, the Second World Meteorological Congress (held in Geneva) determined that a comprehensive ocean observing system is an essential component of the Global Climate Observing System (GCOS). In 1998, the Conference of the Parties to the United Nations Framework Convention on Climate Change (UNFCCC) called on the governments worldwide to enhance full and systematic monitoring and data collection activities over and within the oceans. In 2001, the WMO and the IOC of the UNESCO jointly established the JCOMM, which is responsible for the coordination of VOS scheme internationally. The JCOMM aperiodically holds Ship Observations Team (SOT) and Port Meteorological Officers (PMO) conferences, which are known as the VOS scheme conferences.

The WMO's VOS scheme is an important component of the World Weather Watch (WWW). Under this framework, the National Meteorological Services (NMSs) recruit ships for recording and transmitting meteorological observations, namely air pressure, air temperature, sea-surface temperature, wind, and sea state. Port Meteorological Officers (PMOs) are representatives of the NMS, contributing directly to the effectiveness and efficiency of the VOS scheme. An office of PMO is often located at the main ports in

most of the countries, which is responsible for collecting non-real-time information from ships under VOS scheme and maintaining equipment and instruments of VOSs. Meteorological observations made by officers onboard vessels under the VOS scheme are recorded in meteorological logbooks and subsequently transmitted to shore instantly after standardized coding of these data. They are then routed on the WMO's Global Telecommunication System (GTS) for use by meteorologists, ship routing services, radio and television broadcasts, and other clients around the world.

2 Status of VOS observations management

2.1 Current situation

Ship monitoring refers to the use of ship-borne equipment for monitoring the marine environment, which includes ship observations (VOS observations), sectional monitoring, trend monitoring, emergency monitoring, and ecological monitoring. Ship observations are hydrographic and meteorological monitoring by merchant ships or fishing boats on fixed shipping routes globally. Sectional monitoring refers to the hydrographic, meteorological, conventional chemical, and geological monitoring at the fixed sections of the major sea areas of China, which are carried out annually by marine monitoring vessels. Trend monitoring is periodic monitoring of changes of contaminants at more than 400 stations and points throughout sea areas of China. Emergency monitoring refers to the temporary on-site monitoring of sudden contaminative disasters, such as oil spoil, red tide, and viral breakout. In 2005, more than 180 monitoring vessels were responsible for marine environment monitoring in China, with more than 16,000 hours of navigation time.

Currently, China only has 35 VOSs, with 9 under the South China Sea Branch, 15 under the East China Sea Branch, and 11 under the North China Sea Branch. These ships are mainly composed of merchant ships on the regular shipping lanes. The observations made by these VOSs include: wind direction, wind speed, air pressure, temperature, and humidity. No hydrographic observations are reported. The five ship observation stations are responsible for the collection and management of the data collected by these VOSs.

With the development of aerospace technology, satellite marine exploration technology has advanced rapidly. Its advantageous features of all-weather, all-time, and large area coverage along with monitoring of ocean stations, wave radar monitoring of coastal bases, conventional sectional monitoring, VOS observations, and monitoring of buoys and submerged buoys have composed a complementing and powerful three-dimensional monitoring network. Moreover, satellites can be used as a relay platform for data transmission, which has solved the long-dated fundamental problem of real-time data transmission

Currently, the monitoring data received by all levels of the marine environmental monitoring institutions are mutually transmitted mainly through the marine environmental monitoring data communication network. Marine environmental monitoring data communication network uses cable networks, namely frame relay, DDN, CHINAPAC, and PSTN, of the national public telecommunication

network and wireless telecommunication technology, namely VSAT, INMMARSAT-C, and shortwave and ultra shortwave radio telecommunications, to build connections with the data transmission networks of the followings: marine monitoring stations, island stations, offshore platform stations, monitoring vehicles, monitoring vessels, monitoring buoys, satellite remote sensing ground stations, aerial remote sensing monitoring, all levels of operation centers and stations, and the administrative and law enforcement authorities. The connections are composed of: (1) Marine Environmental Monitoring Stations → Marine Environmental Monitoring Center Stations; (2) Marine Environmental Monitoring Center Stations → Regional Operation Centers; (3) VOS (including Island Stations and Offshore Platform Stations) → Regional Operation Centers; and (4) Regional Operation Centers → National Operation Center.

The transmission of real-time data from VOS is as follows: IMARSAT-C Satellite → Ship Observation Stations → Various Regional Forecast Centers → VSAT Stations → the National Marine Environment Forecast Center.

2.2 Management mode

In accordance with the "Three-Decision Plan" of the State Council, the national oceanic administrative departments are responsible for the management of oceanic affairs, including coordination of VOS. Currently, a national forecast center and three regional forecast centers have been established, which are responsible for the task of real-time reception and redistribution of VOS observation data. Moreover, the five ship reporting stations are established in Dalian, Tianjin, Qingdao, Shanghai, and Guangzhou, which are directly under the command of Dalian Center Station, Tang-gu Center Station, the North China Sea Forecast Center, the East China Sea Forecast Center, and the South China Sea Forecast Center, respectively. The stored data are handed over to the respective reporting stations after vessels have docked. The media are then passed to the three regional sea forecast centers. From there, the data are finally given to the National Marine Data & Information Service for filing, administration, analysis, reporting, and services.

The national oceanic administrative departments are responsible for the organization, coordination and administration of China's participations in international maritime cooperation, including ocean observations, marine forecasts and other marine services related to the JCOMM. China has participated the VOS Observation Scheme of the JCOOM. However, the result has not been very satisfactory so far. The VOSs transmit real-time data to the WMO through INMARSAT, and these data are subsequently sent by the WMO to the entire world through GTS, which are then used for marine forecasts and weather forecasts. In China, only the meteorological bureaus are capable of receiving these real-time data through GTS. An exclusive GTS transmission line exists between the National Marine Forecast Center and the National Meteorological Bureau, but only VOS observation data are transmitted through this exclusive line.

2.3 Existing problems

Resources of VOS observations have not been put into good use in the past. Concurrently, the issue of underfunding has weakened the administrative ability of the five reporting stations under the State Oceanic Administration, responsible for coordination of VOS. As a result, the gap between China and the rest of the world maritime powers has been widened. For example, the ADCP Current Profiler manufactured by RD Instruments of USA is technologically advanced and very expensive. Yet, the Japanese government is the largest buyer internationally. Japan has passed regulations requiring its domestic ocean merchant ships and fishing ship to be equipped with this ADCP instrument according to the proportion of the number of vessels, which, in return, allows Japan to acquire the current profile data of major ports and shipping routes throughout the world.

With the gradual strengthening of the national power in the recent years, the task of VOS observations has been recovered gradually. For example, despite collection of simple observations, ocean fishing vessels under VOS scheme may sail to any region and port worldwide with minimal restrictions. This advantage of navigation freedom of VOS is extremely precious, especially under the viewpoint of the "threat from great powerful nation" commonly shared in the international community. Furthermore, these ocean fishing boats often have to operate in the same sea areas for a long time, which frequently happen to be the marine environments that the Chinese military desperately wants to be familiar with. Under the current circumstance of no other more economical and reliable ways of obtaining the needed information, the role of VOS observations is irreplaceable.

However, VOS observations in China still have many problems, including scarce VOSs, outdated observational means and measures, limited observational parameters, and insufficient observational data. The lack of effective laws and regulations for support has caused VOS unable to carry out the necessary observations. The utilization ratio of VOS resources is very low. These resources (including ocean fishing boats, merchant ships, and survey ships) have not been fully utilized to obtain the observation data in high seas, oceans, and major shipping lanes. Observation parameters are often limited to the conventional marine meteorological information, lacking information on sea currents, CTD (conductivity, temperature, and depth), seabed topography, and luminous biological organisms. Furthermore, equipment and instruments of the survey ships and monitoring stations are aging and badly outdated with very little automation, which have contributed to the hindrance of real-time reception, collection, and transmission of VOS observation data.

Currently, the key existing problems of VOS include: (a) The scale of fleet of VOSs is small. Currently, China only has 35 VOSs, and the actual number of operational ships is much smaller than that. Only five ships are able to carry out real-time data transmission. Furthermore, due to the route restrictions, the actual information obtained is very minimal. (b) Most of equipment and instruments of VOSs have aged considerably. No replacement parts are available onboard to promptly repair the

damaged equipments and instruments. Furthermore, the situation of strong sea wind with high salinity has worsened the problem, damaging equipment and instruments readily. (c) Real-time data transfer is very poor. Due to the lack of proper telecommunication system, some of the VOS observations cannot be transmitted in real-time. These data can only be collected after the ships returned to ports. (d) Funding is severely insufficient. In the current operation process of VOS, the funding for the necessary instrumentations and equipment, labor fees, service fees, maintenance fees, and telecommunication are all seriously underfunded, making very difficult for normal operations of VOS observations to be carried out. (e) Development and management are difficult. Regulations governing VOS observations are basically non-existent. Currently, the activities of VOS observations are all voluntary. Moreover, no one onboard VOS is responsible for handling observation equipment and instruments, and the management of ship observation stations is inadequate. Consequently, many VOSs have failed to operate normally.

The direct result from the above mentioned problems is that China cannot effectively fulfill its international obligations. International VOS scheme is part of the World Weather Watch of the WMO. As a member of the WMO, China is obligated to share its observations in real-time as China is receiving VOS observations from other countries concurrently. However, due to the restraints, such as departmental interests, the fulfillment of this international obligation has been very poor, affecting the status of China as a permanent member of the United Nations. Consequently, China has clearly lost its position over this issue as a major country actively participating international affairs.

3 Conclusion

The frequent occurrences of natural marine disasters, such as tsunamis and storm surges, have led to huge social and economic losses, which have constantly threatened the life and assets security of the coastal residents. Yet, the task of undergoing research, development, and application of the relevant scientific and technological oceanographic observations still remains very difficult. Chinese government must place great attention to ship monitoring, which has important significance in accessing marine meteorological data. The development of VOS industry must meet the requirements of fulfilling international obligations. China should actively promote international cooperation and exchanges, participate the related international activities, study the key scientific problems, and provide accurate information and countermeasure proposals to safeguard national interests and image.

China should promptly formulate its own VOS Observation Action Plan Scheme with consideration and incorporation of its own characteristics and advantages. Furthermore, it should timely promulgate a ship observation study plan related to VOS observations. With integration of the existing projects and considering advantages comprehensively, this VOS observation system of China should be promoted internationally and incorporated into the international research plan. The result will continuously improve the status and role of China in the international oceanographic observation science plan.

As a large developing country, China faces many prominent issues, namely society, environment,

economic, and development, in the international community. Consequently, China must earnestly perform its international obligations and act in accordance with the international conventions, which will help China to establish a good image of a responsible large nation in its development.

中国海洋志愿观测船现运行状态及发展

刘家沂

（国家海洋局 海洋发展战略研究所，北京 100860）

摘 要：志愿船观测是中国必须履行的国际义务。目前，中国海洋志愿观测船只呈逐年减少趋势，从过去的百余艘船只降至三、四十艘，并且从观测能力上也存在较多问题，比如观测手段比较落后、观测要素单一、观测资料缺乏。从根本上讲，志愿船运行机制缺乏有效的制度化保障，因此难以形成业务化能力，并且不能有效的履行国际义务。本文将对志愿船现运行状态及发展进行论述。

关键词：志愿船；海洋观测；船舶监测

海 洋 通 报（英文版）

HAIYANG TONGBAO

2009 年 5 月　第 11 卷　第 1 期

目　次

冬季鄂霍次克海海冰对北太平洋风暴轴年际变化的影响 …… 何冬燕 等 (12)

珠江口二类水体水色三要素的优化反演 …… 杨锦坤 等 (23)

黄、东海溶解态无机砷的分布及其季节变化 …… 任景玲 等 (36)

雨生红球藻中 IPP 异构酶基因表达调控机制的初步研究 …… 高政权 等 (42)

南海南部表层沉积物中生物硅的分布及其环境意义……张兰兰 等 (52)

新村湾海龟草(*Thalassia hemprichii*)的生长策略研究…… 许战洲 等 (61)

应力－应变过程中海底沉积物微结构变化对其声速的影响 …… 李赶先 等 (69)

南海南部断裂的分形研究 …… 姚衍桃 等 (81)

我国海岸线确定和管理模式研究 …… 林　宁 等 (89)

中国海洋志愿观测船现运行状态及发展…… 刘家沂　(96)

Marine Science Bulletin

Marine Science Bulletin publishes papers on marine science and technology including physical oceanography, chemical oceanography, marine biology, marine geology, environmental oceanography, estuarine & coastal sciences, marine technology, digital ocean, coastal zone management, ocean engineering, marine economics, etc., and aims to promote international academic exchange.

Editor-in-Chief: XU Sheng (徐　胜)
Associate Editor-in-Chief: HE Guang-shun (何广顺)　LU Ming-sheng (卢明生)
Executive Editor: YANG Rui (杨　瑞)　QIU Wen-jing (邱文静)　LI Xue (李　雪)
ZHANG Xiao-xian (张潇娴)　YUAN Ze-yi (袁泽轶)
English proofed by: WANG Qi (王琦)

Semi-annually (started in 1999, sum 21)
Publication date: May. 15th and Oct. 15th

Marine Science Bulletin **(Vol. 11, No. 1, May 2009)**

Responsible Institution:
State Oceanic Administration of China
Sponsored by:
National Marine Data and Information Service
Edited by:
Office of Marine Science Bulletin (English edition)
Printed by:
Printery of National Marine Date and Information Service

Published by:
Office of Marine Science Bulletin (English edition)
E-mail: msb@mail.nmdis.gov.cn
Tel: (022) 24011287
Address: 93 Liuwei Rd., Hedong District, Tianjin 300171, China

ISSN1000-9620
CN12-1271/N

Price: $ 30.00 / ￥18.00 Per year